A METAMORPHIC AND GEOCHEMICAL STUDY OF MAFIC ROCKS ACROSS THE PENCKSÖKKET-JUTULSTRAUMEN DISCONTINUITY, WESTERN DRONNING MAUD LAND, EAST ANTARCTICA

Eugene Gerald Grosch
B.Sc. (Hons)

Thesis presented for the Degree of
MASTER OF SCIENCE

Department of Geological Sciences
University of Cape Town
August 2005

DECLARATION

I, Eugene G. Grosch, declare that the work presented in this thesis is my own, unless otherwise stated.

Signature:

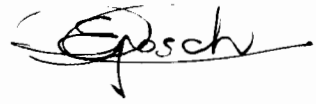

Eugene Gerald Grosch

ABSTRACT

A petrological and metamorphic comparison of Mesoproterozoic metabasic rocks on the eastern margin of the Archaean Grunehogna Craton and the adjacent Maud Belt in western Dronning Maud Land, East Antarctica, revealed a difference in peak metamorphic conditions from T = ~275°C to 730°C and P = 2 to 10.7 kbar over a distance of only 30 km across a major glacial valley. The lower grade constraints were derived from average P-T calculations using THERMOCALC and thermodynamic modeling of phase equilibria together with chlorite geothermometry. The high-grade P-T constraint for the westernmost part of the Maud Belt closest to the glacier, derived from hornblende-plagioclase thermometry and geobarometric calculations with a garnet amphibolite assemblage, is very similar to that reported for the eastern Maud Belt and, therefore, does not support the concept of a westward decreasing metamorphic field gradient as previously proposed. In conjunction with a recent geochronological study on the eastern Maud Belt, this study suggests that the inferred sub-glacial boundary between the Grunehogna Craton and the Maud Belt, known as the Pencksökket-Jutulstraumen Discontinuity, may represent a major thrust that developed during Pan-African orogenesis (possibly as the continuation of the East African Mozambique Belt into East Antarctica) prior to extension and its development as a normal listric fault or succession of fault slices during the Mesozoic break-up of Gondwana.

Bulk major-, trace- (including rare earth) element and isotopic data of variably metamorphosed mafic rocks in the polymetamorphic Maud Belt, in conjunction with limited geochronological data, indicate that the Maud Belt was once an active continental volcanic arc that formed on the southeastern margin of the Kaapvaal-Grunehogna Craton during the late Mesoproterozoic (1160-1130 Ma). This is in contrast to models of an oceanic island arc that was obducted onto the craton margin in analogy with the evolution of the Natal Belt in southern Africa. Four groups of amphibolite are distinguished on the basis of new lithogeochemical and Rb-Sr as well as Sm-Nd isotope data. Group 1 is the oldest and is interpreted as representing volcanic arc-related mafic protoliths in the Maud Belt. It is characterized by Archaean Sm-Nd model ages (2500 to 3300 Ma), depletion in Nb and Ta, and strong enrichment in light rare earth and large ion lithophile elements. Its ϵ_{Nd} (1110 Ma) values show a wide spread ranging between –6.0 and –15.0. The mafic protoliths to the Group 2 amphibolites are ascribed to the 1107 Ma

Umkondo/Borgmassivet thermal event on the basis of comparable Sm-Nd model ages (~1800 Ma) and trace element distributions. Group 3 amphibolites are distinguished by flat, E-type MORB-like rare earth element patterns and low Th/Yb ratios. They are interpreted to represent largely juvenile oceanic basalts/dykes that were emplaced during opening of a Neoproterozoic ocean basin. Group 4 amphibolites show overall enrichment in rare earth elements and elevated Zr concentrations. They are interpreted to be related to a phase of c. 530 Ma syn-tectonic mafic magmatism that was derived from partial melting of late Mesoproterozoic lithosphere. Post-tectonic, c. 490 Ma gabbro and mafic dykes have a geochemical signature with subduction-zone characteristics. From their chronometric, isotopic and field relationships it is evident, however, that they are related to partial melting of lower calc-alkaline, arc-related Mesoproterozoic crust during orogenic collapse and not to melt formation in an active supra-subduction-zone setting. This demonstrates the limitations and problems of conventional tectonic discrimination diagrams.

CONTENTS

LIST OF FIGURES AND TABLES

List of figures:

Figure 7. Tetrahedral Al versus trioctahedral chlorite content (x) for selected samples.

Figure 8. Amphibole compositions in Nashalkalvane metabasites classified after Leake et al. (1997).

Figure 9. Amphibole compositions in selected Straumsvola metabasites classified after Leake et al. (1997). Recrystallized amphibole displays the highest variation in Si, but similar X_{Mg} (Inset B). Open symbols: all Fe = Fe^{2+}, black symbols: maximum Fe^{3+} estimation.

Figure 10. Plagioclase compositions for Nashalkalvane and Straumsvola metabasites. Feldspar in metamorphic domains of Nashalkalvane metabasite is albite. Plagioclase grains in the recrystallized amphibolite sample EG-028 shows the greatest compositional variability.

Figure 11. *P-T* diagram in the system NCMASH showing activity isopleths with activities derived from mineral compositions in EG-N2. All reactions with clinochlore, quartz and H_2O in excess. PA, PP, and PrA indicate the pumpellyite-actinolite, prehnite-pumpellyite, and prehnite-actinolite facies, respectively. GS = greenschist facies. Point *X* is the intersection between the two reactions defining the lowermost boundary of the greenschist facies. The location of the Act-Hbl boundary is after Apted & Liou (1983).

Figure 12. The influence of water pressure on the lower boundary of the greenschist facies, modeled using THERMOCALC v.2.75 (Holland & Powell, 1998; and references therein).

Figure 13. Relationship between modal proportion of mafic hydrous phases and temperature calculated by chlorite geothermometry. A temperature of 259°C is a minimum estimate obtained from fine-grained chlorite growing along a cleavage plane in the core of a clinopyroxene grain in sample EG-N10 and chlorite in the smallest observed metamorphic domain in sample EG-14a.

Figure 14. Temperature curves yielded by the Holland & Blundy (1994) geothermometer for amphibole-plagioclase pairs (a-e) in Straumsvola amphibolites.

Figure 15. P-T constraints on metamorphic conditions at Nashalkalvane (eastern Grunehogna Craton) and Straumsvola (western Maud Belt) compared with those from eastern Maud Belt (eastern H.U. Sverdrupfjella; Board, 2005). Granulite facies conditions are derived from mafic boudins after Groenewald & Hunter (1991) and Groenewald et al. (1995). Aluminosilicate triple point is after Bohlen et al. (1991). Reactions (15), (16) and (17) are from Pattison (2003) calculated on the basis of a pargasite composition with X_{Mg} = 0.5. Reaction (18) is the approximate position of the wet tonalite solidus (Johannes, 1978; Piwinskii, 1968, Wyllie and Wolf, 1993). P-T conditions calculated in this study for the western Maud Belt correspond to that of M_{2b} in the eastern Maud Belt with age constraints from Board et al. (2005). Note a metamorphic hiatus of T = 450°C and P = 6.5 – 8.7 kbar across the Jutulstraumen glacier.

Figure 16. Tectonic map of Western Dronning Maud Land, (after Board et al., 2005) showing the study area and the various sample localities.

Figure 17. AFM diagram for (a) 1107 Ma Borgmassivet Suite sills on the Grunehogna Craton and the Maud Belt amphibolites, and (b) post-tectonic 490 Ma Stabben Gabbro and mafic dykes from the Gjelsvikfjella.

Figure 18. Zr/TiO_2 versus Nb/Y diagram (after Winchester and Floyd, 1977) for the mafic rocks from Western Dronning Maud Land.

Figure 19. Major and trace element versus Zr plots distinguishing between the effects of possible magmatic fractionation and remobilization of elements during high-grade metamorphism.

Figure 20. REE patterns of mafic rocks included in this study from Western Dronning Maud Land normalized to the C1 chondrite (Sun and McDonough, 1989). Note that the Nashornkalvane mafic sill on the easternmost margin of the craton has a REE pattern identical to the data available (Krynauw, 1986) for the 1107 Ma Borgmassivet Suite mafic sills (a). The REE patterns of post-tectonic mafic intrusions are shown in (b). The majority of the amphibolites of unknown age (c-f) from the Maud Belt compare well with the on-craton 1107 Ma Borgmassivet Suite sills sharing a similar LREE enriched pattern. Some amphibolites from the Gjelsvikfjella differ in that they show overall enrichment in REE or much flatter profiles to the rest (g). Heimefrontfjella 1030 Ma and 600 Ma amphibolite groups (h; data from Bauer et al., 2003).

Figure 21. Zr/Y versus Zr diagram after Pearce and Norry (1979) for mafic rocks from the Maud Belt.

Figure 22. REE patterns of amphibolite samples displaying evidence for secondary alteration. Amphibolites showing concave-upward, LREE-depleted patterns due to metamorphic alteration correspond to those with severe depletion in Zr (a). Similarly, amphibolites showing pronounced negative Eu anomalies correspond to the samples also showing enrichment in 'immobile' trace elements due to metasomatism (c). The negative Ce and Eu anomalies in the REE patterns in some samples are attributed to interaction with seawater (b). A positive correlation between Zr concentration and LREE depletion is observed in some amphibolites suggesting the mobility of these elements during high-grade metamorphism (d).

Figure 23. Nb-Zr-Y diagram after Meschede (1986), data fields include: within-plate alkaline basalts (AI + AII), within-plate tholeiites (AII + C), P-MORB (B), N-MORB (D), volcanic arc basalts (C + D). Amphibolite dykes and mafic sills of known age are shown on this diagram (a). All data for amphibolites in this study of unknown age are compared (b, d). Samples of unknown age from the Gjelsvikfjella with differences in REE chemistry and those, which have been affected by metamorphism, are shown separately of this diagram in (c) and (b), respectively.

Figure 24. Zr-Ti/100-Y*3 diagram after Pearce and Cann (1973), data fields include: island arc tholeiites (A), MORB, island arc tholeiites and calc-alkali basalts (B), calc-alkali basalts (C), within-plate basalts (D). As in Fig. 25, amphibolites of unknown age are compared to those, which have been dated (b, d). Samples with different REE patterns and those showing evidence for fluid remobilization are shown separately in (c) and (b), respectively.

Figure 25. Th/Yb versus Nb/Yb plot for the mafic rocks in Western Dronning Maud Land; EM = enriched mantle. DM = depleted mantle (after Pearce, 1983; Pearce and Peate, 1995). Note that most of the amphibolites in the Maud Belt and the on-craton mafic intrusives are displaced above the mantle array suggesting the influence of subduction zone metasomatism for these rocks. The three samples from the Gjelsvikfjella with the flat REE profiles plot close to the data for the c.590 Ma amphibolite dykes near the enriched mantle part of the array.

Figure 26. N-type MORB-normalized trace element variation diagrams (after Pearce, 1983) for various amphibolites in the Maud Belt in comparision to the Borgmassivet Suite mafic sills and the two groups of amphibolite dykes in the Heimefrontfjella dated at 1030 and 590 Ma. Most of the amphibolites in the Maud Belt have very similar patterns to that of the Borgmassivet sills (e-f).

Figure 27. Primitive mantle-normalized diagrams for the majority of the Maud Belt amphibolites in comparision to the Borgmassivet and Umkondo Suite mafic sills. Average southern Karoo basalt composition of southern Africa shown for comparision (Duncan et al., 1984).

Figure 28. Ba/Nb versus La/Nb diagram (after Sun and McDonough, 1989) for Nashornkalvane mafic sill and the amphibolites in the Maud Belt. Fields for primitive mantle, EM-type OIB = Enriched Mantle-type Ocean Island Basalt, HIMU OIB = HIMU Ocean Island Basalt, MORB = Mid-Ocean Ridge Basalt and arc basalts after Sun and McDonough (1989).

Figure. 29. Tectonic discrimination diagrams (after Mullen, 1983; Shervais, 1982; Wood, 1980) for the post-tectonic mafic dykes in the Gjelsvikfjella (A. Bisnath, unpubl. data 2005). (a) CAB = Calc-Alkaline Basalt, IAT = Island Arc Tholeiite, MORB = Mid-Ocean Ridge Basalt, OIA = Ocean Island Andesites, OIT = Ocean Island Tholeiites. (b) WPB = Within-Plate Basalt.

Figure 30. The Nashornkalvane sill (this study) of the 1109 Ma Borgmassivet Suite and 1105 Umkondo mafic sills in comparision to various Mesozoic Karoo-Dronning Maud Land basalt groups of Riley et al. (2005). Data: Umkondo sills from Munyanyiwa (1999); Average composition of southern Karoo basalt from Duncan et al. (1984). Mesozoic Dronning Maud Land-Karoo (DML-Karoo) age Group 1 and 4 basalts from the Ahlmannryggen region, Antarctica from Riley et al. (2005).

List of Tables:

ACKNOWLEDGEMENTS

This research was funded through the South African National Antarctic Programme. The various expedition team leaders and the staff from the South African Department of Environmental Affairs and Tourism are thanked for their guidance and logistic support. Avinash Bisnath is thanked for providing unpublished geochemical data on mafic rocks from the Gjelsvikfjella area. Dr. Andreas Späth is acknowledged for his help with the electron microprobe analyses. I am grateful for the assistance provided by Shireen Govender with the Rb-Sr and Sm-Nd isotope analyses. My supervisor, Prof. Hartwig Frimmel is thanked for his encouragement and guidance during my MSc and for giving me the opportunity of experiencing Antarctica. Dr Marian Tredoux, Prof. David Reid, Prof. Steve Richardson, and Prof. Anton. le Roex are all thanked and will always be remembered for their much appreciated support. Finally, I would like to thank my parents, Gerald and Patsy; brothers, Warren and Garreth; sister-in-law, Ramona and my baby nice, Allison; especially for her heart-warming smile.

1. INTRODUCTION

The high-grade Maud Belt of western Dronning Maud Land, East Antarctica, has been interpreted to originate as a juvenile island arc that was tectonically accreted on to the margin of an Archaean cratonic block, known as the Grunehogna Craton at the end of the Mesoproterozoic (Basson et al., 2004; Bauer et al, 2003; Golynsky and Jacobs, 2001; Grantham et al., 1995; Groenewald et al., 1995; Paulsson and Austrheim, 2003, Jacobs, 1993; Figs. 1 and 2). The marked metamorphic contrast between the relatively undeformed Mesoproterozoic volcano-sedimentary Ritchersflya Supergroup overlying Archaean basement granite of the Grunehogna Craton and the high-grade gneisses of the Maud Belt, has led to the inference of a sub-glacial boundary known as the Pencksökket-Jutulstraumen Discontinuity (PJD; e.g. Ravich & Soloviev, 1969; Grantham et al., 1988; Grantham & Hunter, 1991). Extensive mafic sills of the 1107 Ma Borgmassivet Suite (Krynauw, 1991; M. Knoper, unpubl. data reported in Frimmel, 2004) intruded the Ritcherflya Supergroup, whereas in the Maud Belt numerous mafic bodies occur as pre- to post-tectonic amphibolite dykes, sills and boudins.

General agreement exists on the Grunehogna Craton having formed part of the Kaapvaal Craton prior to the break-up of Gondwana. The geodynamic evolution prior to Gondwana remains highly speculative. Three different tectonic models have been suggested for the oceanic area to the south of the Kaapvaal-Grunehogna Craton, including western Dronning Maud Land: (i) a complex "Tugela Ocean" with one or more intra-oceanic arcs but generally southward directed subduction zones (Arima et al., 2001); (ii) a southward directed subduction, followed by a northward directed subduction in western Dronning Maud Land (Bauer et al., 2003); and (iii) two southward directed subduction zones, with the northern one separating the Grunehogna Province from the Kaapvaal Craton (Basson et al., 2004). All of these models consider the Maud Belt to represent a continuation of the late Mesoproterozoic Namaqua-Natal Belt of southern Africa into East Antarctica and they involve deposition of at least the lower parts of the Ritcherflya Supergroup in a peripheral forearc cratonic basin in response to accretion and continental collision of an island arc (Maud Belt) to the margin of the Grunehogna Craton (e.g. Basson et al., 2004; Groenewald et al., 1995; Moyes & Harris, 1996). The polarity of subduction is, in most cases, assumed to be directed away from the Kaapvaal-Grunehogna Craton to-

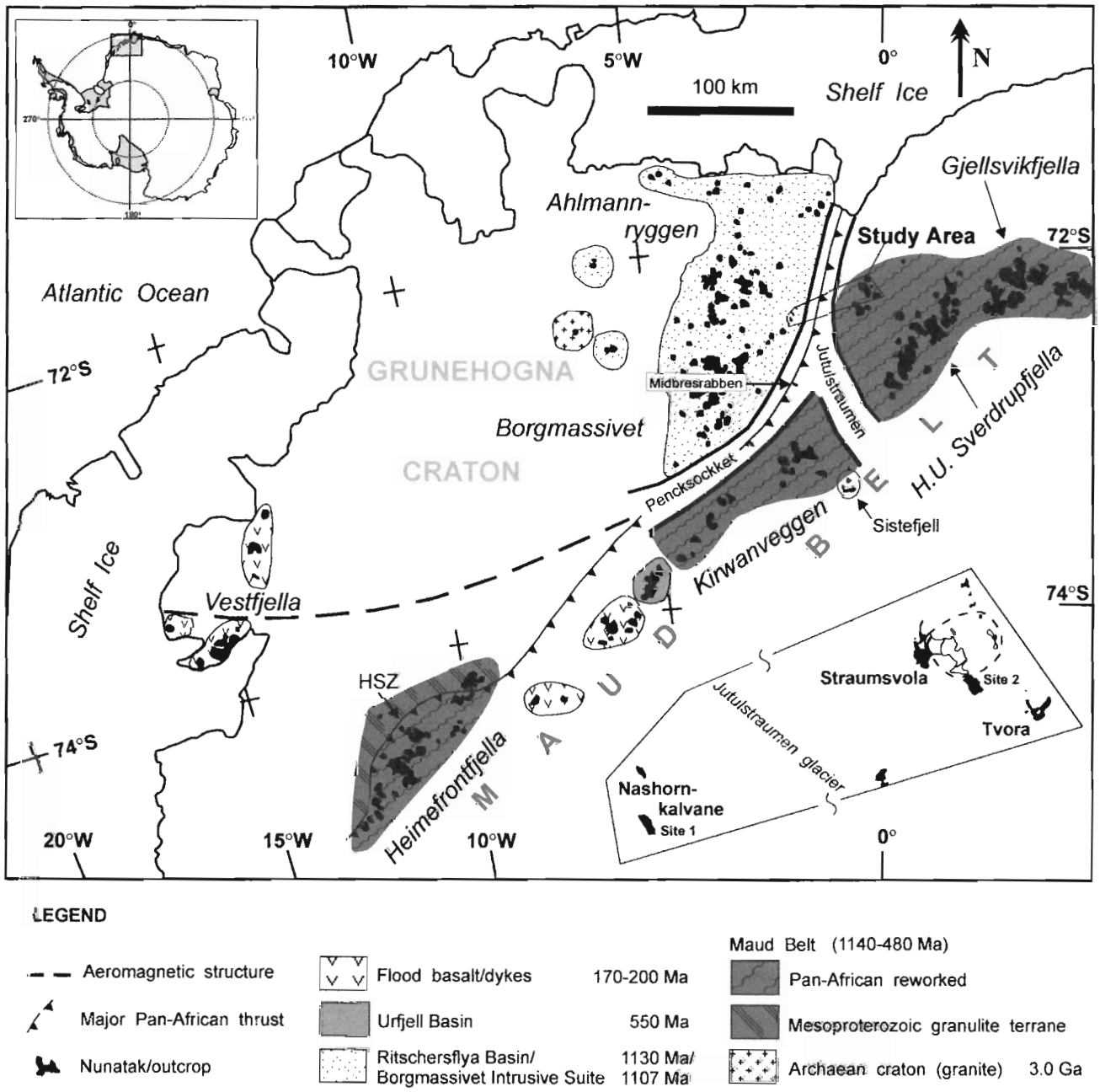

Fig. 1. Tectonic Map of Western Dronning Maud Land (modified after Board et al., 2005) showing an inferred major Pan-African thrust between the Grunehogna Craton and the Maud Belt. Sample localities at Nashalkalvane South (072°19.06S/001°57.46W) and the outcrop near Straumsvola (072°09.775/000°14.52W) are shown (Map of Straumsvola nunatak in the inset after Harris & Grantham, 1993). HSZ = Pan-African Heimefront Shear Zone.

ward allegedly juvenile island arc/s that comprise the Namaqua-Natal and Maud Belts (e.g. Basson et al., 2004; Jacobs, 1993; Golynsky and Jacobs, 2001; Grantham et al., 1995; Groenewald et al., 1995). The PJD was interpreted to have developed as a consequence of major Mesoproterozoic (1060 - 1030 Ma) thrusting during this collisional episode forming a large-scale suture between the oceanic island arc and the southeastern margin of the Kaapvaal Craton (Groenewald et al., 1995).

In contrast, a number of workers considered the discontinuity to be a graben structure that was repeatedly reactivated over the past 2.5 billion years (e.g. Ravich & Soloviev, 1969; Roots, 1969; Wolmarans & Kent, 1982). The interpretation as a rift structure was supported by gravity and aeromagnetic anomalies (Wolmarans & Kent, 1982; Decleir & Van Autenboer, 1982; Golynsky, 1997) as well as the presence of Mesozoic alkaline complexes at Tvora and Straumsvola (Fig. 1; Decleir & Van Autenboer, 1982; Harris & Grantham, 1993). Vertical displacement along the inferred fault plane/s has been estimated at between ~600 to 1500 m (Ravich & Soloviev, 1969) and 8 km (R.C. Wallace, in Wolmarans & Kent, 1982). Groenewald et al. (1995) did not dismiss the idea of crustal extension for the PJD proposed by earlier work of the above authors, but suggested that rifting exploited the pre-existing thrust plane during the break-up of Gondwana (Grantham et al., 1988; Grantham & Hunter, 1991; Harris & Grantham, 1993; Groenewald et al., 1995).

Low-grade metamorphism and deformation of the Ritchersflya Supergroup has recently been noted to increase towards the PJD (Frimmel, 2004). The age of this metamorphism, however, is unknown. On the opposite side of the sub-glacial boundary, an apparent late Mesoproterozoic metamorphic field gradient has been reported. Metamorphic grade is interpreted to decrease from granulite facies conditions in the eastern Maud Belt to amphibolite facies further to the west (Groenewald et al., 1995; Grantham et al., 1995). Recent work in the eastern Maud Belt, however, has revealed that the main, penetrative fabric is Pan-African (c. 540 Ma) in age indicating major Pan-African tectonic reworking of the Grenville-age crust (Board et al., 2005). Reconstruction of a late Mesoproterozoic P-T-t path for the Maud Belt and direct comparison with that recorded in the Namaqua-Natal Belt has was, therefore, shown to be complicated because of Pan-African overprinting (Board et al., 2005; Frimmel, 2004). Thus, the age (that is

'Grenvillian' or Pan-African) and true metamorphic grade on the opposite side of the PJD in the western part of the Maud Belt is also unknown. These new data and field observations present new uncertainties and casts doubt on pre-existing tectonic models for the development of the PJD and the late Mesoproterozoic to Palaeozoic geological evolution of Western Dronning Maud Land. Furthermore, the masking effect of the Pencksökket and Jutulstraumen glaciers, prevents direct measurement of the dip, transport direction and displacement along the inferred discontinuity concealing its true nature as a thrust or thrust zone or an extensional feature such as a normal fault, listric fault or graben-type structure.

The presenting uncertainties and difficulties in interpreting the geological evolution of Western Dronning Maud Land give rise to a number of possible end-member tectonic models other than those proposed in the literature. As the age of the metamorphism on either side of the PJD is not known, it is possible that the two litho-tectonic crustal components record differing geologic and metamorphic histories in independent tectonic settings prior to juxtaposition that resulted in a metamorphic discontinuity. Alternatively, the two crustal domains may be related only by metamorphism and not by their geological origin in the same setting, such as formation and obduction of an oceanic arc onto the continental craton margin forming a large-scale suture or thrust zone, with a section of crust missing below the glaciers. In this model, the allegedly large difference in metamorphic grade may be due to differential exhumation of different crustal levels of the Grunehogna Craton and Maud Belt, related either to Grenvillian or Pan-African orogenesis. As not only the age, but also the extent of the metamorphic hiatus is uncertain, another possibility arises whereby a continuous and progressive change in metamorphic grade exists below the glaciers. That is, the two domains may be genetically related by both, metamorphic history and tectonic setting, arguing for a close spatial relation between the Grunehogna Craton and the former Maud volcanic arc, in which case the Ritcherflya volcano-sedimentary basin may take a back-arc position. Hybrid models may also be possible which involve the PDJ as a major Pan-African thrust, rather than a late Mesoproterozoic feature.

As a penetrative fabric was imprinted on the high-grade metamorphic rocks at c. 540 Ma, the various mafic bodies that occur as deformed dykes, sills and/or boudins must pre-date or be syn-tectonic with respect to the Pan-African orogeny and thus provide potential information on

the late Meso- to Neoproterozoic history of the Maud Belt. To address the problems discussed above, the first part of this study aims at assessing the extent of the metamorphic hiatus as well as the nature and tectonic history of the PJD by quantifying and comparing the P-T conditions on either side of the inferred discontinuity. Peak metamorphic conditions was estimated from amphibolite boudins at Straumsvola nunatak in the western part of the Maud Belt closests to the Jutulstraumen glacier and compared to both the Grenvillian and Pan-African metamorphic constraints from similar amphibolite in the eastern Maud Belt as well as P-T conditions on the southeastern margin of the Grunehogna Craton from a probably contemporaneous (with respect to the protoliths of the amphibolite) mafic sill (Fig. 1).

New major, trace (including rare earth element, REE) as well as Sr and Nd isotopic data for various mafic intrusions and amphibolites from different parts of Western Dronning Maud Land are presented in this study. Geochemical and geochronological data on mafic rocks in Western Dronning Maud Land are scarce in the literature. So far, two geochemically distinct generations of amphibolite could be distinguished in the southernmost part of the Maud Belt with geochronological methods: U-Pb single zircon ages yielded 1033 ± 7 Ma and 586 ± 7 Ma, respectively (Bauer et al., 2003). These late Mesoproterozoic and Neoproterozoic mafic rocks serve as reference for the variety of undated pre- to post-tectonic mafic rocks across the Maud Belt, which are subject of this study. A further reference for lithogeochemical and isotopic comparison is given by the voluminous, effectively unmetamorphosed, 1107 Ma mafic sills of the Borgmassivet Suite on the adjacent Grunehogna Craton. Given that the early metamorphic and tectonic evolution of the Maud Belt is largely unknown due to major Pan-African tectonic overprint, the trace element and isotope geochemistry of the mafic protoliths to the amphibolites is used here in an attempt to constrain their tectonic setting. It will be shown that a number of different generations of mafic protoliths can be distinguished. By assessing the extent to which the Maud Belt represents juvenile, late Mesoproterozoic crust of an intra-oceanic island arc origin or an extensive continental volcanic arc system on the craton margin, a new geodynamic model for the late Mesoproterzoic evolution of western Dronning Maud Land will be proposed.

2. REGIONAL GEOLOGY

Western Dronning Maud Land comprises two major tectonic units, namely the Grunehogna Craton and the Maud Belt (Krynauw, 1996), with the latter recording evidence of two orogenic episodes related to supercontinent formation, once in the late Mesoproterozoic ("Grenvillian" of North America) and again around the Precambrian/Cambrian boundary ("Pan-African" of Africa) during the assembly of Gondwana (Figs. 1 and 2). An inferred boundary between the Grunehogna Craton and the Maud Belt lies concealed below the enormous Pencksökket-Jutulstraumen glacial system and is known as the Pencksokket-Jutulstraumen Discontinuity (or PJD). The only rocks exposed above this glacial system are the highly sheared diorite and mafic dykes at a small nunatak, known as Midbresrabben in the middle of the Pencksökket Glacier (Grantham and Hunter, 1991; Fig. 1).

The Proterozoic volcano-sedimentary Ritcherflya Supergroup, overlying Archaean basement granite on the craton, is sub-divided into the lowermost Ahlmannryggen Group, interpreted as a marginal-marine to braided/meandering river, regressive, marine sequence (Ferreira, 1988), and the upper Jutulstraumen Group, which consists of tuff layers and mafic to intermediate lava flows (Watters, 1991). Similarity between this volcano-sedimentary succession and the Umkondo Supergroup of southeastern Zimbabwe has led Ferreira (1988) to interpret the Grunehogna Craton as an Archaean fragment of the southeastern Kalahari (amalgamated Kaapvaal-Zimbabwe) Craton that became tectonically disconnected during the break-up of Gondwana. Numerous mafic sills of the Borgmassivet Suite intrude the Ritcherflya Supergroup and have been geochemically correlated with the flood basalts of the Jutulstraumen Group (Krynauw, 1991). U-Pb zircon data from one of the sills indicates an emplacement age of approximately 1107 Ma (M. Knoper, unpubl. data in Frimmel, 2004). A U-Pb age of 1130 ± 7 Ma, derived from single zircon grains in tuff beds from the Ahlmannryggen Group (Frimmel, 2004), provides so far the best constraint on the timing of sedimentation in the Ritcherflya basin. The tectonic setting for these sediments remains problematic.

A U-Pb zircon age of 1109.6 ± 0.6 Ma from an Umkondo dolerite sill on the eastern margin of the Archaean Zimbabwe Craton (Hanson et al., 2004) is identical with that of the Borgmassivet

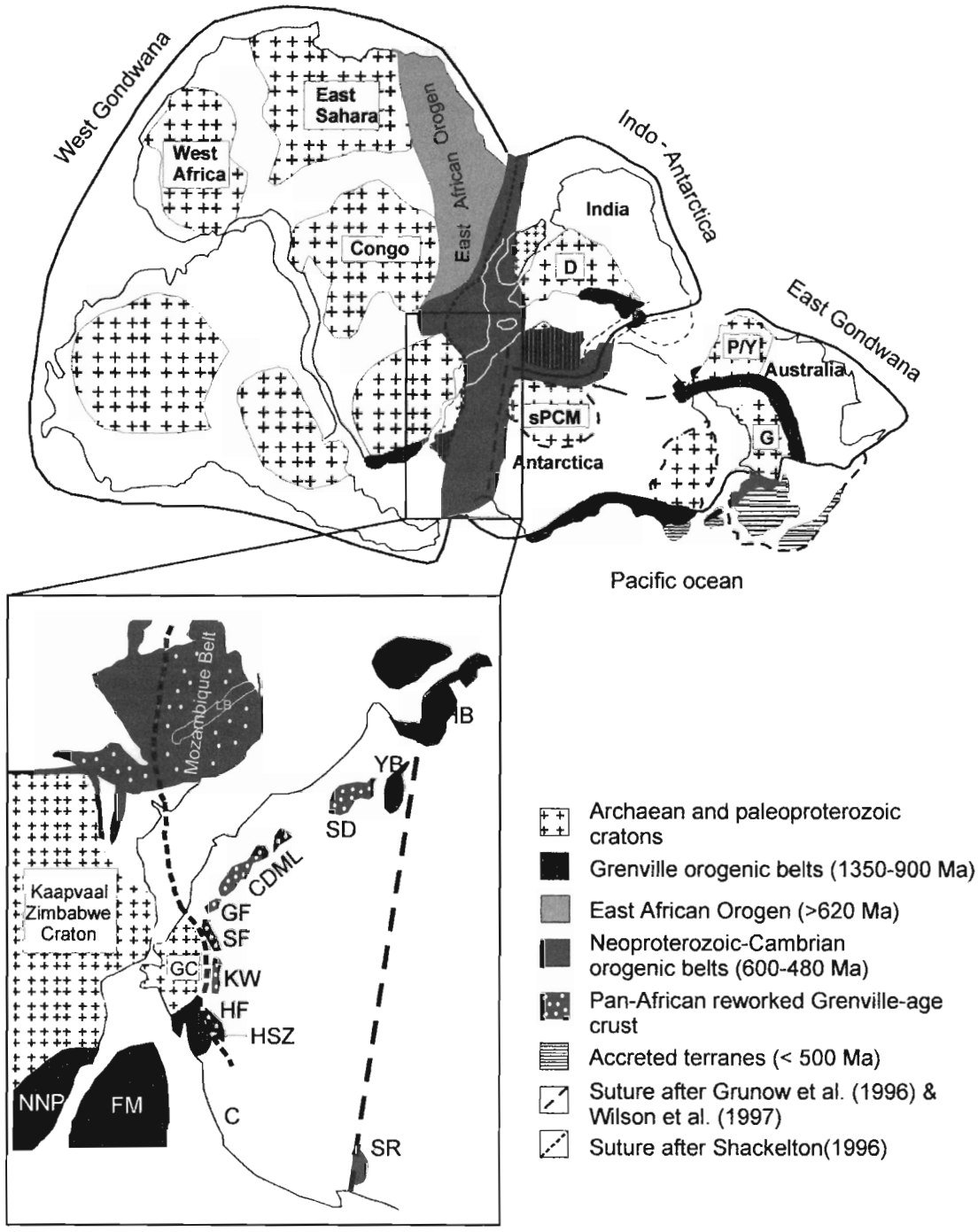

Fig. 2. East Antarctica within a Gondwana configuration at ~ 500 Ma (modified after Boger and Miller, 2004). Inset B shows Western Dronning Maud Land and the Maud Belt consisting of the Heimefrontfjella (HF), Kirwanveggen (KW), H.U. Sverdrupfjella (SF), Gjelsvikfjella (GF) and Central Dronning Maud Land (CDML) as the continuation of the Mozambique Belt into East Antarctica (modified after Kröner, 2001). C: Coats Land, FM: Falkland Microplate, GP: Grunehogna Craton, LB: Lurio Belt, NNP: Namaqua-Natal Belt, LHB: Lützow-Holm Bay, SD: Sor Rondane, YB: Yamato-Belgica Complex, SL: Sri Lanka. HSZ= Heimefront Shear Zone (after Jacobs et al., 1995). The proposed suture between East and West Gondwana is after Shackelton (1996) and Grunow (1996).

Suite. Magmatism at around that time has also been documented about 1200 km southwest of the Grunehogna Craton in southern Coats Land (Gose et al., 1997; Fig. 2). Zircon grains from rhyolite and granophyre in that area yielded U-Pb ages of 1112 ± 4 Ma and 1106 ± 3 Ma, respectively (Gose et al., 1997). It is now known that the Coats Land Block could not have been attached to the Kalahari Craton since recent age data for the Umkondo sills (Hanson et al., 2004) confirm a similar age of intrusion to that of the Coats Land magmatic suite, yet the palaeomagnetic data from these rocks indicate that the Coats Land pole is different to the Kalahari pole (Gose et al., 1997). The Umkondo and Borgmassivet Suites have been interpreted to reflect part of a large-scale intra-plate magmatic event that took place between 1112 and 1106 Ma that, although short-lived, affected both the Kalahari (including the Grunehogna) and Laurentian Cratons during the assembly of an inferred late Mesoproterozoic supercontinent (Hanson et al., 1998; 2004), be it Rodinia, Palaeopangea, or any other configuration.

Traditionally, the Maud Belt has been considered part of a larger Grenville-age mobile belt around the margin of East Antarctica, known as the Circum East Antarctic Mobile Belt (CEAMB; e.g. Tingey, 1991; Yoshida, 1992; Jacobs et al., 1993; Gose et al., 1997; Golynsky and Jacobs, 2001; Jacobs et al., 2003), which continues into the Namaqua-Natal Belt of southern Africa. It has been proposed that the Maud Belt represents a juvenile island arc that accreted onto the southeastern margin of the Kaapvaal Craton during the late Mesoproterozoic (e.g. Arndt et al., 1991; Jacobs, 1993; Grantham et al., 1995; Groenewald et al., 1995; Golynsky and Jacobs, 2001; Bauer et al, 2003; Paulsson and Austrheim, 2003; Basson et al., 2004). The Maud Belt is exposed in a number of areas from southwest to northeast, namely the Heimefrontfjella, Kirwanveggen, H.U. Sverdrupfjella, Gjelsvikfjella and central Dronning Maud Land (Fig. 1). The U-Pb zircon protolith ages of the oldest volcanic and plutonic rocks of this proposed island arc of between 1160 and 1130 Ma (Arndt et al., 1991; Harris et al., 1995; Jacobs et al., 1999; Jackson, 1999; Paulsson and Austrheim, 2003; Board et al., 2005) are in good agreement with the U-Pb single zircon ages of 1130 ± 7 Ma from tuff layers in the Ahlmannryggen Group, pointing to a close spatial relationship between the cratonic depositional basin of the Ritcherflya Supergroup and the former Maud Belt volcanic arc.

The tectonothermal evolution of the Maud Belt is complex. In contrast to the Namaqua-Natal

Belt, reconstruction of a late Mesoproterozoic P-T-t path has been severely complicated due to major Pan-African reworking of pre-existing Mesoproterozoic crust (Frimmel, 2004; Board et al. 2005). Mesoproterozoic metamorphism has been documented from various exposed parts of the Maud Belt. A SHRIMP U-Pb age of 1061±14 Ma from 300 km long megacrystic augen gneiss is recorded in the northeastern Maud Belt (Harris et al., 1995). Similar metamorphic zircon ages from anatectic leucosome and metamorphic zircon overgrowths indicate high-grade metamorphism that occurred between 1060 and 1030 Ma in the Central Kirwanveggen (Jackson, 1999) and H.U. Sverdrupfjella (Board et al., 2005). Although Arndt et al. (1991) reported a metamorphic U-Pb zircon age of 1104±5 Ma; high-grade Grenville-age metamorphism in the southeastern Heimefrontfjella area has more recently been bracketed between c.1090 and 1060 Ma (Jacobs et al., 2003). The older age is therefore interpreted as derived from an inherited zircon and most likely dates an earlier large-scale thermal event on the Kaapvaal Craton (Hanson et al., 1998; 2004). A similar U-Pb age of 1098±5 Ma from leucosome material has also been reported from the Northern Kirwanveggen (Harris et al., 1995).

The extent of Pan-African tectonic overprinting in the belt has been a contentious issue, with some workers suggesting a mainly thermal overprint (Grantham et al., 1995; Groenewald et al., 1995, Jackson, 1999) and others a tectono-thermal overprint (Jacobs et al., 1995; Board et al., 2005). In particular, U-Pb ages of c.540 Ma from syn-tectonic monazite inclusions within metamorphic minerals that define a penetrative top-to-the-northwest shear fabric in the H.U. Sverdrupfjella provided strong support for a tectono-thermal Pan-African overprint (Board et al., 2005). This shear fabric developed under upper amphibolites-facies conditions (M_{2b}) that followed decompression from eclogite-facies (M_{2a}) conditions (Board et al., 2005). Although the age of this eclogite-facies metamorphism is not resolved, an early Pan-African age is preferred because of rare U-Pb zircon overgrowth ages around 565 Ma (Board et al., 2005).

Two pulses of high-grade Pan-African tectonism have also been reported from the Gjelsvikfjella (Bisnath et al., in review) and central Dronning Maud Land (Jacobs et al., 2003) further to the northeast between c. 580-560 Ma and 530-510 Ma. In central Dronning Maud Land, the second pulse was associated with a phase of syn- to post-tectonic mafic magmatism during orogenic collapse (Jacobs et al., 2003). In the Kirwanveggen, the intensity and extent of deforma-

tion and metamorphism contributed by 'late-Grenvillian' and Pan-African tectonothermal episodes has proven to be difficult to differentiate due to co-planar and co-linear superposition of structural elements (i.e. southeast plunging kinematic indicators), and the lack of Pan-African magmatism in that area (Grantham et al., 1995; Jackson, 1999). In the amphibolite facies Sivorg Terrane, east of an extensive Pan-African shear zone (known as the Heimefront Shear Zone or HSZ) in the Heimefrontfjella, metamorphic zircon overgrowths also indicate a ~500 Ma tectonothermal overprint (Jacobs et al., 2003). The extent of Pan-African tectonothermal overprinting of Mesoproterozoic reworked volcanic arc crust apparently increases towards the northeast (e.g. Jacobs et al., 1998; Jacobs et al., 2002; Paulsson & Austrheim, 2003), which has lead to Cambrian migmatization and the more common occurrence of post-tectonic (<510 Ma) mafic and felsic intrusions (e.g. granitoids, gabbros, syenites, aplite dykes) in the northeastern areas of the belt (Harris et al., 1995; Mikhalsky et al., 1997; Jacobs et al., 2003; Paulsson and Austrheim, 2003; Bisnath et al., in review).

The recognition and timing of Pan-African tectonism in the Maud Belt and other related areas of East Antarctica (Zhao et al., 1992; Shiraishi et al., 1992; Dirks et al., 1993; Jacobs et al., 1996, 1998; Fitzsimons et al., 1997) has supported the concept of continuation of the East African Orogen into East Antarctica (e.g. Pinna et al., 1993; Jacobs et al., 1998). Jacobs et al. (1995, 1996, 1999) interpreted the Pan-African Heimefront Shear Zone (HSZ) in the Heimefrontfjella to represent the continuation of the Mozambique Belt into East Antarctica, but only as the western front to the East African Orogen in their Gondwana reconstruction (Fig. 2). The suture between East and West Gondwana is generally considered to be contained within the East African Orogen and is attributed to the closure of the Mozambique Ocean between ~700 and 600 Ma (e. g. Grunow et al., 1996; Shackleton, 1996; Fitzsimons, 2000a, 2000b; Nedelec et al., 2000; Boger et al., 2001). However, the exact location of this suture in both the East African Orogen and East Antarctica remains problematic.

Three Mesozoic alkaline intrusions occur in the Maud Belt east of the Jutulstraumen Glacier (Fig. 1). These include the Straumsvola, Tvora and Sistefjell syenite intrusions (e.g. Harris and Grantham, 1993; Harris et al., 2002) and are believed to record rift-related magmatism related to the break-up of Gondwana (e.g. Grantham and Hunter, 1991; Harris and Grantham, 1993).

3. METAMORPHIC HISTORY OF THE MAUD BELT

Groenewald et al. (1995) proposed a westward decreasing Grenville-age metamorphic field gradient in the H.U. Sverdrupfjella with granulite facies rocks in an eastern domain thrust over an amphibolite facies domain in the west that developed during collision and accretion of the Maud Belt as a former oceanic island arc to the southeastern margin of the Kaapvaal-Grunehogna Craton. Temperature and pressure estimates of ~12±2 and 675-750°C for the eastern part were obtained from an early inferred M_1 mafic assemblage consisting of Grt + Cpx + Pl + Qtz (Grantham et al., 1995), with only the pressure estimate being in agreement with the proposed M_1 eclogite facies assemblage of Groenewald et al. (1995). Subsequent decompression during thrust-related uplift and partial hydration was suggested, leading to the development of the mineral assemblage Cpx + Hbl + Grt + Pl + Qtz (M_2) for which P-T constraints of 7-9.5 kbar and 600-700°C were obtained (Grantham et al., 1995). This temperature estimate for M_2 is much lower than that proposed by Groenewald et al. (1995) and Groenewald & Hunter (1991) who suggested decompression during thermal relaxation to granulite facies conditions (8-10 kbar, 850°C). These discrepancies most likely reflect uncertainty regarding the timing of metamorphic and deformation events in that area. In contrast to the above authors, Board et al. (2005) identified pervasive fabric development and upper amphibolite facies metamorphism (M_{2b}) in the eastern Sverdrupfjella as being Pan-African (c. 540 Ma) in age based on U-Pb isotope data from syn-tectonic monazite inclusions in the metamorphic minerals defining a penetrative S_2 fabric and from U-Pb zircon ages. These recent data imply a Pan-African age for the major top-to-northwest thrusting. Although not dated by geochronological means, an early Pan-African age is also inferred for a garnet-omphacite M_{2a} eclogite facies assemblage, due to evidence for an earlier Pan-African pulse at c. 565 Ma from U-Pb zircon overgrowth ages (Board et al., 2005).

Hornblende-plagioclase geothermometry applied to metabasites that contain retrograde decompression-related hornblende-plagioclase symplectite surrounding garnet and clinopyroxene has been shown to be more reliable and consistent than garnet-hornblende geothermometry (Board et al., 2005). Temperature estimates from garnet-hornblende thermometry are variable, indicating that Fe-Mg exchange between garnet and amphibole did not achieve equilibrium. Previous

constraints on peak metamorphic temperatures from 'eastern' and 'western' domains (Grantham et al. 1995) using this geothermometer are, therefore, problematic as the garnet and amphibole belong to two separate metamorphic assemblages (M_1 and M_2, respectively) and most likely did not attain chemical equilibrium. Metamorphic temperature constraints on the M_1 garnet-clinopyroxene assemblage are also doubtful as they were derived from garnet and clinopyroxene separated by retrograde symplectite, and most likely reflect diffusional resetting during Pan-African M_{2b} conditions.

A lower pressure limit of ~3 kbar is derived for the proposed western domain using clinopyroxene-plagioclase-quartz geobarometry (Grantham et al., 1995). The same geobarometer is also used in constraining a pressure for M_1 and M_2/M_3 conditions in the eastern domain. Difficulty in obtaining accurate analyses of Na_2O in clinopyroxene is known to be a problematic aspect in the application of clinopyroxene-plagioclase-quartz geobarometry. Order-disorder transitions in both clinopyroxene and albite and the limited activity-composition data for the calcic-sodic pyroxenes are other problematic factors (Carswell & Harley, 1989). Grantham et al., (1995) noted that clinopyroxene and plagioclase compositions from two of their samples yielded unrealistic pressure estimates. Board et al. (2005) considered all the plagioclase in textural equilibrium with the clinopyroxene as being secondary, due to petrographic evidence for decompression from the surrounding hornblende-plagioclase symplectite. Decompression from M_{2a} eclogite facies to M_{2b} upper amphibolite facies conditions resulted in the decomposition of omphacitic clinopyroxene and the net transfer of jadeite and Ca-tschermakite components to albite and anorthite, respectively, in the secondary symplectitic plagioclase. On this basis, the lower pressure limit of 3 kbar for the western domain is also unreliable.

A closer inspection of the Grantham et al. (1995) P-T data allows a distinction to be made between their M_2/M_3 metamorphism. Pressure estimates derived from garnet-rutile-ilmenite-plagioclase-quartz geothermometry (referred to as GRIPS by Grantham et al., 1995) for both eastern and western domains of ~7-8 kbar, are identical to later Pan-African M_{2c} conditions described by Board et al. (2005) in the southeastern H.U. Sverdrupfjella (derived from metapelitic rocks), suggesting that the plagioclase compositions in the metabasites used by these authors were reset during late Pan-African metamorphism. Garnet-hornblende-plagioclase-quartz geo-

barometry, on the other hand, yields a more reliable pressure constraint of ~9 kar, consistent with the lower pressure estimate (9.2 kbar) for M_{2b} in Board's study. If the interpretation of Board et al. (2005) is correct, the granulite facies mineral assemblage (i.e. M_1) described by Groenewald & Hunter (1991) might be the only preserved relict of earlier, Grenvillian high-grade metamorphism in the H.U. Sverdrupfjella area, apart from geochronological evidence of leucosome formation around 1035 Ma.

4. LOCAL GEOLOGY

Samples for this study were taken from two localities directly on either side of the Pencksökket-Jutulstraumen glacial valley, namely at Nashornkalvane South on the eastern margin of Grunehogna Craton and at Straumsvola in the western part of the Maud Belt (Fig. 1 and Fig. 3).

4.1 Nashornkalvane

Nashornkalvane comprises two nunataks, namely, Nashornkalvane North and South. Both nunataks are exposures of the Ahlmannryggen Group, the southern of which is host to a large, 50-120 m thick, mafic sill of the Borgmassivet Suite. At Nashornkalvane South the bedding planes dip at a significantly steeper angle of ~ 25° SE, as opposed to the general sub-horizontal attitude further west from the discontinuity. The succession consists predominantly of brown-grey, massive thickly bedded siltstone interlayered with thin beds of shale, greywacke and pale yellow felsic tuff.

Field observations are consistent with a regressive marine depositional environment (Ferreira, 1988). Symmetrical bifurcating ripple marks found on the eastern side of Nashalkalvane North indicate a shallow marine to tidal flat environment. Rounded globule-like structures observed in thin mudstone layers represent intraformational, clay pebble conglomerates (Ferreira, 1988). Well preserved cross bedding at Nashalkalvane South indicates changes to a more fluvial dominated depositional environment. In outcrop, the mafic sill at the southern nunatak appears dioritic to gabbroic in composition. On the hand specimen scale, the green colouration points to possible greenschist facies metamorphism.

4.2 Straumsvola

Metabasic boudins were sampled from a unit mapped as Banded Gneiss Complex of the Jutulrora Formation (Grantham et al., 1988) at the southern end of the Straumsvola nunatak (Fig. 3 and Fig. 4). The gneiss complex comprises regularly alternating dark amphibolite and felsic layers, which define a strong planar fabric and form the host rock to the Straumsvola nepheline syenite complex (Harris & Grantham, 1993). The Straumsvola alkaline pluton, together with the nearby quartz syenite Tvora complex intruded the gneisses at around 170-180 Ma during Gond-

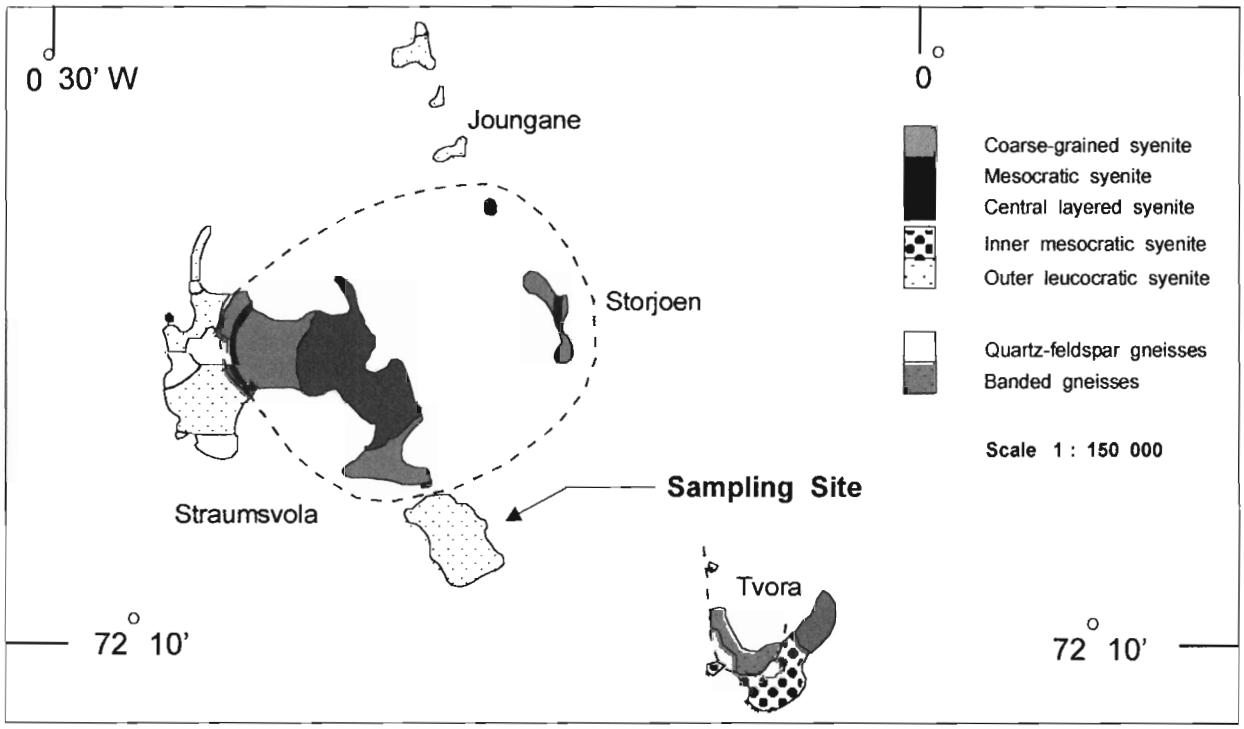

Fig. 3. Geological map of the Straumsvola nunatak (Harris & Grantham, 1993) showing the sampling site with the Straumsvola and Tvora alkaline complexes also shown.

wana break-up (Grantham et al., 1988; Harris & Grantham, 1993). Oxygen isotope data indicated that extensive fluid alteration (fenitization) of the country rock and the development of a hydrothermal system around the pluton was not achieved (Harris & Grantham, 1993).

The orientation of the large, up to 8 m thick, mafic boudins in the country rock is parallel to the foliation throughout the area with the thickness of the gneissic layers ranging from centimeters to metres (Fig. 4). Thinner, centimeter-scale layers commonly display ptygmatic folds. The general appearance of the boudins in outcrop suggests that they may represent thick mafic sills that intruded into a volcano-sedimentary succession before deformation. In places, mafic boudins display an outer well-foliated zone that surrounds a more resistant, less strained, core. Some amphibolite boudins are garnet-rich, while others are devoid of garnet. High-grade metamorphism generated anatectic leucosomes comprising alkali and plagioclase feldspar, quartz and large sheets of biotite, which appear in both, the country rock and in the cores of boudins. Abundant quartzofeldspathic veins and pegmatite post-date folding and foliation in the area and

cut across the mafic boudins with xenoliths of amphibolitic country rock present in the larger pegmatitic dykes.

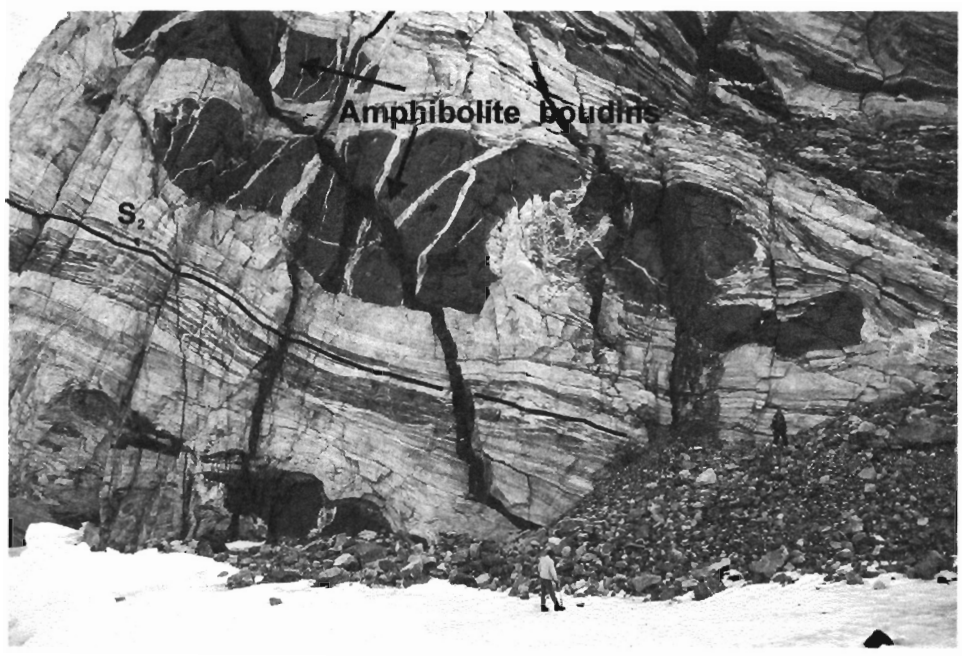

Fig. 4. Outcrop south of the Straumsvola syenite complex displaying the Jutulrora Banded Gneiss Complex with amphibolitic boudins. The boudins are syn-tectonic with respect to the regional S_2 fabric. Post-tectonic mafic dykes are related to the nearby syenite complex.

Numerous, mostly near vertical, melanocratic dykes were found to truncate the folds, boudins and pegmatite dykes. These dykes are probably similar in age with a similar compositional range to those cross-cutting the neighbouring Straumsvola complex for which a Mesozoic age has been established (Harris & Grantham, 1993). As field evidence points to pre- and post-syenite emplacement for the dykes, the approximate parallel orientation (north-south) of the dykes with the Jutulstraumen glacier is interpreted to indicate the continuation of rift-related extension after intrusion of the Straumsvola pluton (Harris & Grantham, 1993).

5. PETROGRAPHY

5.1 Nashornkalvane

Petrographic examination of the Borgmassivet Suite samples from Nashornkalvane revealed the presence of actinolite, chlorite, epidote, albite and quartz. These metamorphic minerals are randomly scattered throughout individual thin sections with their occurrence restricted to local domains between dominant relic igneous phases. The mafic rocks appear unstrained with no preferred orientation of any mineral developed.

In many cases, most of the thin section consists of corroded clinopyroxene (augite) grains and highly sericitized plagioclase (Fig. 5a). Clinopyroxene is uralitized to fine actinolite and/or chlorite along grain boundaries. The fine dusting on the plagioclase consists of white mica. Minor ilmenite is typically replaced by metamorphic sphene and/or rutile. The sphene exists as a reaction rim around ilmenite, as triangular shaped crystals with an opaque core, or as larger skeletal-shaped pseudomorphs after poikilitic-skeletal ilmenite crystals. The type and proportion of metamorphic minerals present in the greenschist microdomains vary considerably. All the minerals defining the metamorphic domains are very fine-grained and usually occur as mono-, bi-, or tri-mineralic assemblages. Chlorite is usually the most abundant phase. Figure 5 (c) , for example, illustrates textural equilibrium between chlorite, actinolite, epidote and quartz, whereas in places only actinolite exists as pseudomorphs after clinopyroxene. In most places chlorite and actinolite may be found in textural equilibrium within microdomains varying between 4 and 140 mm^2 in area.

Actinolite is commonly found as small needles fringing relic augite grains. Long, fibrous needles are also found scattered randomly or concentrated in zones associated with other metamorphic minerals (Fig. 5b, c, e). In some domains, the dominant actinolite habit was found to be minute blades occurring in aggregates within chlorite-rich domains rather than existing as fine-grained nematoblasts (Fig. 5d). A third morphological type manifests itself where clinopyroxene is completely replaced and the resulting actinolite pseudomorph exists as an independent grain with well formed crystal faces. In this case, the actinolite occurs as larger, elongated prismatic crystals. In some of the grains, well-developed cleavage can clearly be observed. Light

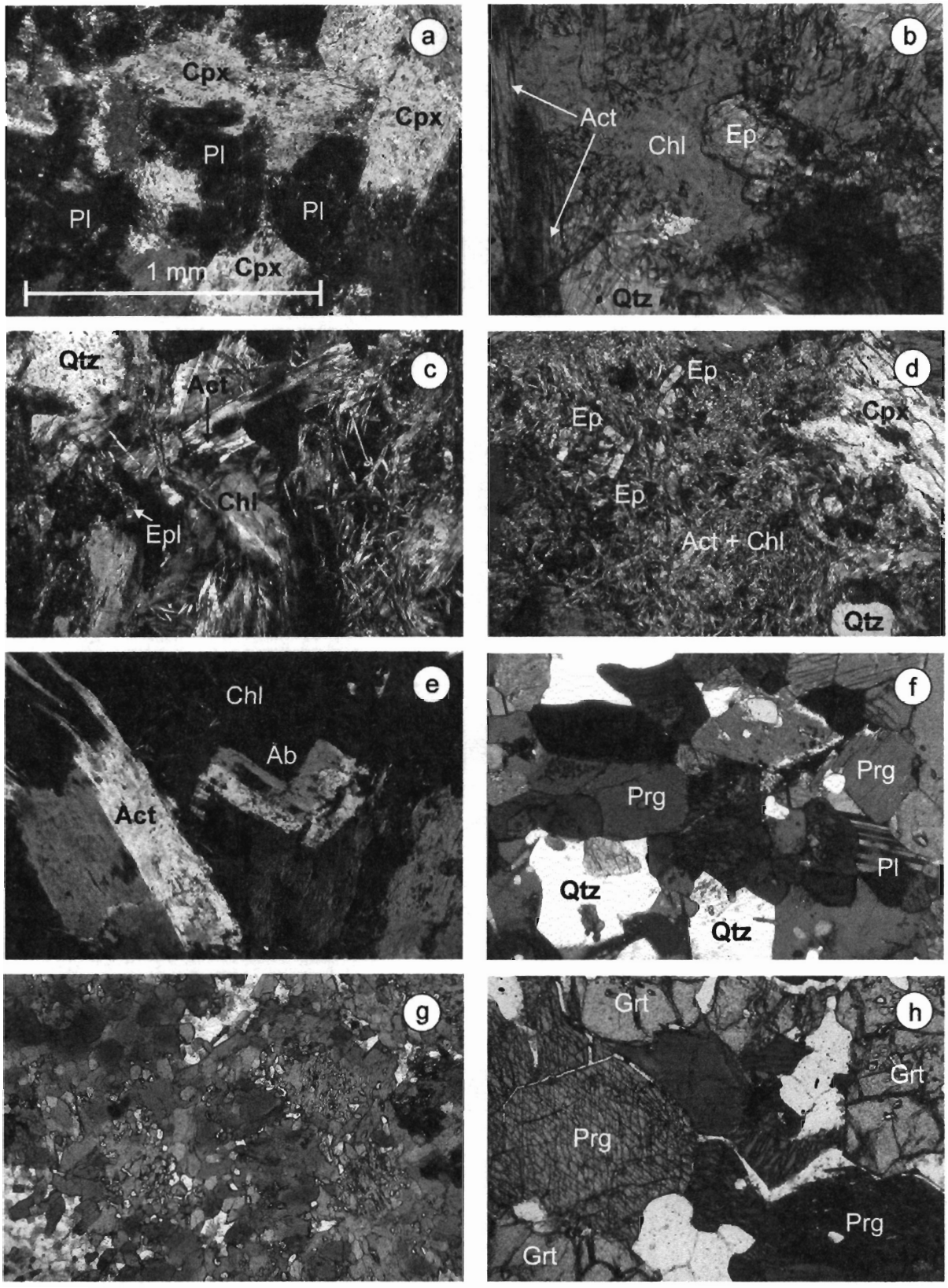
a
Cpx
Cpx
Pl
Pl
Pl
1 mm
Cpx
b
Act
Chl
Ep
Qtz
c
Qtz
Act
Chl
Epl
d
Ep
Ep
Ep
Cpx
Act + Chl
Qtz
e
Chl
Ab
Act
f
Prg
Prg
Pl
Qtz
Qtz
g
h
Grt
Grt
Prg
Prg
Grt

Fig. 5 Photomicrographs of metabasic rocks from Nashalkalvane, (a-e), and Straumsvola, (f-h), all in cross-polarized light, except (h) taken in plane-polarized light. Field of view =1.5mm. (a) Relic clinopyroxene and plagioclase outside metamorphic domains (sample EG-N3). (b) Large metamorphic microdomain in sample EG-N2 showing partial replacement of clinopyroxene along rim by actinolitic nematoblasts, with chlorite and a euhedral, crystal of epidote. (c) Smaller microdomain similar to (b) showing quartz, chlorite, actinolite and epidote (EG-14a). (d) Finer-grained aggregate of chlorite, actinolite and epidote with quartz (EG-14c). (e) Domain showing albite (after plagioclase), actinolite (after clinopyroxene) with chlorite (EG-N2). (f) Amphibole + plagioclase + quartz assemblage in textural equilibrium (EG-021b) typical of the Straumsvola amphibolites. (g) Recrystallized texture due to second generation amphibole (EG-028). (h) Poikiloblastic garnet in garnet amphibolite (EG-016).

green chlorite is present as abundant aggregates surrounding the other metamorphic minerals, such as quartz, actinolite and epidote (Fig. 5(b-e)). It also exists around clinopyroxene relics where it is associated with actinolite. Its low, anomalous blue interference colour indicates an Fe-rich composition. Higher birefringence mixed-layer chlorite/smectite was not observed.

Epidote/clinozoisite is present as granular aggregates (i.e intergrowths of two or more crystals), six-sided sections or as long prismatic crystals (Fig. 5(b-d)). Crystal size varies considerably. Grains (and aggregates) of various sizes generally tend to cluster in groups but can also occur isolated. Many of the crystals display compositional zoning.

The scattered occurrence and restriction of the metamorphic minerals to microdomains may possibly reflect a lack of pervasive fluid infiltration, which appears to have limited their growth. This fluid phase most probably had a composition with a low CO_2 partial pressure as no carbonate phases were observed.

5.2 Straumsvola

Amphibolite samples were collected from mafic boudins within the banded gneiss country rock to the nearby Straumsvola syenite complex. In contrast to the Nashornkalvane metabasites, igneous textures of the Straumsvola mafic protolith(s) have been completely obliterated due to high-grade metamorphism. Typically, the amphibolite consists of syn-kinematic green-brown amphibole, plagioclase and quartz with accessory metamorphic sphene and/or rutile replacing relict ilmenite (Fig. 5f). Randomly oriented, post-kinematic biotite is present as a minor phase

in variable amounts. Textural evidence for recrystallization of pre-existing amphibole is indicated in some of the samples that were collected from less hydrated, strain- protected cores of boudins. In these domains, former, relatively coarse-grained amphibole grains recrystallized to a second generation of smaller, subhedral amphibole grains (Fig. 5g). Towards the boudin margins, the second-generation amphibole is progressively more aligned and coarser-grained. This indicates that the fabric-defining amphibole belongs to the second generation, with evidence of a previous amphibolite-facies metamorphic event only preserved in strain-protected, less hydrated and equilibrated cores of larger boudins. Particularly well foliated amphibolite tends to show a higher degree of saussuritisation and partial replacement of amphibole by biotite. Most of the amphibolite is garnet-free, but rarely a garnet-bearing variety occurs as well (Fig. 5h).

6. MINERAL CHEMISTRY

Mineral compositions were measured using a Cameca CAMEBAX electron microprobe at the University of Cape Town. Representative mineral compositions are listed in Tables 1-6 (for entire data set see Appendix 3). Mineral abbreviations are after Kretz (1983) and Bucher & Frey (1994). Five representative polished sections from the Nashornkalvane and nine from the Straumsvola localities were selected. The analyses were carried out using an accelerating potential of 15 kV and a beam current of 40 nA. All minerals were analyzed with an electron beam diameter of about 10 μm, except for feldspar (~ 30-40 μm). Natural mineral standards were used for calibration. Typical detection limits at 1-sigma of background for element oxides were (in wt%): SiO_2, 0.2; Na_2O, 0.1; K_2O, 0.01; Al_2O_3, 0.2; FeO, 0.3; MnO, 0.03; MgO, 0.1; TiO_2, 0.02; CaO, 0.1. Data were reduced using a Cameca PAP correction (Pouchou & Pichoir, 1984).

6.1 Nashornkalvane

For the Nashornkalvane metabasites at least 15 chlorite grains from each of five samples were analyzed (Table 1). The x-parameter, or proportion of chlorite content in the phyllosilicate structure, was obtained from the sum of the non-interlayer cations and extrapolation between the pure chlorite end-member (for clinochlore, x = 1) and smectite end-member (for saponite, x = 0) according to the method of Schiffman & Fridleifsson (1991). Chlorite compositions are close to that of ideal tri,trioctahedral chlorite (Fig. 6 and 7). All of the metamorphic amphibole grains straddle the boundary between actinolite and ferro-actinolite (after Leake et al., 1997) plotting within a narrow X_{Mg} range of between 0.49-0.59 (Table 2). Actinolite compositions within some of the metabasites samples are homogeneous, whereas others display variable Si content per formula unit for a relatively constant X_{Mg} ratio (Fig. 8). Actinolite compositions appear to differ depending on actinolite crystal habit/morphology. Fine-grained actinolite needles found along clinopyroxene grain boundaries have a higher Si content for a given X_{Mg} compared to discrete, lath-shaped pseudomorphs of actinolite formed after complete clinopyroxene replacement.

Ten analyses from a large metamorphic domain in sample EG-14c revealed a significant variation in epidote composition between the clinozoisite and epidote end-members (Table 3). Epi-

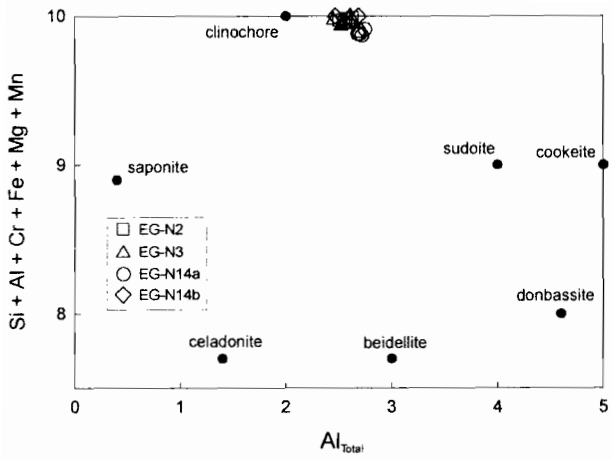

Fig. 6. Non-interlayer cations versus Al_{Total} indicating chlorite compositions. End-member compositions (filled circles) after Robinson et al. (1993).

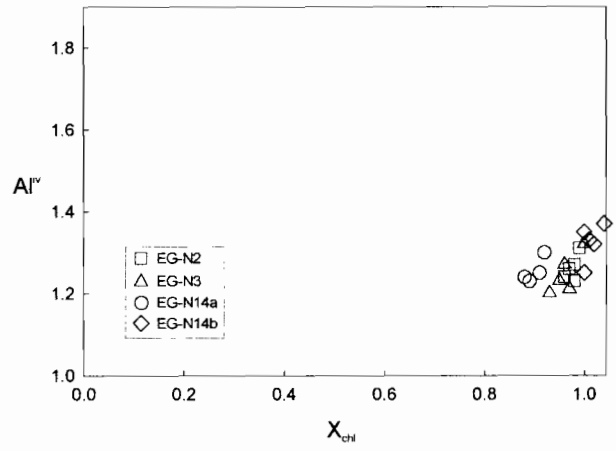

Fig. 7. Tetrahedral Al versus trioctahedral chlorite content (x) for selected samples.

dote analyses yielded X_{Fe3+} values between 0.12 and 0.28. This compositional spread is independent of the domain size. The feldspar in metamorphic microdomains is albite. Where present, it has a restricted composition of 98-95 mol% Ab (Fig. 10).

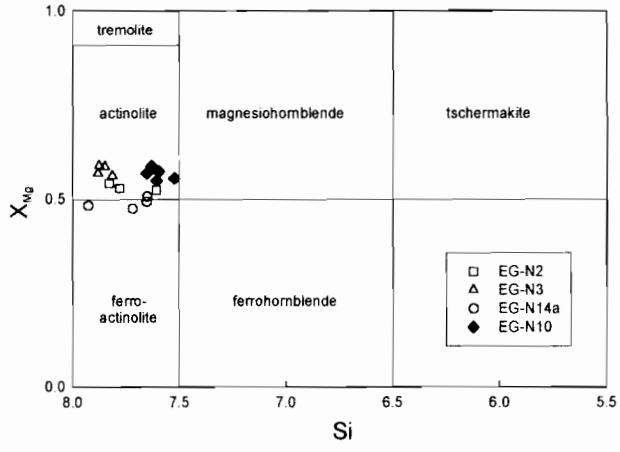

Fig. 8. Amphibole compositions in Nashalkalvane metabasites classified after Leake et al. (1997).

6.2 Straumsvola

The amount of Fe^{3+} in amphibole was estimated using the method of Leake et al. (1997) on the basis of 23 O. In all cases, normalization on an all-ferrous assumption assigns the majority of the amphiboles to the ferropargasite compositional field (Table 5; Fig. 9). Recalculation assuming the maximum amount of Fe^{3+} with the formula based on 13 cations excluding K, Na and Ca, forces amphibole compositions in samples EG-024, EG-031, EG-028 and EG-016 into the

pargasite compositional field. On an all-ferrous assumption, the amphibole data plotted for these samples appear to overlap and cluster tightly near the top left corner of the ferropargasite field. Most grains are compositionally homogeneous. Second generation, recrystallized amphibole displays the highest variation in Si composition, for the same X_{Mg} (Fig. 9, inset B).

Plagioclase compositions range between An_{40} and An_{25} (Table 6; Fig. 10). Plagioclase compositions in the recrystallized sample, EG-028, shows the greatest compositional variability (Fig. 10). Samples with plagioclase compositions between An_{40} and An_{29} are associated with a slightly more edenitic variety of amphibole, reflecting variations in Si and Mg content in the mafic precursor rocks. The garnet in sample EG-016 is predominantly almandine but with a significant grossular component ($Py_{11}Alm_{55}Spess_2Gro_{28}$, Table 4).

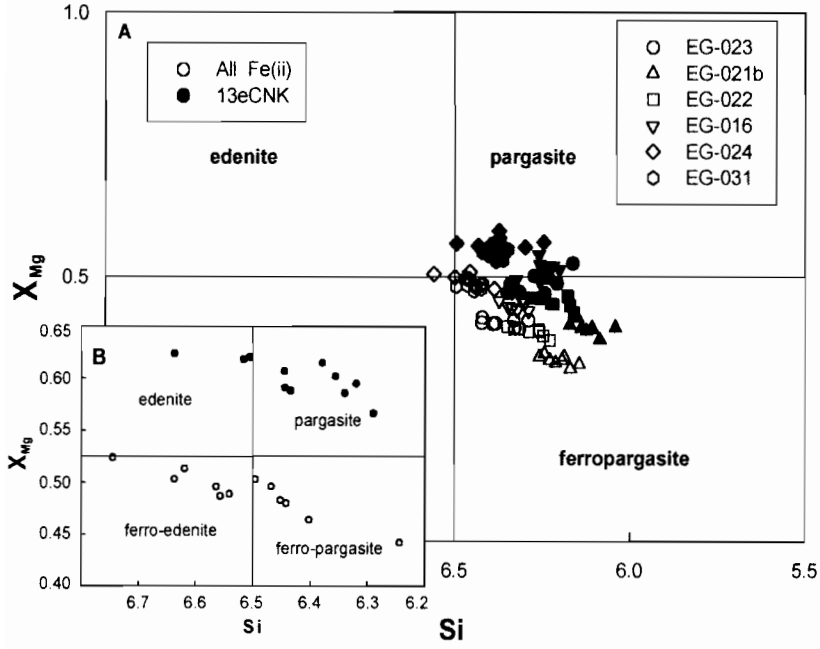

Fig. 9. Amphibole compositions in selected Straumsvola metabasites classified after Leake et al. (1997). Recrystallized amphibole displays the highest variation in Si, but similar X_{Mg} (Inset B). Open symbols: all Fe = Fe^{2+}, black symbols: maximum Fe^{3+} estimation.

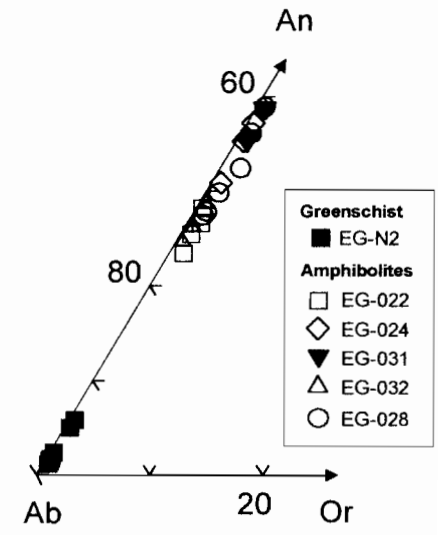

Fig. 10. Plagioclase compositions for Nashalkalvane and Straumsvola metabasites. Feldspar in metamorphic domains of Nashalkalvane metabasite is albite.

Table 1. Representative electron microprobe analyses of chlorite in the Nashornkalvane metabasites

	EGN2(1)	EGN2(11)	EGN2(7)	EGN2(5)	EGN2(8)	EGN3(12)	EGN3(16)	EGN3(2)	EGN3(1)	EGN3(3)
SiO_2	25.38	24.84	25.88	25.70	26.00	26.73	26.29	26.00	25.46	26.57
TiO_2	0.02	0.01	0.00	0.04	0.01	0.00	0.04	0.02	0.02	0.02
Al_2O_3	21.04	20.20	20.56	20.50	20.40	20.42	20.53	21.08	21.05	19.77
FeO	30.36	29.71	30.40	29.76	29.88	28.39	29.34	29.40	28.61	29.60
MnO	0.39	0.41	0.47	0.45	0.39	0.47	0.39	0.39	0.38	0.44
MgO	12.33	13.15	12.10	12.53	12.45	13.21	12.75	12.75	13.68	13.28
CaO	0.02	0.00	0.05	0.02	0.03	0.05	0.05	0.00	0.01	0.02
Na_2O	0.02	0.05	0.00	0.00	0.08	0.00	0.03	0.05	0.04	0.05
K_2O	0.00	0.00	0.01	0.02	0.01	0.00	0.00	0.01	0.01	0.01
Total	89.55	88.37	89.48	89.00	89.25	89.25	89.43	89.70	89.26	89.76
Si	2.69	2.67	2.74	2.73	2.76	2.80	2.77	2.73	2.68	2.79
Al^{+4}	1.31	1.33	1.26	1.27	1.24	1.20	1.23	1.27	1.32	1.21
T site	4.00	4.00	4.00	4.00	4.00	4.00	4.00	4.00	4.00	4.00
Al^{+6}	1.32	1.23	1.31	1.30	1.31	1.33	1.32	1.34	1.30	1.24
Fe^{+3}	0.00	0.00	0.00	0.00	0.00	0.00	0.00	0.00	0.00	0.00
Ti	0.00	0.00	0.00	0.00	0.00	0.00	0.00	0.00	0.00	0.00
Mg	1.95	2.11	1.91	1.99	1.97	2.07	2.00	2.00	2.15	2.08
Fe^{+2}	2.69	2.67	2.70	2.65	2.65	2.49	2.58	2.58	2.52	2.60
Mn	0.04	0.04	0.04	0.04	0.04	0.04	0.03	0.03	0.03	0.04
Ca	0.00	0.00	0.01	0.00	0.00	0.01	0.01	0.00	0.00	0.00
Na	0.00	0.01	0.00	0.00	0.02	0.00	0.01	0.01	0.01	0.01
K	0.00	0.00	0.00	0.00	0.00	0.00	0.00	0.00	0.00	0.00
O site	6.00	6.05	5.97	5.98	5.98	5.93	5.96	5.97	6.01	5.98
X_{Fe}	0.58	0.56	0.58	0.57	0.57	0.55	0.56	0.56	0.54	0.56
x	0.99	1.04	0.97	0.98	0.96	0.93	0.95	0.96	1.00	0.97
(T^oC)										
Z & F	273	279	261	265	260	252	258	266	279	253
C	360	366	342	346	339	323	334	347	362	326
C & N	296	300	284	287	282	272	279	287	297	274
K & Mc	200	200	194	195	192	185	190	194	198	187

	EG14a(11)	EG14a(9)	EG14a(14)	EG14a(6)	EG14a(7)	EG14b(15)	EG14b(13)	EG14b(6)	EG14b(8)	EG14b(5)
SiO_2	26.10	25.99	25.26	25.82	26.23	25.05	24.81	24.85	24.99	25.81
TiO_2	0.06	0.02	0.02	0.02	0.02	0.04	0.01	0.02	0.04	0.04
Al_2O_3	21.42	21.55	21.84	21.53	21.70	20.79	21.09	21.36	20.41	19.68
FeO	30.16	29.77	29.63	29.84	29.92	30.79	30.51	30.92	30.81	29.93
MnO	0.40	0.45	0.46	0.47	0.43	0.44	0.48	0.47	0.49	0.46
MgO	10.79	11.35	11.05	10.49	11.08	12.30	12.72	11.65	12.20	13.04
CaO	0.04	0.04	0.03	0.05	0.03	0.07	0.02	0.06	0.03	0.06
Na_2O	0.01	0.04	0.04	0.04	0.03	0.00	0.01	0.00	0.02	0.00
K_2O	0.01	0.02	0.01	0.00	0.01	0.01	0.00	0.00	0.00	0.00
Total	88.97	89.21	88.34	88.25	89.45	89.48	89.65	89.32	89.00	89.01
Si	2.77	2.75	2.70	2.76	2.77	2.67	2.63	2.65	2.68	2.75
Al^{+4}	1.23	1.25	1.30	1.24	1.23	1.33	1.37	1.35	1.32	1.25
T site	4.00	4.00	4.00	4.00	4.00	4.00	4.00	4.00	4.00	4.00
Al^{+6}	1.45	1.43	1.46	1.48	1.46	1.28	1.27	1.34	1.26	1.22
Fe^{+3}	0.00	0.00	0.00	0.00	0.00	0.00	0.00	0.00	0.00	0.00
Ti	0.00	0.00	0.00	0.00	0.00	0.00	0.00	0.00	0.00	0.00
Mg	1.71	1.79	1.76	1.67	1.74	1.95	2.01	1.85	1.95	2.07
Fe^{+2}	2.68	2.63	2.65	2.67	2.64	2.74	2.71	2.76	2.76	2.67
Mn	0.04	0.04	0.04	0.04	0.04	0.04	0.04	0.04	0.04	0.04
Ca	0.00	0.00	0.00	0.01	0.00	0.01	0.00	0.01	0.00	0.01
Na	0.00	0.01	0.01	0.01	0.01	0.00	0.00	0.00	0.00	0.00
K	0.00	0.00	0.00	0.00	0.00	0.00	0.00	0.00	0.00	0.00
O site	5.88	5.91	5.92	5.88	5.89	6.02	6.05	6.00	6.03	6.01
X_{Fe}	0.61	0.60	0.60	0.61	0.60	0.58	0.57	0.60	0.59	0.56
x	0.89	0.91	0.92	0.88	0.89	1.01	1.04	1.00	1.02	1.00
(T^oC)										
Z & F	253	259	269	254	255	278	286	280	275	262
C	334	341	356	336	336	367	378	372	363	341
C & N	278	283	293	280	280	300	307	304	298	283
K & Mc	194	195	200	195	194	203	205	205	201	192

Spot number for individual analysis is shown in parentheses after the sample name. All analysis recalculated on the basis chlorite structural formula with normalization based on 14 O. Note: all Fe expressed as FeO. X_{Fe} = Fe/(Fe + Mg) calculated on a molecular proportions basis. x = estimate of the proportion of trioctahedral chlorite (x = 1) relative to saponite component (x = 0). Z & F = Zang and Fyfe (1995) chlorite thermometer. C = Cathelineau (1988) chlorite themometer. C & N = Cathelineau and Nieva (1985) thermometer. K & Mc = Kranidiotis and MacLean (1987) thermometer

Table 2. Representative electron microprobe analyses of actinolite for Nashornkalvane metabasites.

Sample	EG-N14b(7)	EG-N2(3)	EG-N3(8)	EG-N14a(3)	EGN-10(5)
SiO_2	50.58	51.63	54.56	51.88	52.34
TiO_2	0.07	0.05	0.01	0.04	0.09
Al_2O_3	4.42	4.40	2.63	4.13	2.97
Fe_2O_3	0.00	0.00	0.00	0.00	0.00
FeO*	18.53	18.02	15.84	18.66	16.72
MnO	0.38	0.40	0.26	0.35	0.34
MgO	11.64	11.13	12.65	10.24	13.13
CaO	12.61	11.73	12.59	12.59	12.83
Na_2O	0.41	0.30	0.23	0.58	0.26
K_2O	0.10	0.18	0.12	0.10	0.11
Total	98.73	97.83	98.88	98.56	98.79
Si	7.45	7.61	7.85	7.63	7.62
Al^{+4}	0.55	0.39	0.15	0.37	0.38
T site	8.00	8.00	8.00	8.00	8.00
Al^{+6}	0.21	0.37	0.29	0.35	0.13
Fe^{+3}	0.00	0.00	0.00	0.00	0.00
Ti	0.01	0.01	0.00	0.00	0.01
Mg	2.56	2.45	2.71	2.24	2.85
Fe^{+2}	2.22	2.18	1.90	2.29	1.97
Mn	0.00	0.00	0.03	0.04	0.04
M1,2,3	5.00	5.00	4.94	4.93	5.00
Fe^{+2}	0.06	0.04	0.00	0.00	0.07
Mn	0.05	0.05	0.00	0.00	0.00
Ca	1.99	1.85	1.94	1.98	2.00
Na	0.00	0.00	0.06	0.02	0.00
M4	2.09	1.95	2.00	2.00	2.07
Ca	0.00	0.00	0.00	0.00	0.00
Na	0.12	0.09	0.00	0.15	0.07
K	0.02	0.03	0.02	0.02	0.02
A site	0.14	0.12	0.03	0.17	0.10
Total	15.23	15.06	14.97	15.10	15.16

*All Fe calculated as FeO.
Calculation of formula based on 23 O. Number for individual analysis shown in parentheses.

Table 3. Selected electron micrprobe analyses of epidote in samples EG-N14(c) and EG-N2 (Nashornkalvane)

Sample	EG-N14(c)							EG-N2						
SiO_2	36.85	37.51	38.26	38.38	37.72	37.44	38.22	41.24	36.67	37.13	39.11	38.77	38.18	37.07
TiO_2	0.03	0.04	0.03	0.02	0.07	0.02	0.11	0.04	0.03	0.00	0.00	0.00	0.00	0.00
Al_2O_3	22.84	28.83	29.79	29.45	28.66	24.91	29.53	24.46	24.11	25.55	29.63	28.78	29.01	23.71
Fe_2O_3	13.57	7.45	6.47	6.46	6.60	11.56	6.16	9.10	12.44	11.18	5.44	6.27	5.72	12.32
FeO	0.00	0.00	0.00	0.00	0.00	0.00	0.00	0.00	0.00	0.00	0.00	0.00	0.00	0.00
MnO	0.03	0.05	0.11	0.08	0.06	0.06	0.09	0.15	0.05	0.02	0.00	0.00	0.00	0.00
MgO	0.01	0.00	0.04	0.03	0.00	0.03	0.02	2.69	0.03	0.00	0.02	0.02	0.01	0.00
CaO	24.03	24.44	24.42	24.74	25.11	24.12	24.86	21.62	24.11	24.20	24.26	24.38	24.25	23.33
Na_2O	0.06	0.01	0.05	0.00	0.04	0.02	0.00	0.11	0.01	0.00	0.02	0.02	0.04	0.00
Total	97.41	98.32	99.17	99.14	98.26	98.17	98.97	99.40	97.45	98.09	98.48	98.23	97.20	96.43
Si	2.97	2.92	2.94	2.95	2.93	2.96	2.94	3.15	2.94	2.94	3.00	3.00	2.98	2.99
Al^{+4}	0.03	0.08	0.06	0.05	0.07	0.04	0.06	0.00	0.06	0.06	0.00	0.00	0.02	0.01
Z site	3.00	3.00	3.00	3.00	3.00	3.00	3.00	3.15	3.00	3.00	3.00	3.00	3.00	3.00
Al^{+6}	2.13	2.56	2.63	2.61	2.56	2.29	2.62	2.51	2.22	2.32	2.68	2.62	2.65	2.24
Fe^{+3}	0.82	0.44	0.37	0.37	0.39	0.69	0.36	0.52	0.75	0.67	0.31	0.36	0.34	0.75
Ti	0.00	0.00	0.00	0.00	0.00	0.00	0.01	0.00	0.00	0.00	0.00	0.00	0.00	0.00
Y site	2.96	3.00	3.01	2.99	2.95	2.98	2.98	3.03	2.97	2.99	3.00	2.99	2.99	2.99
Fe^{+2}	0.00	0.00	0.00	0.00	0.00	0.00	0.00	0.00	0.00	0.00	0.00	0.00	0.00	0.00
Mn	0.00	0.00	0.01	0.00	0.00	0.00	0.01	0.01	0.00	0.00	0.00	0.00	0.00	0.00
Mg	0.00	0.00	0.00	0.00	0.00	0.00	0.00	0.31	0.00	0.00	0.00	0.00	0.00	0.00
Ca	2.07	2.04	2.01	2.04	2.09	2.05	2.05	1.77	2.07	2.05	2.00	2.02	2.03	2.02
Na	0.01	0.00	0.01	0.00	0.01	0.00	0.00	0.02	0.00	0.00	0.00	0.00	0.01	0.00
X site	2.09	2.04	2.03	2.04	2.10	2.06	2.06	2.11	2.08	2.05	2.00	2.02	2.04	2.02
X_{Fe3+}	0.28	0.15	0.12	0.12	0.13	0.23	0.12	0.21	0.25	0.22	0.10	0.12	0.11	0.25

Table 4. Selected electron microprobe analyses of garnet in Straumsvola metabasite.

	EG-016G2	EG-016G7	EG-016G10	EG-016G5	EG-016G6	EG-016G14
SiO_2	37.10	37.65	37.75	37.32	37.50	37.90
TiO_2	0.22	0.06	0.16	0.19	0.12	0.10
Al_2O_3	21.44	20.92	20.98	21.19	21.16	21.26
Cr_2O_3	0.01	0.03	0.09	0.06	0.13	0.00
FeO*	26.32	26.26	26.34	26.36	25.62	25.58
MnO	1.47	1.36	1.08	1.11	1.06	0.65
MgO	2.88	2.77	2.82	2.79	2.71	2.53
CaO	10.68	10.40	10.91	10.78	11.43	11.70
Na_2O	0.05	0.05	0.06	0.05	0.02	0.05
K_2O	0.00	0.00	0.00	0.00	0.00	0.00
ZnO	0.00	0.00	0.00	0.00	0.00	0.00
Total	100.18	99.49	100.20	99.86	99.75	99.77
Si	5.84	5.97	5.94	5.90	5.92	5.98
Al^{+4}	0.16	0.03	0.06	0.10	0.08	0.02
	6.00	6.00	6.00	6.00	6.00	6.00
Al^{+6}	3.82	3.89	3.84	3.84	3.86	3.94
Fe^{+3} **	0.30	0.14	0.19	0.22	0.17	0.07
Cr	0.00	0.00	0.01	0.01	0.02	0.00
	4.12	4.02	4.04	4.07	4.05	4.01
Mg	0.68	0.66	0.66	0.66	0.64	0.60
Fe^{+2}	3.16	3.35	3.28	3.26	3.21	3.30
Mn	0.20	0.18	0.14	0.15	0.14	0.09
Ca	1.80	1.77	1.84	1.83	1.93	1.98
	5.84	5.95	5.92	5.89	5.93	5.96
py	11.57	11.01	11.18	11.15	10.76	9.98
alm	54.20	56.23	55.33	55.33	54.20	55.39
spess	3.36	3.06	2.44	2.53	2.40	1.46
gro	23.51	26.24	26.08	25.33	27.99	31.33
and	7.33	3.37	4.70	5.46	4.26	1.84
uv	0.03	0.08	0.27	0.19	0.39	0.00
	100.00	100.00	100.00	100.00	100.00	100.00

Garnet formula calculated to 24 O and a cation total of 16.
*All Fe reported as FeO.
Fe^{3+} ** calculated using the method of Droop (1987).

Table 5. Representative electron microprobe analyses of amphibole for selected amphibolites from the southern end of Straumsvola nunatak.

Sample	EG22 (14)		EG24(8)		EG31(3)		EG32(4)		EG28(rim)		EG28(core)	
SiO_2	40.85		43.58		42.44		41.58		43.79		42.60	
TiO_2	1.27		0.80		1.00		1.08		0.78		0.79	
Al_2O_3	12.55		10.95		12.03		12.37		11.17		11.71	
FeO*	20.88		17.68		18.16		20.26		18.74		0.00	
MnO	0.36		0.26		0.31		0.28		0.29		18.91	
MgO	7.64		10.15		9.15		8.34		10.07		0.30	
CaO	11.80		12.01		11.81		11.52		12.12		9.78	
Na_2O	1.55		1.46		1.59		1.62		1.24		11.86	
K_2O	1.53		1.02		0.82		0.94		0.56		1.34	
F	0.00		0.00		0.00		0.00				0.59	
Total	98.42		97.91		97.32		97.98		98.75		97.86	
	a	b	a	b	a	b	a	b	a	b	a	b
Si	6.26	6.19	6.56	6.49	6.44	6.38	6.34	6.24	6.54	6.43	6.44	6.32
Al^{+4}	1.74	1.81	1.44	1.51	1.56	1.62	1.66	1.76	1.46	1.57	1.56	1.68
T site	8.00	8.00	8.00	8.00	8.00	8.00	8.00	8.00	8.00	8.00	8.00	8.00
Al^{+6}	0.53	0.43	0.50	0.42	0.60	0.51	0.57	0.43	0.51	0.37	0.53	0.37
Fe^{+3}	0.00	0.50	0.00	0.46	0.00	0.46	0.00	0.72	0.00	0.75	0.00	0.87
Ti	0.15	0.15	0.09	0.09	0.11	0.11	0.12	0.12	0.09	0.09	0.09	0.09
Mg	1.75	1.73	2.28	2.26	2.07	2.05	1.90	1.87	2.24	2.21	2.20	2.16
Fe^{+2}	2.58	2.15	2.13	1.75	2.22	1.83	2.41	1.82	2.16	1.55	2.18	1.47
Mn	0.00	0.05	0.00	0.03	0.00	0.04	0.00	0.04	0.00	0.04	0.00	0.04
M1,2,3	5.00	5.00	5.00	5.00	5.00	5.00	5.00	5.00	5.00	5.00	5.00	5.00
Fe^{+2}	0.10	0.00	0.10	0.00	0.09	0.00	0.17	0.00	0.18	0.00	0.21	0.00
Mn	0.05	0.00	0.03	0.00	0.04	0.00	0.04	0.00	0.04	0.00	0.04	0.00
Ca	1.94	1.92	1.94	1.92	1.92	1.90	1.88	1.85	1.94	1.91	1.92	1.89
Na	0.00	0.08	0.00	0.08	0.00	0.10	0.00	0.15	0.00	0.09	0.00	0.11
M4 site	2.08	2.00	2.07	2.00	2.05	2.00	2.09	2.00	2.16	2.00	2.17	2.00
Ca	0.00	0.00	0.00	0.00	0.00	0.00	0.00	0.00	0.00	0.00	0.00	0.00
Na	0.46	0.37	0.43	0.34	0.47	0.37	0.48	0.32	0.36	0.26	0.39	0.27
K	0.30	0.29	0.19	0.19	0.16	0.16	0.18	0.18	0.11	0.10	0.11	0.11
A site	0.76	0.67	0.62	0.53	0.63	0.52	0.66	0.50	0.46	0.36	0.51	0.38
Total	15.84	15.67	15.69	15.53	15.68	15.52	15.75	15.50	15.62	15.36	15.68	15.38

*All Fe reported as FeO.

Calculation of formulae based on 23 O: (a) an all-Fe^{2+} assumption; (b) 13 cations exclusive of K, Na and Ca.

Spot number for individual analysis is shown in parentheses after the sample number for amphibole in amphibole-plagioclase pairs.

Table 6. Corresponding representative electron microprobe analyses of plagioclase for selected amphibolites from the southern end of the Straumsvola nunatak.

Sample	EG22 (14)	EG24(8)	EG31(3)	EG32(4)	EG28(3)
SiO_2	61.05	58.56	59.22	60.12	61.254
TiO_2	0.00	0.00	0.00	0.00	0
Al_2O_3	24.36	26.50	26.31	25.01	23.983
Fe_2O_3	0.00	0.00	0.00	0.00	0
FeO	0.09	0.12	0.14	0.15	0.444
MgO	0.00	0.03	0.00	0.00	0.12
CaO	5.38	7.68	7.50	5.77	6.579
Na_2O	8.62	7.72	7.51	8.95	7.392
K_2O	0.16	0.11	0.17	0.12	0.313
Total	99.67	100.72	100.84	100.12	100.085
Mol. %					
Ab	73.66	64.12	63.84	73.26	65.80
An	25.42	35.26	35.23	26.11	32.36
Or	0.92	0.62	0.93	0.64	1.83

Spot number for individual analysis is shown in parentheses after the sample number for plagioclase in amphibole-plagioclase pairs.

7. THERMOBAROMETRY

7.1 Nashornkalvane

An estimate of the peak metamorphic conditions experienced at this locality was achieved by combining chlorite geothermometry with experimental phase equilibria studies, together with phase diagram and average P-T calculations using the program THERMOCALC v.2.75 (Holland & Powell, 1998; and references therein).

7.1.1 Phase equilibria

The metamorphic minerals present within restricted low-grade microdomains comprise chlorite, actinolite, epidote, albite and quartz. The first appearance of these minerals in textural equilibrium is diagnostic of mafic rocks that have undergone the transition to the greenschist facies (Frey et al., 1991; Liou et al., 1987, 1985a,). Various low-grade, temperature-sensitive indicator minerals have been used to help assign mafic rocks to a particular metamorphic facies. Epidote is known to form at temperatures in excess of 200°C (Cho et al., 1986; Liou et al., 1985b; Bird et al., 1984). Actinolite is reported to appear at about 300°C (Bevins et al., 1991; Bird et al., 1984). The minimum temperature for the formation of discrete tri,trioctahedral chlorite is given as 240°C (Kristmannsdóttir, 1979) or 270°C (Schiffman & Fridleifsson, 1991).

As a first approximation for the metamorphic conditions recorded in the metabasite at Nashornkalvane, the position of various univariant end-member reactions with relatively steep slopes in P-T space were calculated with THERMOCALC v.2.75 using the activities of ten end-members (calculated by the AX program; www.esc.cam.ac. uk/astaff/holland) from representative metamorphic mineral compositions in sample EG-N2 (Table 7). This particular sample was chosen, because it contains the highest number of co-existing metamorphic minerals in the same microdomain. The uni-variant end-member reactions involve the breakdown of chlorite into actinolite and an Fe-Mg exchange reaction between these two minerals:

$$Cln + 6Czo + 7Qtz = Tr + 10An + 6H_2O \quad (1)$$

$$Fe\text{-}Chl + 6Czo + 7Qtz = Fac + 10An + 6H_2O \quad (2)$$

$$Cln + Fac = Fe\text{-}Chl + Tr \quad (3)$$

Temperatures of between 220°C and 410°C are indicated from the above reactions for pressures of between 1 and 4 kbar (Table 8).

Table 7. Calculated activities for pure end members from the greenschist phases in EG-N2 using THERMOCALC v. 2.75 (Powell & Holland, 1998)

System	Phase	Analysis	End member*	Activity (a)	std. (a)
NCMASH	Chlorite	11	clin	0.0238	0.0070
			daph	0.0560	0.0118
			ames	0.3625	0.0725
	Amphibolie	3	tr	0.1000	0.0249
			fact	0.0100	0.0036
			ts	0.0008	0.0005
	Plagioclase	3	an	0.2600	0.0285
			ab	0.9800	0.0489
	Epidote	3	cz	0.64	0.0635
			ep	0.36	0.0365
	Quartz		q	1	
			H_2O	1	

* clin - clinochlore. daph - daphnite. ames - amesite. tr - tremolite. fact - ferroactinolite. ts - tschermakite. an -anorthite. ab - albite. cz - clinozoisite. ep - epidote.
std. = standard deviation.

Table 8. Calculated temperatures* for the position of univariant reactions.

Pressure (kbar)		1.0	2.0	3.0	4.0
Reaction no.					
1	T(°C)	321	351	381	410
2	T(°C)	315	344	373	402
3	T(°C)	222	239	255	271

* temperatures calculated using THERMOCALC with the activities calculated using the AX program.

An approximation of a minimum temperature constraint for the assemblage in EG-N2 may, however, be estimated by calculating the position of reactions in P-T space, which define the sub-greenschist/greenschist facies boundary. The most commonly used petrogenetic grid for illustrating the boundary between the subgreenschist and greenschist facies in metabasites is that of Frey et al. (1991), which is based on the model basaltic system NCMASH. Two intersecting reactions mark the subgreenschist-greenschist facies boundary. At pressures above 3 kbar, this

boundary is defined by the decomposition of pumpellyite given by,

$$Pmp + Chl + Qtz = Czo + Tr + H_2O \quad (4)$$

whereas at lower pressures, this boundary is given by the breakdown of prehnite following the reaction:

$$Prh + Chl + Qtz = Czo + Tr + H_2O \quad (5)$$

Frey et al. (1991) pointed out that the reaction boundary in the NCMASH system should be regarded as a P-T zone or band as the position of reactions defining the boundary between two facies in P-T space are sensitive to the activities of the metamorphic minerals (bulk rock composition) and other variables such as the partial pressure of water (P_{H2O}). Extensive overlap in metamorphic facies was shown to occur with the transition from the prehnite-actinolite and pumpellyite-actinolite to greenschist facies at about 250 to 300°C at 1 to 3 kbar and at about 250 to 350°C at 3 to 8 kbar.

Similar calculations were performed for the Nashornkalvane metabasite in the system NCMASH and the calculated Mg end-member activities from the minerals in the EG-N2 assemblage (Fig. 11). As the remaining phases belonging to the subgreenschist facies in the NCMASH system are not present in any of the samples, their activities are unknown and were included as unit activities in the above calculations. The reaction curves in the constructed P-T diagram occur as fixed activity isopleths with the position of the reactions defining the lower boundary of the greenschist facies, indicating a minimum temperature of about 300°C.

Although the activity isopleths indicate that the transition to the greenschist facies for the metabasite at Nashornkalvane South must have occurred at temperatures above ~300°C, they are all based on the assumption that the partial pressure of H_2O at the time of metamorphism was equal to the lithostatic pressure. However, as many of the reactions defining the boundaries between different facies are dehydration equilibria, the position of these reactions will shift towards lower temperatures when $P_{H2O}<P_{Total}$ (Fig. 12). Petrographic evidence indicates possible

limited and variable fluid infiltration for the Nashornkalvane metabasite with local metamorphic domains of varying size scattered randomly within and between thin section samples. As exemplified by sample EG-N2, the intersection point between the two boundary reactions could be displaced to temperatures as low as 250°C if the partial pressure of H_2O is lowered to 0.5 (Fig. 12). Therefore, a minimum temperature could possibly be estimated to lie between ~250 and 300°C.

An average P-T estimate of T = 274 ± 30 °C and P = 2 ± 1.9 kbar was derived from all ten EG-N2 end-member activities listed in Table 7 using THERMOCALC in average P-T mode (with unit activities for prehnite and pumpellyite included to obtain a complete set of independent reactions). The temperature thus obtained is further compared to that derived from chlorite geothermometry.

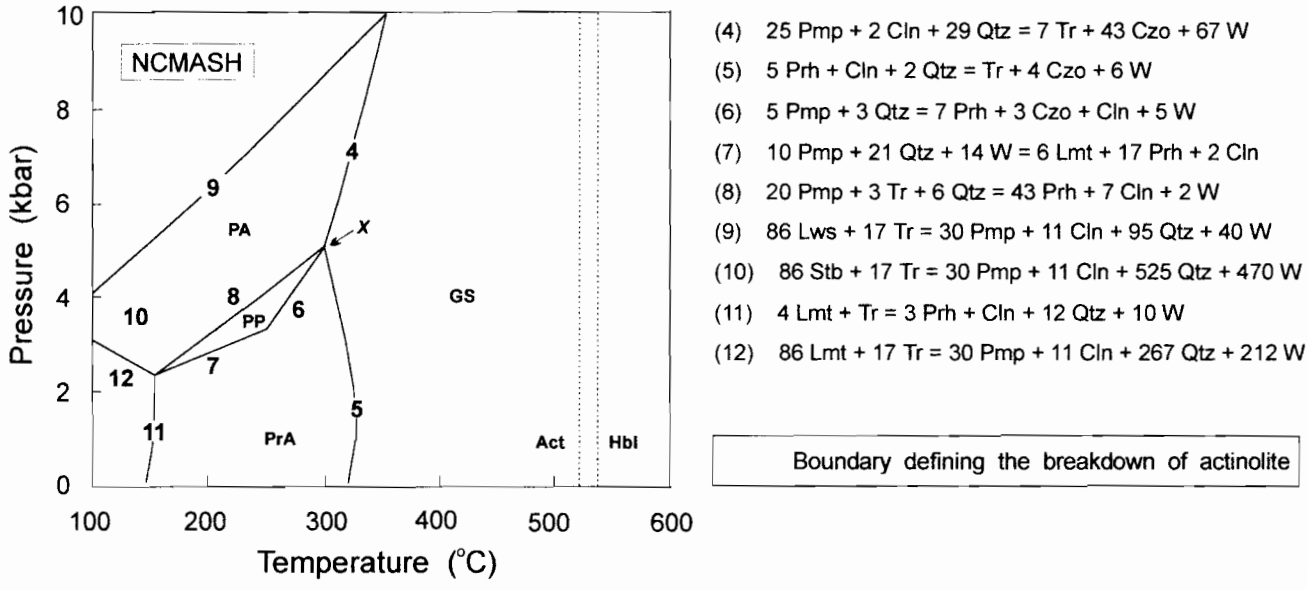

Fig. 11. *P-T* diagram in the system NCMASH showing activity isopleths with activities derived from mineral compositions in EG-N2. All reactions with clinochlore, quartz and H_2O in excess. PA, PP, and PrA indicate the pumpellyite-actinolite, prehnite-pumpellyite, and prehnite-actinolite facies, respectively. GS = greenschist facies. Point *X* is the intersection between the two reactions defining the lowermost boundary of the greenschist facies. The location of the Act-Hbl boundary is after Apted & Liou (1983).

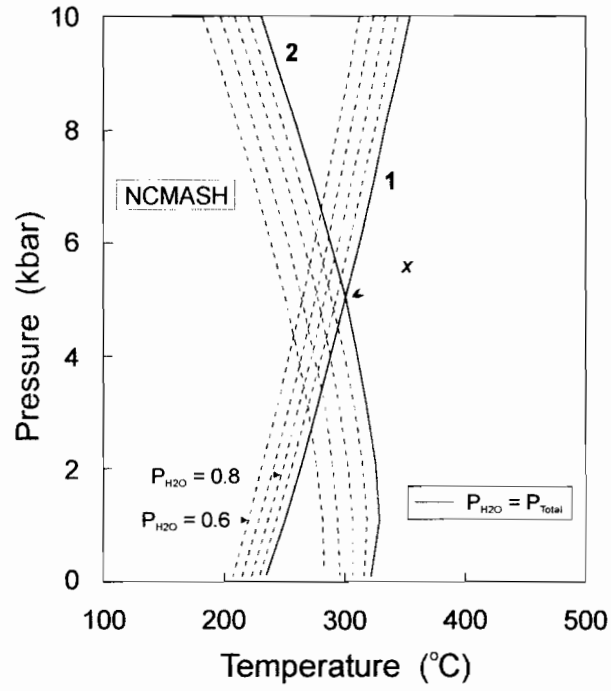

Fig. 12. The influence of water pressure on the lower boundary of the greenschist facies, modeled using THERMOCALC v.2.75 (Holland & Powell, 1998; and references therein).

7.1.2 Chlorite geothermometry

Cathelineau and Nieva (1985) proposed a chlorite geothermometer based on an empirical calibration of tetrahedral Al content and temperature increase in chlorite from the Los Azufres geothermal field, Mexico. Subsequently, Cathelineau (1988) included a larger dataset and concluded that increases in tetrahedral Al content is dependant on increasing temperature, and is independent of factors such as fluid composition. The relation between temperature and Al^{iv} was described as:

$$T\ (^{o}C) = -\ 61.92 + 321.98\ (A^{iv})$$

Kranidiotis & MacLean (1987) also suggested variation in chlorite composition to be a function of increasing temperature, but modified the calibration of Cathelineau & Nieva (1985) to take into account the influence of bulk rock composition. The more recent themometer of Zang and Fyfe (1995), similar to that of Kranidiotis & MacLean (1987), takes into account the change in Fe/Fe+Mg ratio of chlorite with temperature and is given by the equation:

$$T\ (^{o}C) = 17.5 + 106.2[2(Al^{iv}) - 0.88(X_{Fe} - 0.34)]$$

Many other researchers have considered chlorite geothermometry to yield inaccurate temperature estimates and suggested that it should be applied with caution because of the unknown influences of other variables such as oxygen fugacity, fluid and bulk rock composition, and contamination with other phases (e.g. Jiang et al., 1994; De Caritat et al., 1993). Jiang et al. (1994), for example, pointed out that the correlation between octahedral occupancy (and therefore, tetrahedral Al) and temperature is a product of chlorite contamination by microscopic inclusions and mixed layer smectite and correctly predicted that irrespective of the geothermometer used, chlorite with substantial amounts of Ca, Na and K would always yield lower temperatures.

All of the chlorite grains analyzed in this study have very low levels of Ca and the sum of Ca + Na + K does not exceed 0.02 (Table 1). Discrete chlorite growth with effectively no contamination is thus indicated. The association of albite (as well as epidote and white mica) with the chlorite indicates Al-saturation, thus fulfilling an essential requirement for the application of chlorite geothermometry. Chlorite temperature estimates are presented from metamorphic microdomains in the Nashornkalvane sill using different calibrations of the chlorite thermometer (Table 1), including those of Zang & Fyfe (1995), Cathelineau (1988), Kranidiotis & MacLean (1987) and Cathelineau and Nieva (1985). A wide spread in temperatures is obtained from the different calibrations. However, the independent temperature estimate of 274°C obtained from THERMOCALC falls within the range of average chlorite temperature estimates (258 - 276°C) calculated for various sample microdomains using the Zang and Fyfe (1995) calibration. Average temperature ranges yielded by the other chlorite thermometers are either to high as in the case of the calibrations of Cathelineau (1988; T = 338 - 364°C) and Cathelineau and Nieva (1985; T = 282 - 298°C) or too low as for the Kranidiotis & MacLean (1987; T = 191 - 201°C) thermometer (Table 3). In conjunction with other thermometric techniques, Frimmel (1997) pointed out that the chlorite thermometer of Zang & Fyfe (1995), which includes a correction for a change in Fe/(Mg + Fe) ratio, yields more accurate temperature estimates for chlorites with $X_{Fe} > 0.5$. As all the analyzed chlorites in this study have X_{Fe} ranging between 0.5 and 0.61 (Table 3), the thermometer by Zang & Fyfe (1995) is favoured here.

All thermometer calibrations yield significantly higher average chlorite temperatures from analyses within larger metamorphic domains (as in thin section sample EG-14b) than those from smaller microdomains (EG-14a; Table 3). A lower average temperature from an apparently less hydrated part of the sill points to a possible relationship between the temperature yielded by chlorite geothermometry and fluid/rock ratio, as approximated by the modal proportion of the hydrous metamorphic phases, namely chlorite and actinolite (Fig. 13). The chlorite temperature estimate of 276°C from the microdomain with the highest proportion of chlorite and actinolite is identical to the temperature estimate of 274 ± 30 °C from the average P-T calculation. The lower chlorite temperatures probably do not reflect the true formation temperatures but are rather an artifact of lower local fluid/rock ratios.

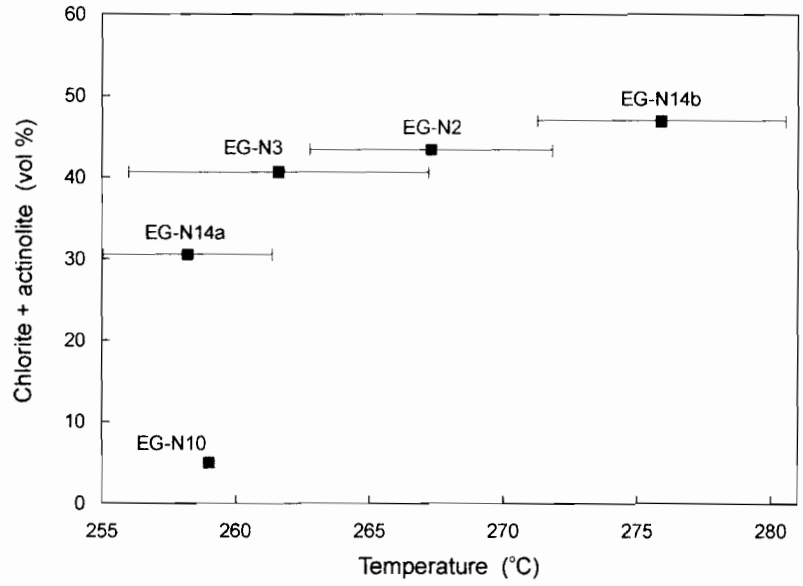

Fig. 13. Relationship between modal proportion of mafic hydrous phases and temperature calculated by the chlorite geothermometry. A temperature of 259°C is a minimum estimate obtained from fine-grained chlorite growing along a cleavage plane in the core of a clinopyroxene grain in sample EG-N10 and chlorite in the smallest observed metamorphic domain in sample EG-14a.

This possible relation between fluid/rock ratio and chlorite temperature may be the result of the variance of the greenschist facies mineral assemblage. The assemblage chlorite + actinolite + epidote + albite + quartz has four degrees of freedom. At a given temperature and pressure, as

many as five compositional variables determine the state of the system, which may have remained closed, except for H_2O:

(i) Fe-Mg variation in chlorite

(ii) Al^{3+}-Si variation in chlorite

(iii) Fe-Mg variation in actinolite

(iv) Fe^{3+}-Al^{3+} in epidote

(v) variation in fluid composition or P_{H2O}

Consequently, any change in one of the above, such as P_{H2O}, will cause a change in all other variables. However, the spread in chlorite temperatures may also be due to a number of variables other than fluid/rock ratio (degree of hydration) such as oxygen fugacity and slight variations in chemical composition of primary phases on a microscale or possibly a combination of more than one of these variables. For example, the low calculated temperature of ~259°C from fine-grained chlorite, which has grown along fractures/cleavage of a clinopyroxene grain in sample EG-N10, may have been the product of both a low fluid/rock ratio and nucleation of chlorite in an Al-poor micro-environment (Fig.13). Therefore, in order for the dependence of calculated chlorite temperature on fluid/rock ratio to be true, many other variables affecting both the nucleation rate and the intra-crystalline chemical composition of chlorite are required to remain constant. As it is difficult to directly quantify these variables, it becomes correspondingly difficult to interpret the spread in calculated chlorite temperature estimates of between 250 and 276°C. The chlorite temperatures may indicate formation of chlorite and actinolite within each microdomain under different P-T conditions reflecting more than one metamorphic event. Alternatively, the highest chlorite temperature estimate (which coincides with the calculated average temperature) of ~275°C may record peak metamorphic conditions related to a single metamorphic event with the spread towards lower artificial chlorite temperatures being a function of changes in one or more other physical and compositional variables.

7.2 Straumsvola

7.2.1 Hornblende-plagioclase geothermometry

Blundy and Holland (1990) suggested, based on a strong positive correlation, that compositional variation in amphiboles is essentially controlled by a coupling between Al^{iv} substitutions and the introduction of cations (Na ± K) into the A-site. Further evidence was provided by a dominant compositional vector lying parallel, but intermediate to the joins edenite-tremolite and pargasite-hornblende in triangular plots of Al^{iv}, Al^{vi} and A-site vacancy for the natural and synthetic amphiboles in their data set. This vector was characterized as an $(Na, K)Al^{vi} \square_{-1}Si_{-1}$ cation exchange, since it was taken as an expression of the strong coupling between Al^{iv} and A-site substitution. The Al^{iv} substitution was shown to be more strongly dependent on temperature, rather than pressure. The $(Na, K)Al^{vi} \square_{-1}Si_{-1}$ exchange was written in the form of two reactions:

$$\text{edenite} + 4\text{quartz} = \text{tremolite} + \text{albite} \quad (13)$$

$$\text{pargasite} + 4\text{quartz} = \text{hornblende} + \text{albite} \quad (14)$$

Various activity-composition models in, which ideal mixing in amphibole and non-ideal behaviour in coexisting amphibole, were assumed to calibrate the above reactions with equilibrium relations of the form $-\Delta G^0 = RT\ln K$ written for each. The resulting amphibole-plagioclase geothermometer of Blundy and Holland (1990) based on the derived equilibrium constant, K, was found to yield good temperature estimates for amphiboles with similar compositions to that in the dataset of Blundy and Holland (1990) but erroneous results for aluminium-rich amphiboles coexisting with plagioclase in garnet-amphibolites (Mengel and Rivers, 1991). The failure of the thermometer to yield reasonable results was attributed to two incorrect assumptions: firstly, that of ideal mixing in amphiboles and secondly, that all amphiboles, including the aluminium-rich varieties, display strong coupling between Na in the A-site and Al in the T1 (tetrahedral) site (Holland and Blundy, 1994).

Using a more expanded dataset, as well as incorporating the influence of non-ideality as far as possible into the activity models, Holland and Blundy (1994) derived two geothermometers. The first of these (Thermometer A) was a revised edenite-tremolite thermometer based on the

reaction:

$$\text{(A) edenite + 4quartz = tremolite + albite}$$

The new, second thermometer (Thermometer B) was based on the reaction:

$$\text{(B) edenite + albite = richterite + anorthite}$$

and may be used for silica under-saturated rocks. Considering non-ideal mixing between the six sites in amphibole, a maximum of 36 possible interaction terms (or interaction parameters (W)) were derived, including 24 independent cross-site interaction terms and 12 independent within-site terms. However, in a balanced chemical reaction involving the two end-members, many of the interaction terms cancel reducing the total number of terms to only 8. For example, both within-site and cross-site interaction terms for non-ideal mixing on the M2, M1,3 and M4 sites between edenite and tremolite cancel out (Holland and Blundy, 1994). It was only these 8 non-ideal interaction terms, which were considered to affect the equilibrium constant (K_A) for reaction A.

The condition of equilibrium for reaction A on which the improved edenite-tremolite thermometer was based therefore, included an ideal and non-ideal component and expressed as:

$$\Delta\mu_A = 0 = \Delta G_A^{\circ} + RT\ln K_A$$
$$= \Delta H_A^{\circ} - T\Delta S_A^{\circ} + P\Delta V_A^{\circ} + RT\ln K_{ideal} + RT\ln \gamma_{ab} + RT\ln \gamma_{trem} - RT\ln \gamma_{ed}$$

K_{ideal} remains the same as given in Blundy and Holland (1990), where as the last three terms in the equation take into account the excess energy associated with non-ideality in plagioclase and amphibole. A revised expression for the edenite-tremolite thermometer is given as:

$$T_A = [\Delta H_A^{\circ} + P\Delta V_A^{\circ} + Y_{ab} + Y_{(ed-trem)}] / [\Delta S_A^{\circ} - R \ln K_{ideal}]$$

As in the previous thermometer the factor Y_{ab} depends on the albite composition of the plagioclase. $Y_{(ed-trem)}$, however, is given by,

$Y_{(ed-trem)} = RT\ln \gamma_{trem} - RT\ln \gamma_{ed}$

and is obtained from the 8 interaction parameters. Regression of the expanded experimental and natural amphibole-plagioclase dataset allowed the determination of ΔH_A^o and ΔS_A^o as well as the components comprising $Y_{(ed-trem)}$ (Holland and Blundy, 1994). The success of the new thermometer was reflected in the calculated temperatures from hornblende-plagioclase pairs of, which 83% fell within $\pm 50^oC$ of the measured values.

As all the amphibolite samples display at least 5% quartz, the edenite-tremolite (Thermometer A) of Holland & Blundy (1994) was used. Application of the hornblende-plagioclase geothermometer to the amphibolite in the gneiss complex near Straumsvola in the western H.U. Sverdrupfjella yielded temperatures between 685 and 790°C (Table 9; Fig. 14(a-e)). Temperatures were calculated from amphibole-plagioclase pairs (6-8 pairs per sample) in five samples at pressures of 5, 10 and 15 kbar (Table 9). The temperatures calculated at 15 kbar are unlikely as the amphibolites should be eclogite under such high pressure conditions. The temperature estimates calculated from the compositions of amphibole-plagioclase pairs at 10 kbar and 5 kbar are similar. However, the temperature estimates calculated at 10 kbar display narrower temperature ranges than those calculated at 5 kbar (Table 9). A pressure estimate from a garnet-bearing sample EG-016 (see section 7.2.2 below) indicate peak pressures of between 8.5 and 10.7 kbar at Straumsvola, depending on the geobarometer used. Thus, the temperature estimates at 10 kbar are preferred. Mineral chemical analyses of the plagioclase in these amphibolite samples show a significant spread, which possibly reflects a thermal retrograde overprint. Plagioclase grains in sample EG-031 have the highest anorthite content and a low spread in composition. The calculated temperature range of 713-748°C (at 10kbar) from the amphibole-plagioclase pairs in this sample is, therefore, regarded as the minimum temperature estimate for metamorphic conditions at Straumsvola in the western H.U. Sverdupfjella. This temperature estimate is indistinguishable from that of Pan-African M_{2b} conditions (T=687-758°C; Board et al., 2005) in the eastern part of the belt where a pressure estimate for upper amphibolite facies conditions has been constrained at 9.2 to 11.3 kbar.

Many of the amphibolite boudin cores are host to anatectic leucosome. As this leucosome consists predominantly of K-feldspar and biotite with minor plagioclase and muscovite, it is most likely derived from the migmatized Banded Gneiss Complex rather than from melting of the mafic boudins themselves. Considering the calculated upper amphibolite temperatures, this petrographic observation suggests that metamorphism of the mafic precursor rocks occurred below the experimentally determined solidus at P_{H2O} lower than P_{Total}. The position of the tonalite solidus in P-T space and an approximation of the P_{H2O} during metamorphism has been estimated from the mineral chemistry of the amphibole in conjunction with a recent study by Pattison (2003).

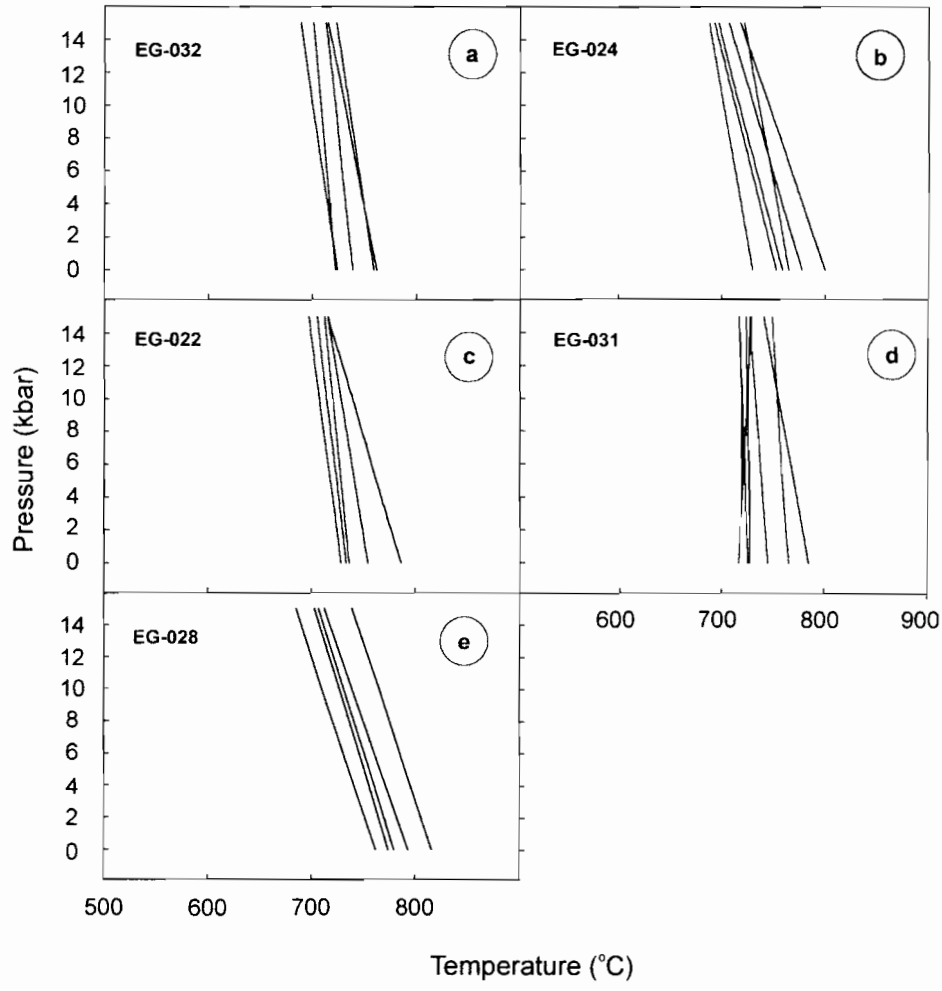

Fig. 14. Temperature curves yielded by the Holland & Blundy (1994) geothermometer for amphibole-plagioclase pairs (a-e) in the Straumsvola metabasites.

As pointed out by Pattison (2003), poorly understood discrepancies occur between P-T data obtained from natural paragenesis, experimental constraints and thermodynamic modelling in mafic amphibolite and granulite-facies rocks. One of the reasons for these discrepancies is the lack of a well-constrained melt composition for thermodynamic modeling. As a result, complex 'natural' reactions in metabasites are modelled using only dehydration reactions as analogues.

Table 9. Calculated temperatures from Hbl-Pl compositions in Straumsvola amphibolites.

Pressure (kbar)	5	10	15
Sample no.			
EG-032	712-747	700-735	689-723
EG-024	716-773	702-746	688-722
EG-022	717-761	706-738	696-714
EG-031	714-763	713-748	710-742
EG-028	736-790	710-765	685-739

Temperature estimates calculated from compositions of Hbl-Pl pairs using the Holland & Blundy (1994) geothermometer.

Physical conditions for the analogue reaction,

$$2Prg + 8Qtz = 3Fsl + 2Hd + 2Ab + 2An + 2H_2O \quad (15)$$

representing the amphibolite-granulite facies transition in metabasites at low to intermediate pressures were modelled by Pattison (2003) using THERMOCALC including the thermodynamic data of Dale et al. (2000) for a range of bulk rock X_{Mg} values of between 0.35 and 0.65. As pargasitic amphibole is essentially the only mafic mineral in the Straumsvola metabasites and displays a X_{Mg} of about 0.4 to 0.5, analogue reaction (10) representing a bulk X_{Mg} of 0.5 was used in this study. A down-temperature shift of 150 to 200°C was calculated assuming a H_2O activity of 0.3 for reaction (10). A similar displacement towards higher temperatures may be envisaged for the experimentally determined tonalite solidus (Fig. 14). Consequently, as no petrological evidence for partial melting of the metabasites exists, the P_{H2O} must have been considerably less than P_{Total}, estimated at less than or equal to 0.5.

7.2.2. Pressure estimate

Pressure could only be constrained for garnet-bearing amphibolite (sample EG-016), which displays a mineral assemblage garnet + hornblende + plagioclase + quartz. The activities of the various end-members in this assemblage were calculated with the AX program (Table 10). An average pressure estimate of 10.7 kbar was derived for this amphibolite using THERMOCALC in average pressure mode and an independent temperature estimate (of ~735°C) derived from hornblende-plagioclase thermometry. Application of the Kohn & Spear (1990) geobarometer yielded a pressure of 8.5 kar. In summary, the best constraints on peak temperature and pressure for these amphibolite samples are T = 713-748°C at P = 8.5 - 10.7 kbar.

Table 10
Activities for phases in EG-016 using THERMOCALC (estimated with a-x program)

Phase	End-member*	Activity (a)	std. (a)
Garnet	alm	0.1400	0.0208
	py	0.0046	0.0019
	gr	0.0370	0.0098
	spss	0.000014	0.000008
Amphibole	tr	0.014480	0.004725
	fact	0.001600	0.000838
	ts	0.0007	0.0008
	parg	0.032000	0.007900
Plagioclase	an	0.4400	0.0277
	ab	0.6900	0.0345
	q	1	
	H_2O	1	

* alm - almandine. py - pyrope. gr - grossular. spss - spessartine. tr - tremolite. fact - ferroactinolite. ts - tschermakite. parg - pargasite. an - anorthite. ab - albite.

7.3 Discussion and integration of P-T data with the eastern Maud Belt

The data presented in this study indicates the presence of a major metamorphic discontinuity with a temperature and pressure difference of 450°C and 6.5 to 8.7 kbar, respectively, between the Grunehogna Craton and the Maud Belt. Metamorphism at Nashornkalvane is assigned to the lowermost greenschist facies (T = 250 - 276°C, P = 2 kbar), whereas peak metamorphic conditions only 30 km away at Straumsvola in the far western part of the Maud Belt reached upper-

most amphibolite facies conditions (T = 713 - 748 °C; P = 8.5 -10.7 kbar). The temperature estimate of 713-748°C is a minimum estimate that takes into account the possibility of a thermal retrograde effect, either during the late Pan-African or due to the intrusion of the nearby Straumsvola syenite intrusion. Temperature estimates from amphibolite, which have a significantly more sodic composition possibly due to resetting during a retrograde thermal effect, are slightly lower but do not differ significantly from that calculated from sample EG-031 containing plagioclase with the most calcic (anorthite-rich) composition. This indicates that any thermal effect on the amphibolite following peak regional metamorphic conditions was probably minimal. A similar geological situation involving a Mesozoic syenite body that has intruded amphibolite facies country rock occurs in the northeastern part of the Northern Kirwanveggen area (see Fig. 1). There, the Sistefjell intrusion, a large 10km wide syenite pluton (twice the size of the Straumsvola body) intrudes lower amphibolite facies country rock (Harris et al., 2002). An oxygen isotope study has shown that amphibole growth in the country rock was the result of an earlier lower amphibolite facies event rather than being related to any contact thermal metamorphic effect of the adjacent intrusion (Harris et al., 2002). Despite the size of the syenite intrusion, no extensive fenitization and no recrystallization of the pre-existing earlier formed amphibole was observed in the country rock (Harris et al., 2002). Therefore, the compositional and thermal effect of these Mesozoic syenite intrusions on surrounding amphibolite facies country rock appear to be minimal.

A large-scale metamorphic hiatus of 450°C and 6.5 to 8.7 kbar indicates that a section of crust with an estimated thickness of between ~ 20 to 30 km is missing below the Pencksökket and Jutulstraumen glaciers. This metamorphic discontinuity may have formed in response to different tectonic compressional and/or extensional regimes. The lack of a P-T-t path for the western part of the Maud Belt as well as the lack of an extensive structural dataset to help constrain the kinematic history (transport direction) along the sub-glacial PJD boundary lead to various possible tectonic models for its development. Possible models may include the PJD as a major thrust zone, a low-angle normal fault, an oblique-strike-slip fault, a listric fault or a graben-type structure. Hybrid models may be invoked for the PJD involving a combination of thrusting followed by normal or oblique-strike slip faulting. The discontinuity may have developed in an extensional setting possibly as a tilted crustal block during rotation on a listric fault plane between

the craton and the Maud Belt subsequent to either major late Mesoproterozoic and/or Pan-African tectonism.

The only exposed rock outcrop in the entire Pencksökket-Jutulstraumen glacial valley occurs at the Midbresrabben nunatak located at (72.73°S, 2.10°E). There, an ~400m wide mylonitic shear zone in a diorite intrusion, together with highly sheared 40m wide mafic dykes, protrudes above the Pencksökket Glacier (Grantham and Hunter, 1991; Grantham et al., 1995). The intense planar mylonitic fabric at Midbresrabben strikes N-NNE and dips steeply E (70-80°), with the mineral lineation defined by epidote (after plagioclase) and biotite (probably after amphibole) plunging steeply (70-80°) toward the SE (Grantham and Hunter, 1991). The orientation and record of kinematic shear sense of this exposed major mylonitic shear zone is in agreement with the pervasive Pan-African top-to-northwest shear fabric in the eastern Maud Belt reported by Board et al. (2005). Both, the dykes and the diorite yielded whole-rock Rb-Sr ages of ~800 Ma (Moyes et al., 1993a). These ages could either reflect the time of rock emplacement or resetting of the Rb-Sr isotope system during later tectono-thermal overprinting. As no other magmatic rocks of comparable age are known from the entire Maud Belt, partial resetting during the Pan-African orogeny is the preferred explanation for these ages.

Contrary to previous suggestions (Groenewald et al., 1995; Grantham et al., 1995), our new data suggest that there is no significant difference in metamorphic grade from east to west across the H.U. Sverdrupfjella (Fig. 15). Considering that the geographical orientation of the PJD is consistent with the pervasive, Pan-African (540 Ma) top-to-northwest shear fabric in the Maud Belt, a more likely tectonic scenario could be that the metamorphic hiatus represents a large-scale Pan-African thrust (Fig. 1). This model has not previously been considered. P-T conditions in the westernmost part of the belt at Straumsvola (T = 713 - 748 °C; P = 8.5 -10.7 kbar) directly adjacent to the Pencksökket-Jutulstraumen Discontinuity are indistinguishable from Pan-African M_{2b} conditions in the eastern H.U.Sverdrupfjella (T = 687-758°C, P = 9.2-11.3 kbar). By analogy with the dated fabric in the latter domain, it is suggested that the entire H.U. Sverdrupfjella experienced upper amphibolite facies metamorphism during major Pan-African tectonic re-working of older, Mesoproterozoic crust. Most of the previous metamorphic mineral assemblages and structures imprinted during the Grenvillian orogeny were completely

obliterated. Only in the cores of competent boudins, an earlier amphibole generation attests to an older, most likely late Mesoproterozoic amphibolite-facies metamorphic event.

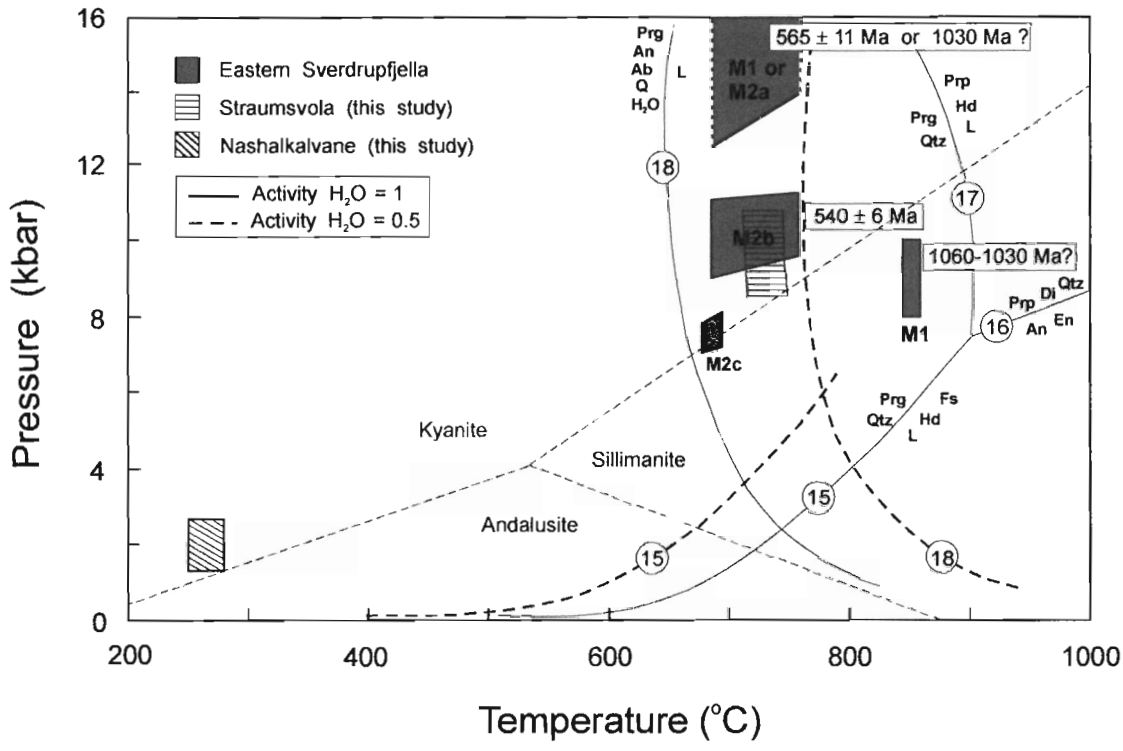

Fig. 15. P-T constraints on metamorphic conditions at Nashalkalvane (Grunehogna Craton) and Straumsvola (western Maud Belt) compared with those from the eastern Maud Belt (eastern H.U. Sverdrupfjella; Board, 2005). Granulite facies conditions are derived from mafic boudins after Groenewald & Hunter (1991) and Groenewald et al. (1995). Aluminosilicate triple point is after Bohlen et al. (1991). Reactions (15), (16) and (17) are from Pattison (2003) calculated on the basis of a pargasite composition with $X_{Mg} = 0.5$. Reaction (18) is the approximate position of the wet tonalite solidus (Johannes, 1978; Piwinskii, 1968, Wyllie and Wolf, 1993). P-T conditions calculated in this study for the western Maud Belt correspond to that of M_{2b} in the eastern Maud Belt with age constraints from Board (2005). Note a metamorphic hiatus of T = 450°C and P = 6.5 – 8.7 kbar across the Jutulstraumen glacier.

In the absence of any structural evidence of more than one tectonothermal overprint along the eastern flank of the Ritscherflya Basin, the lowermost greenschist facies conditions established here for the Nashornkalvane outcrop is ascribed to a single tectonothermal (M_{2b}) event. The southeasterly dip of the strata matches the top-to-northwest transport direction established for the Pan-African orogeny (Board et al., 2005). Consequently, a Pan-African age is assigned to the low-grade metamorphic imprint there, which would then correspond to M_{2b} in the high-grade Maud Belt.

To date, no temperature and age constraints for the early M_{2a} eclogite-facies metamorphism are available, but an Early Pan-African age is preferred for reasons discussed by Board et al. (2005). The previously reported granulite facies metamorphic assemblage (Groenewald et al., 1995; Groenewald & Hunter, 1991) preserved in shielded, anhydrous mafic boudin cores and mafic dykes may therefore, represent relicts of the older, Grenvillian high-grade metamorphism. High-T granulite facies metamorphism at that time has also been documented in the Heimefrontfjella west of the Pan-African Heimefront Shear Zone (Jacobs et al., 2003).

If the PJD is a large-scale Pan-African thrust, it could represent an extension of the orogenic front from the Mozambique Belt into East Antarctica. Continuation of the PJD into the south-eastern-most part of the belt would be in agreement with the spatial alignment, kinematic record (top-to-NNW or NW) and age of the exposed Heimefront Shear Zone in the Heimefrontfjella, which has been interpreted as the western front of the Pan-African suture between East and West Gondwana (Jacobs et al., 1999, 1996, 1995).

8. GEOCHEMISTRY

8.1 Results

A total of 14 mafic samples were analyzed for their major and trace element concentrations (Table 11), as well as Rb-Sr and Sm-Nd isotopic compositions (Table 12). Samples were taken from a Borgmassivet Suite sill on the eastern margin of the Grunehogna Craton at Nashornkalvane and from amphibolite boudins at Straumsvola in the western H.U. Sverdrupfjella (western Maud Belt). This limited geochemical data set (Table 11 and Table 12) is compared with unpublished data on various mafic rocks from the eastern H.U. Sverdrupfjella (Board, 2002) and from the Gjelsvikfjella (A. Bisnath, unpubl. data 2005; Fig. 16). The geochemistry of the amphibolites of unknown age is further compared to that of the on-craton 1107 Ma Borgmassivet Suite sills (this study and Krynauw, 1986) and the contemporaneous Umkondo dolerites (Munyanyiwa, 1999) as well as two geochronologically distinct groups of amphibolite dykes from the Heimefrontfjella (Bauer et al., 2003) in the southernmost part of the Maud Belt.

Major and some trace element concentrations, excluding the REE, were determined by conventional x-ray fluorescence spectrometry (XRF) on a Philips X'Unique II PW1480 spectrometer (see Appendix 4) following the techniques described by Duncan et al. (1984) and le Roex (1985). Typical detection limits are below 0.01 wt% and 2 ppm for the major and trace elements, respectively. Concentrations of other trace elements, including the REE (Table 11), were determined by inductively coupled plasma mass spectrometry (ICP-MS) using a Perkin Elmer/ Sciex Elan 6000 mass spectrometer (see Appendix 4) following the methods described by Frimmel et al. (2001). Sr- and Nd - isotope ratios (Tables 12) were measured on a VG Sector 7-collector mass spectrometer in multi-dynamic mode, following the standard chemical separation techniques described by le Roex and Lanyon (1998). The model ages are discussed according to DePaolo (1981) and the decay constant 6.54×10^{-12} was used for the decay of ^{147}Sm (Lugmair and Marti, 1978), whereas a decay constant 1.42×10^{-11} was used for ^{87}Rb (Steiger and Laeger, 1977). The chondritic uniform reservoir (CHUR) and depleted mantle values of respectively Jacobsen and Wasserburg (1980), i.e., $^{143}Nd/^{144}Nd = 0.512638$ and $^{147}Sm/^{144}Nd = 0.1967$, and Michard et al. (1985), i.e. $^{143}Nd/^{144}Nd = 0.513114$ and $^{147}Sm/^{144}Nd = 0.222$, were used for the

Table 11. Whole rock geochemical analyses of metabasites from Nashornkalvane (eastern Grunehogna Craton) and Straumsvola (western Maud Belt)

Location	Nashornkalvane			W.H.U.S	W.H.U.S	W.H.U.S	W.H.U.S	W.H.U.S	W.H.U.S	W.H.U.S	W.H.U.S	W.H.U.S	W.H.U.S	W.H.U.S
Rock	dolerite	dolerite	dolerite	amphib.	amphib.	amphib.	amphib.	amphib.	amphib.	amphib.	amphib.	amphib.	amphib.	amphib.
Sample	EG-N1	EG-N2	EG-N3	EG-16	EG-23	EG-26	EG-28	EG-30	EG-21B	EG-21A	EG-31	EG-32	EG-22	EG-24
SiO_2	50.52	51.05	51.57	48.38	46.07	43.18	47.69	48.46	47.90	48.43	48.77	49.17	48.76	50.81
Al_2O_3	14.50	14.39	14.90	13.41	14.74	12.62	13.82	14.24	12.59	13.22	14.31	15.02	15.02	14.37
FE2O3	11.78	11.42	10.58	16.68	15.28	17.92	13.26	14.91	17.55	18.06	13.17	14.55	13.91	11.86
FeO*	10.60	10.28	9.52	15.01	13.75	16.13	11.93	13.41	15.79	16.25	11.85	13.10	12.52	10.67
CaO	10.77	10.61	11.23	10.13	7.67	8.28	10.61	9.56	9.08	8.28	10.05	8.59	8.61	9.29
MgO	5.90	5.81	5.94	5.91	7.63	5.04	6.77	5.94	5.04	4.98	6.67	5.76	5.63	6.51
Na_2O	1.72	1.85	1.80	1.91	2.66	2.18	3.04	2.94	2.10	2.72	2.99	3.36	3.68	3.37
K_2O	1.12	1.08	0.94	0.52	2.44	2.24	0.64	0.81	1.40	0.92	0.69	0.88	1.20	0.73
MnO	0.19	0.19	0.17	0.23	0.17	0.33	0.21	0.20	0.24	0.25	0.19	0.19	0.19	0.17
TiO_2	0.86	0.83	0.75	1.71	1.38	4.21	1.75	1.31	2.25	2.37	1.76	1.30	1.38	0.95
P_2O_5	0.11	0.10	0.10	0.21	0.16	2.35	0.21	0.17	0.28	0.28	0.20	0.16	0.16	0.11
H_2O-	0.09	0.09	0.05	0.08	0.19	0.14	0.09	0.09	0.19	0.11	0.08	0.04	0.06	0.33
LOI	1.62	1.62	1.50	0.45	0.64	0.52	1.27	0.39	0.70	0.31	0.47	0.59	0.42	0.68
TOTAL	99.20	99.06	99.57	99.64	99.08	99.01	99.44	99.05	99.35	99.95	99.42	99.68	99.09	99.22
Mg#	0.50	0.50	0.53	0.41	0.50	0.36	0.50	0.44	0.36	0.35	0.50	0.44	0.44	0.52
V	251	248	244	296	269	101	311	260	378	n.d.	320	263	280	263
Cr	110	97	132	121	148	3	140	135	110	n.d.	152	126	129	112
Ni	98	97	108	83	115	6	71	110	52	42	77	109	105	83
Co	45	44	43	59	56	34	45	51	41	n.d.	47	50	51	49
Sc	32	31	33	37	27	15	33	27	38	46	34	27	32	34
Cu	73	101	70	114	178	37	89	239	90	42	141	178	106	64
Pb	12	25	11	7	10	6	3	5	9	8	4	10	14	8
Zn	103	151	93	125	135	137	120	127	168	136	97	98	106	103
Cs	1	1	1	0	11	4	0	1	1	n.d	0	1	2	0
Rb	40	38	39	9	89	81	18	21	35	25	10	21	27	13
Sr	165	157	157	177	171	754	298	159	130	140	246	204	175	228
Ba	272	250	217	79	337	1267	133	141	225	102	86	149	151	108
Th	5	5	4	1	2	8	5	2	2	6	1	2	2	2
U	1	1	1	0	1	1	0	1	1	n.d	0	1	1	1
Ta	0	0	0	0	0	2	0	0	1	n.d	0	0	1	0
Nb	5	5	5	7	7	36	11	6	9	9	8	6	8	5
Zr	111	108	103	113	133	177	121	124	180	190	116	117	125	98
Y	21	20	19	25	25	56	38	26	43	55	24	26	29	21
Hf	2	2	2	1	1	0	0	1	1	n.d	1	1	1	1
La	15.67	14.47	14.17	8.83	12.91	55.62	9.16	13.76	14.42	n.d	9.27	11.52	13.23	10.21
Ce	33.12	31.33	30.26	22.13	28.33	141.28	24.20	29.18	33.65	n.d	22.65	25.90	30.12	22.54
Pr	3.79	3.58	3.48	3.02	3.52	18.93	3.54	3.57	4.46	n.d	3.13	3.19	3.70	2.78
Nd	15.86	15.09	14.48	14.77	15.82	90.28	18.31	15.75	21.28	n.d	15.17	14.34	16.46	12.55
Sm	3.35	3.24	3.10	3.80	3.89	18.24	5.58	3.71	5.74	n.d	3.87	3.52	3.92	2.98
Eu	0.95	0.96	0.89	1.36	1.19	7.13	1.80	1.20	1.84	n.d	1.36	1.20	1.24	0.99
Gd	3.78	3.64	3.52	4.67	4.71	17.05	6.90	4.51	7.48	n.d	4.67	4.44	4.58	3.53
Tb	0.60	0.58	0.56	0.74	0.74	2.18	1.11	0.74	1.21	n.d	0.72	0.71	0.75	0.57
Dy	3.90	3.80	3.74	4.84	4.80	11.90	7.06	4.96	8.06	n.d	4.62	4.73	5.14	3.88
Ho	0.82	0.80	0.76	1.00	1.00	2.16	1.42	1.05	1.69	n.d	0.94	0.99	1.07	0.81
Er	2.33	2.27	2.21	2.83	2.81	5.60	4.01	3.04	4.88	n.d	2.62	2.92	3.20	2.36
Tm	0.34	0.34	0.31	0.41	0.41	0.75	0.56	0.44	0.71	n.d	0.37	0.42	0.47	0.34
Yb	2.18	2.12	2.03	2.61	2.62	4.43	3.46	2.85	4.68	n.d	2.35	2.76	3.20	2.21
Lu	0.32	0.31	0.29	0.39	0.39	0.55	0.48	0.43	0.70	n.d	0.35	0.41	0.48	0.33

FeO* = All Fe as FeO.

W.H.U.S = Straumsvola in western H.U.Sverdrupfjella. amphib. = amphibolite.

calculation of the Sm-Nd model ages and the ϵ_{Nd} values.

Table 12. Rb-Sr and Sm-Nd isotopic data for mafic rocks from Nashornkalvane and Straumsvola

Sample	Rb (ppm)	Sr (ppm)	$^{87}Sr/^{86}Sr$	error (2-sigma)	Sm (ppm)	Nd (ppm)	$^{143}Nd/^{144}Nd$	error (2-sigma)
EG-N1	39.56	165.40	0.72265	0.0029	3.35	15.86	0.51182	0.0009
EG-N2	37.74	157.16	0.72315	0.0017	3.24	15.09	0.51181	0.0008
EG-N3	38.66	157.39	0.72271	0.0025	3.10	14.48	0.51182	0.0009
EG-032	21.26	203.55	0.71969	0.0017	3.52	14.34	0.51172	0.0009
EG-030	21.24	159.18	0.71538	0.0016	3.71	15.75	0.51173	0.0021
EG-021b	35.38	129.78	0.72859	0.0017	5.74	21.28	0.51208	0.0009
EG-022	27.18	175.36	0.72303	0.0019	3.92	16.46	0.51150	0.0010
EG-026	80.68	753.63	0.71755	0.0020	18.24	90.28	0.51175	0.0009

Major and trace element concentrations of most of the western H.U. Sverdrupfjella amphibolites are very similar to that of the Nashornkalvane sill samples. SiO_2 contents for the Nashornkalvane sill samples are about 51 wt%. SiO_2 concentrations for the amphibolites range between 43.18 and 50.81 wt%. The Mg number (Mg #) for the Nashornkalvane samples is about 51 wt%, within the range of that for the amphibolites (0.35 – 0.52 wt%). The influence of metasomatism on major element and trace element mobility is discussed in a subsequent section.

The Zr/TiO_2 and Nb/Y ratios of the Nashornkalvane sill samples are about 0.013 and 0.191, respectively. With the exception of amphibolite sample EG-26, the Zr/TiO_2 and Nb/Y ratios of the Straumsvola western H.U. Sverdrupfjella amphibolites are similar ranging between 0.007 – 0.010 and 0.167 – 0.321, respectively. Sample EG-26 displays a low Zr/TiO_2 ratio of 0.004 (mainly due to its much higher TiO_2 concentration of 4.21 wt%) and a high Nb/Y ratio of 0.520. This sample also differs in that it has much lower concentrations of Ni, Cu, Co and V but higher Ba (1267 ppm) and Sr (754 ppm) contents. The REE patterns displayed by the Nashornkalvane samples is characterized by $(La/Yb)_N$ ratios of between 5.20 and 4.66 and a small negative Eu anomaly. The Straumsvola western H.U. Sverdrupfjella amphibolites have similar REE patterns with overlapping $(La/Yb)_N$ ratios, which range from 4.79 to 2.44. Amphibolite sample EG-26 has the highest $(La/Yb)_N$ ratio of 9.

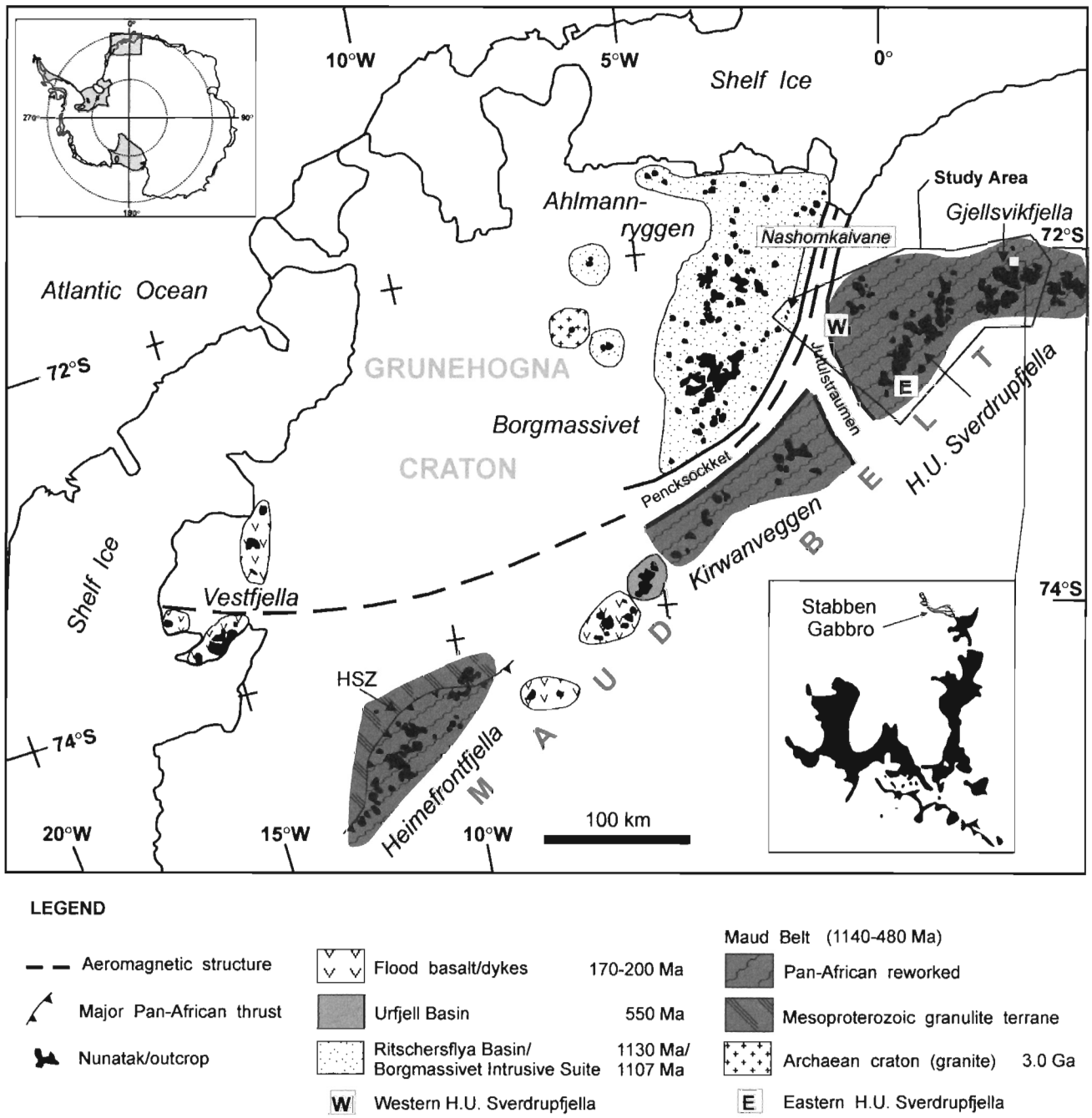

Fig. 16. Tectonic map of Western Dronning Maud Land, (after Board et al., 2005) showing the study area and the various sample localities.

8.2 Major element distribution

The major element compositions of the Nashornkalvane sill, other Borgmassivet Suite mafic sills (Krynauw, 1986) and the amphibolites in the Maud Belt are shown on an AFM diagram, with the majority of the mafic rocks showing an overall tholeiitic trend (Fig. 17a). Although some of the amphibolites plot in the calc-alkaline field, their higher Na_2O and K_2O concentrations are possibly due to alkali metasomatism during high-grade metamorphic overprint. Consequently, the major element distribution is not considered helpful in the characterization of the high-grade amphibolite samples. The increase in Na_2O and K_2O concentrations and greater spread in data points appears to be exemplified by the samples from the Gjelsvikfjella. The Straumsvola amphibolite sample EG-26, from the western H.U. Sverdrupfjella, is distinguished in that it has the highest TiO_2 concentration (4.21 wt%).

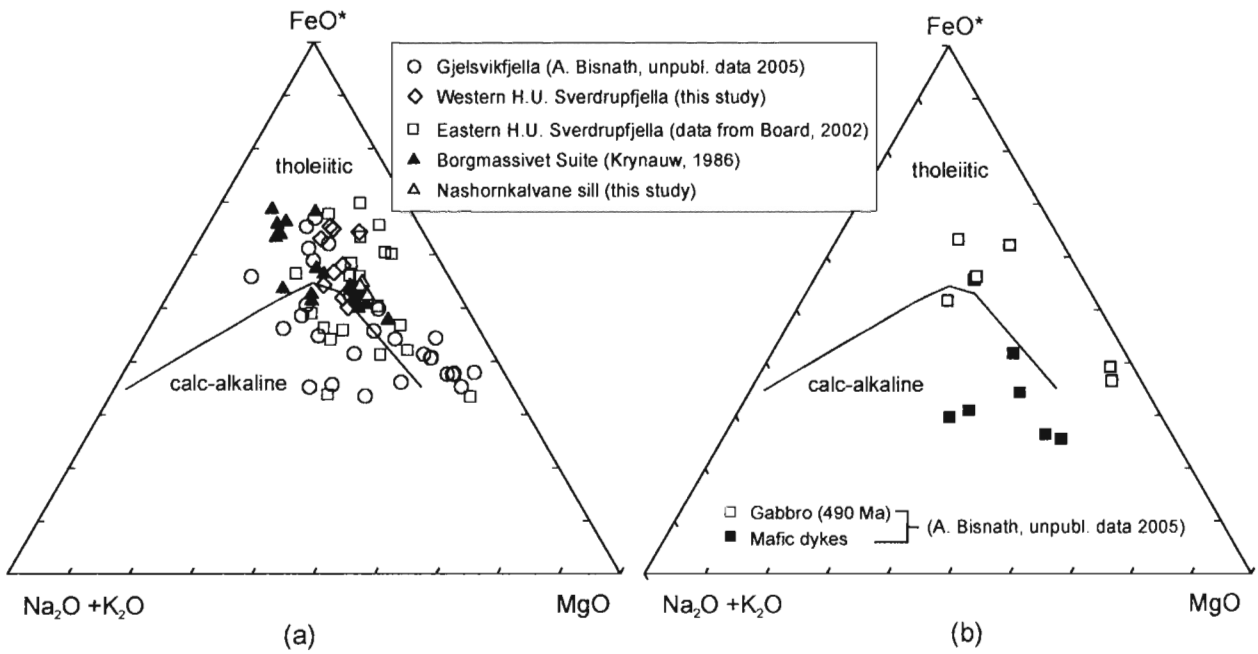

Fig. 17. AFM diagram for (a) 1107 Ma Borgmassivet Suite sills on the Grunehogna Craton and the Maud Belt amphibolites, and (b) post-tectonic 490 Ma Stabben Gabbro and mafic dykes from the Gjelsvikfjella.

The post-tectonic Stabben gabbro displays a tholeiitic trend, whereas the dykes follow a calc-alkaline trend on an AFM diagram (Fig. 17b).

8.3 Trace element distribution

The Nashornkalvane sill has Zr/TiO_2 and Nb/Y ratios of 0.013 and 0.191, respectively, plotting on the boundary between the andesite and andesite/basalt fields in the diagram of Winchester and Floyd (1977). The Zr/TiO_2 (0.01-0.07 ppm) and Nb/Y (0.024-0.885 ppm) ratios of most Maud Belt amphibolite samples are similar (Fig. 18), although many classify as sub-alkaline basalts on this diagram. The wide scatter in the Gjelsvikfjella amphibolite data may be a metamorphic effect whereby even the high-field strength elements (HFSE) became mobile during their polymetamorphic history (see discussion below).

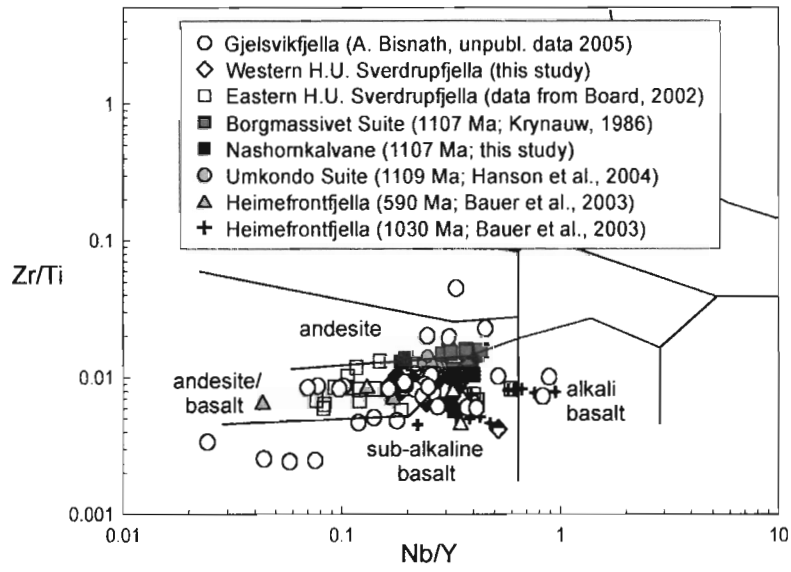

Fig. 18. Zr/TiO_2 versus Nb/Y diagram (after Winchester and Floyd, 1977) for the mafic rocks from Western Dronning Maud Land.

Compared to most of the other amphibolites, a number of samples contain significantly higher large-ion lithophile (LILE) and HFSE concentrations (Figs. 19a-g.). The samples from Gjelsvikfjella, ABA-63, ABA-70, AB-31A, AB-40A, AB-41A, for example, have high concentrations of Cs, Rb, Sr, Nb and Y (Fig. 19a-g.). A similar enrichment in Nb and Y is seen in samples from the H.U. Sverdrupfjella (e.g. WB-109, EG-26). Six samples from the Gjelsvikfjella (ABA-22, AB-7A, AB-9A, AB-13A, AB-33A, AB-38A) are distinguished by their high Zr (280-831 ppm), TiO_2 (> 3.3 wt%) and P_2O_5 (>0.57 wt%) concentrations.

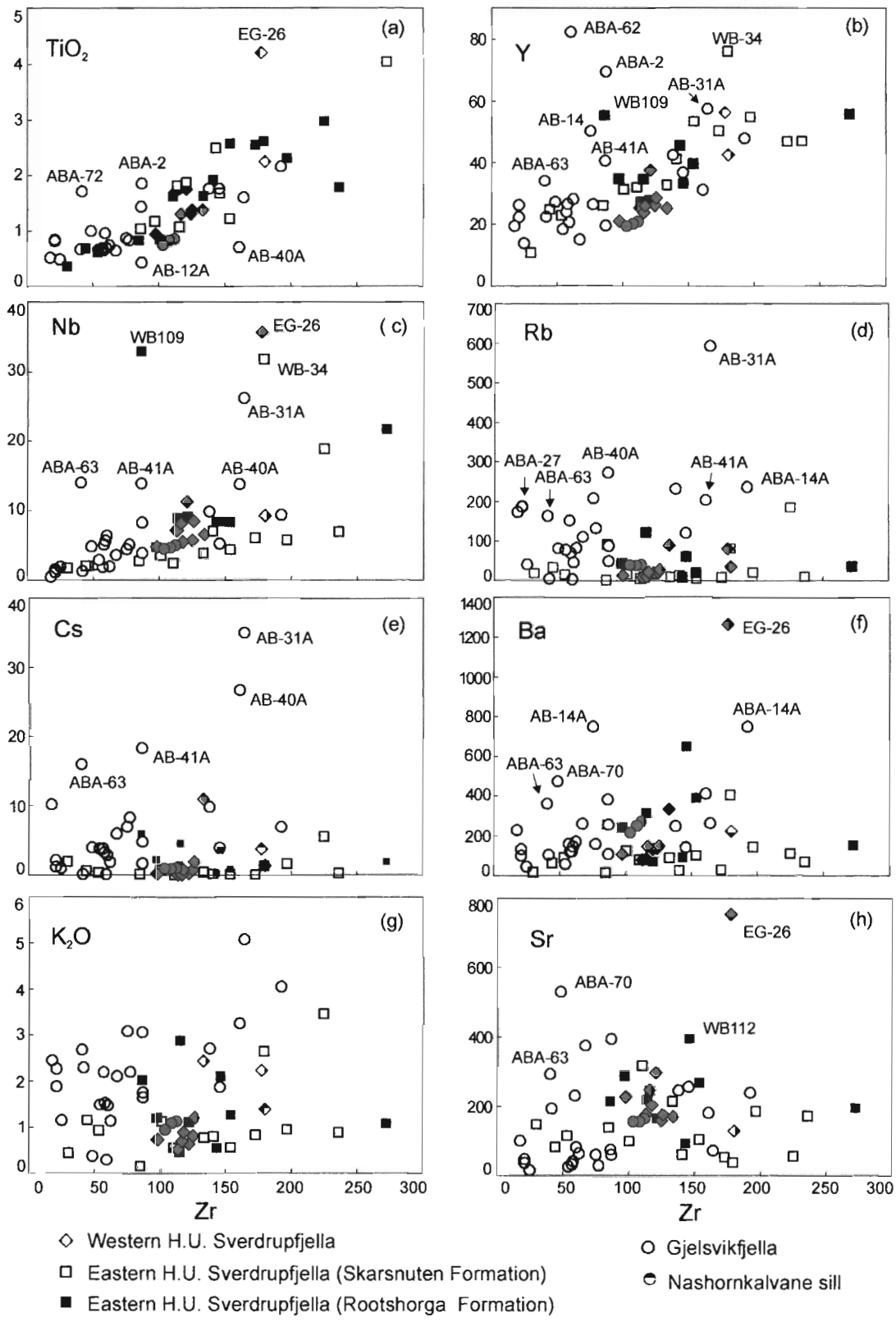

Fig. 19. Major and trace element versus Zr plots distinguishing between the effects of possible magmatic fractionation and remobilization of elements during high-grade metamorphism (For data sources see Fig. 19).

Amphibolite samples with high proportions of amphibole (70 - 95 vol%) from that area have high Ni (262-522 ppm) and Cr (up to 1304 ppm) contents, probably reflecting accumulation of mafic igneous phases, such as olivine.

The Nashornkalvane sill has a chondrite-normalized REE pattern identical to the REE patterns for the Borgmassivet Suite mafic sills. These sills have LREE enriched patterns, with $(La/Yb)_N$ ratios between 5.20 and 4.66 and weak negative Eu anomalies (0.81-0.85; Fig. 20a). The REE patterns of the two amphibolite groups from the Heimefrontfjella are shown separately for comparision (Fig. 20h). The $(La/Yb)_N$ ratios of between 4.79 and 1.67, total REE abundances and weak or absent Eu anomalies (0.85 - 0.99) displayed by the H.U. Sverdrupfjella amphibolites are similar to the REE patterns of the Borgmassivet sills (Fig. 20d,e,f). Sample EG-26 (with the highest TiO2 concentration of 4.21 wt%), from the western H.U. Sverdrupfjella, differs in that it displays the highest $(La/Yb)_N$ ratio of 9 relative to all other amphibolites in this study (Fig. 20d). Amphibolite sample WB-109, taken from a shear zone with abundant quartz veins in the eastern H.U.Sverdrupfjella, displays a shallow, concave upward LREE pattern with a $(La/Yb)_N$ = 1.20 (see Fig. 22a and later discussion on REE mobility). As this sample was taken from a shear zone, its elevated Nb and Y concentrations could reflect metasomatic alteration due to fluid/rock interaction. Thus, the concave upward LREE-depleted pattern may indicate a high fluid/rock ratio and LREE mobility during metamorphism (Grauch, 1989; Fig. 22a). Four other samples (WB-20, WB-64, AB-39A, AB-16A; Fig. 22a) from different parts of the belt also show a similar LREE-depleted, concave upward pattern. The $(La/Yb)_N$ ratios of the remaining amphibolites from the H.U. Sverdrupfjella decrease with distance from the craton margin (Fig. 20d,e,f) from ratios between 4.79 and 2.44, overlapping with those from the Borgmassivet Sill, in the western part of the belt to ratios between 2.45 and 1.67 in its eastern part.

More than one type of pre-Pan-African REE profile is identified in the Gjelsvikfjella amphibolite sample set. Six samples from this area (AB-7A, AB-9A, AB-13A, AB-33A, AB-38A, ABA-22) show high overall enrichment in REE relative to all other samples (excluding the EG-26) and correspond to the six samples identified as having the highest Zr concentrations (Fig. 20g). Three other samples from this part of the belt (ABA-2; ABA-62 and ABA-63) display flat

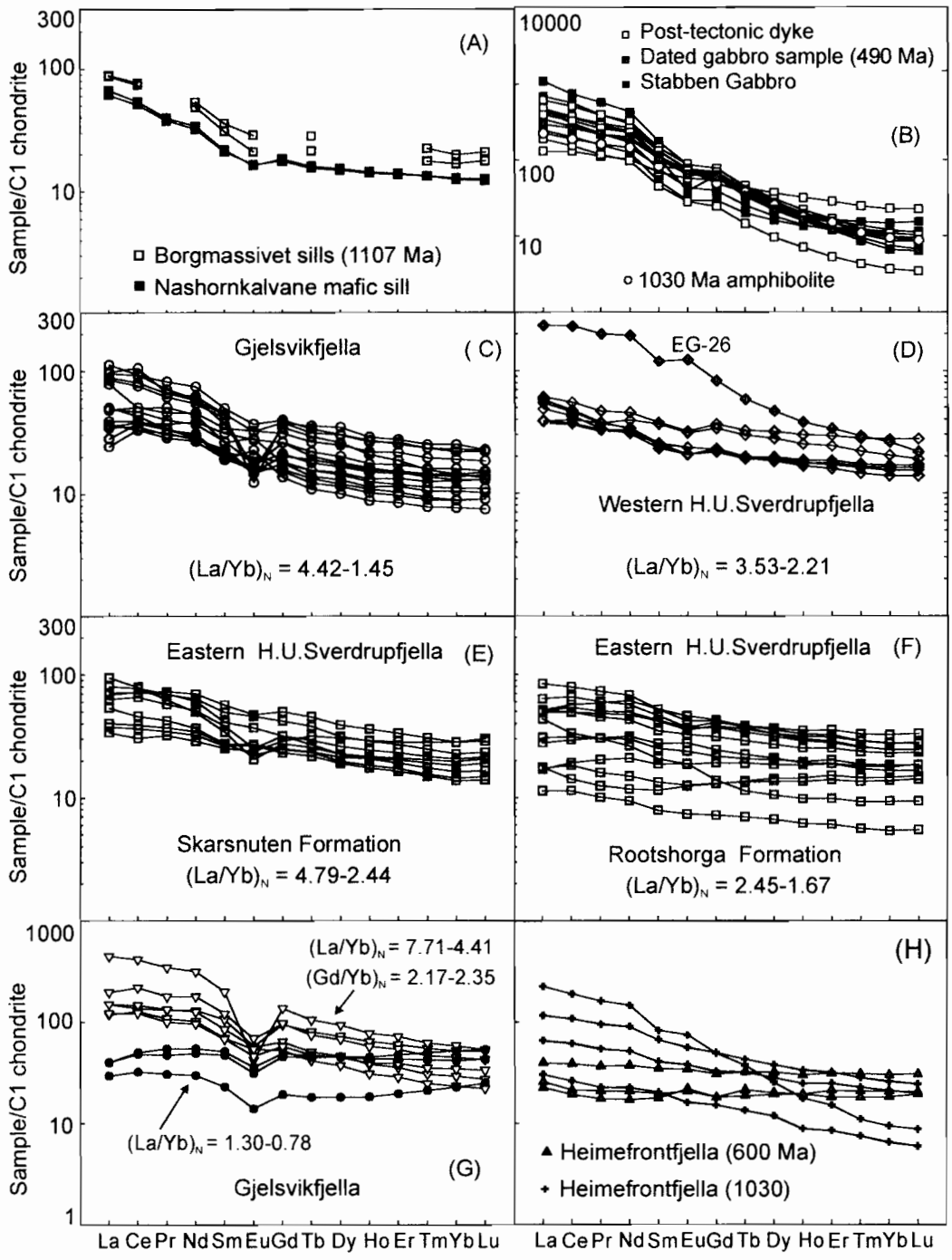

Fig. 20 REE patterns of mafic rocks included in this study from Western Dronning Maud Land normalized to the C1 chondrite (Sun and McDonough, 1989). Note that the Nashornkalvane mafic sill (this study) on the easternmost margin of the craton has a REE pattern identical to the data available (Krynauw, 1986) for the 1107 Ma Borgmassivet Suite mafic sills (a). The REE patterns of post-tectonic mafic intrusions (A. Bisnath, unpubl. data 2005) are shown in (b). The majority of the amphibolites of unknown age (c-f) from the Maud Belt (A. Bisnath, unpubl. data 2005; Board, 2002; this study) compare well with the on-craton 1107 Ma Borgmassivet Suite sills sharing a similar LREE enriched pattern. Some amphibolites from the Gjelsvikfjella (A. Bisnath, unpubl. data 2005) differ in that they show overall enrichment in REE or much flatter profiles to the rest (g). Heimefrontfjella 1030 Ma and 600 Ma amphibolite groups (h; data from Bauer et al., 2003).

REE patterns with the lowest $(La/Yb)_N$ ratios (1.30, 0.96 and 0.78; Fig. 20g). Except for a larger variation in Eu anomaly, the remaining Gjelsvikfjella samples have REE patterns with $(La/Yb)_N$ ratios of 4.42 to 1.45 and overall REE abundances similar to those in the eastern and western H. U. Sverdrupfjella (Fig. 20c) and to those of the Borgmassivet Suite sills. Samples AB-11A and AB-12A have a small positive Eu anomaly and are probably reflecting accumulation of plagioclase, as indicated by a high proportion of plagioclase (70-85 vol%) in these inferred cumulate sills.

8.4 The influence of high-grade metamorphism and metasomatism

Low-grade hydrothermal/metamorphic alteration (e.g. Pearce and Cann, 1973; Pearce, 1975, 1976; Frey, 1983) or processes related to high-grade metamorphism, such as partial melting, dehydration and fluid-rock interaction (e.g. Sawyer, 1991; Zaleski and Pattison, 1993; Kretz, 1994; Bingen et al., 1996) may all contribute to severely affecting the composition of the precursor rock. Some element mobility in the mafic rocks from western Dronning Maud Land has to be expected, because they experienced two high-grade metamorphic episodes. In this section, to evaluate the influence of secondary processes, element mobility is assessed by plotting HFSE correlation diagrams and HFSE against LILE concentrations.

The Zr/Y vs Zr diagram of Pearce and Norry (1979) is conventionally used to distinguish between within-plate, mid-ocean ridge and island-arc basalts. The nature of this diagram (element ratio against element) may be used to identify samples, which have experienced metasomatism as any loss or gain of Zr would result in data plotting along a straight line with positive slope. Six samples from Gjelsvikfjella are enriched in Zr on this diagram (Fig. 21), whereas many of the remaining amphibolite data points scatter away from the general cluster and appear to show a depletion in Zr. Sample AB-39A displays a severe depletion in Zr and LREE (Fig. 21; Fig.22a,). A metasomatically altered sample (WB-109), taken from a shear zone in the eastern H.U. Sverdrupfjella, is also characterized by a REE pattern with a very gentle slope and a concave-upward LREE profile as well as an enrichment in Nb and Y (Fig. 22a; Fig. 19b,c), unlike the majority of the less altered samples, which have moderate LREE-enriched patterns. By analogy with sample AB-39A, WB-109 most likely also suffered Zr-loss (together with Y-enrichment as seen in Fig. 19b) explaining its position on the Zr/Y versus Zr diagram (Fig. 21).

In many of the samples with concave-up LREE-depleted patterns, a general decrease in Zr and Zr/Y ratio is observed (e.g. WB-109, WB-20, WB-64, AB-39A, AB-16A, ABA-13A; Fig. 21; Fig. 22a) suggesting that Zr was more mobile, together with the LREEs, during high-grade metamorphism. The depletion in Zr is also supported by the Y-Zr binary plot showing only WB-109 (excluding the least equilibrated sample, WB-34) with the high Y concentration plotting away from the general trend, indicating that in this sample even Y did not remain immobile (Fig. 19b).

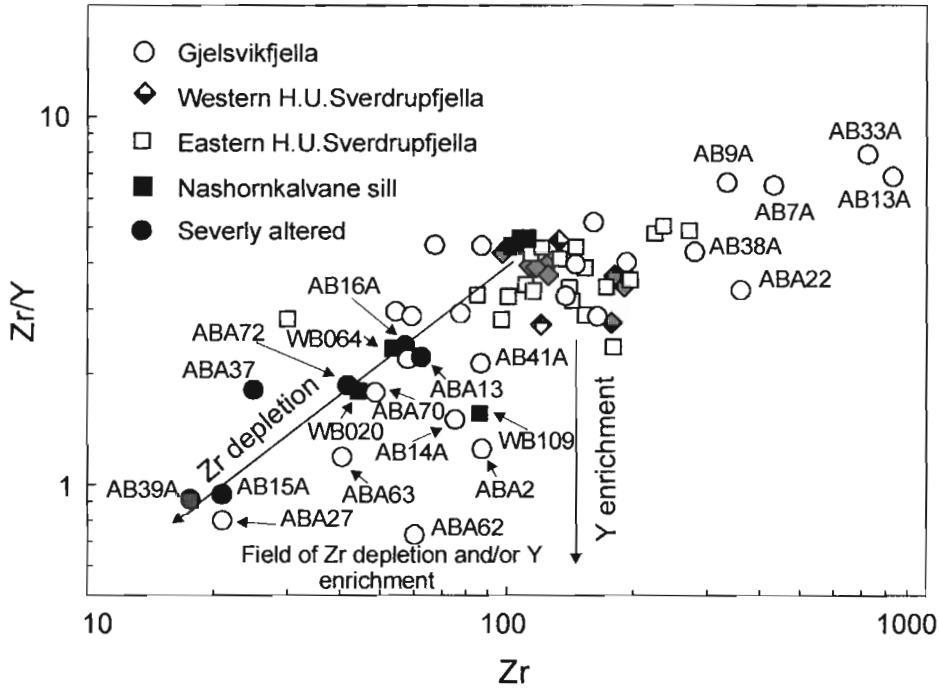

Fig. 21 Zr/Y versus Zr diagram after Pearce and Norry (1979) for mafic rocks from the Maud Belt (for data sources see Fig. 19).

A good positive correlation (r^2=0.83) between La/Yb and Zr/Y points to Zr- and LREE- depletion (mobility) having been coupled (Fig. 22d). Sample AB-39A, showing the lowest La/Yb value, also has the lowest Zr concentration. The presence of zircon overgrowths indicates at least short-range Zr mobility in high-grade metamorphic fluids. Such fluids appear to be also capable of mobilizing the LREEs. Thus, the depletion of amphibolites in both Zr and the LREEs may indicate mobility of these elements possibly as a result of dissolution of zircon grains due to chemical attack by a metamorphic fluid. Some amphibolites display greater depletion in Zr than in LREE (e.g. AB-15A), whereas others show an opposite trend. Although many

studies have shown that HFSE and REE may be mobilized by metamorphic fluids (e.g. Rudashevskiy, 1969; Ludden and Thompson, 1979; Gieré, 1986; Cathelineau, 1987), the behavior of Zr, Ti and REE in metamorphic fluids is still poorly understood. REE-, Zr- and Ti-mobility depends on a variety of factors, such as temperature, pressure and fluid composition, with higher temperatures and high activities of K^+ and/or Na^+, CO_2, B^-, F^-, PO_4^{3-} (e.g. Cullers et al., 1973; Mysen, 1979; Wendlandt and Harrison, 1979; Gieré, 1989) seeming to enhance this mobility. A LREE- and Zr-bearing metamorphic fluid derived from the amphibolites during metamorphism may have migrated to higher crustal levels, eventually being incorporated into the melt derived from partial melting of the felsic country rocks. Deposition of the trace elements may have resulted due to precipitation/crystallization of new zircon grains found in anatectic leucosome, such as those in the northeastern part of the belt where the Pan-African tectonism was most intense (Paulsson and Austrheim, 2003).

Those amphibolite samples that were most intensely altered are readily distinguished on Figure 21 (see Table 13). In general, the amphibolites from the Gjelsvikfjella are more enriched in LILE compared to those from other areas further southwest. This is interpreted to reflect an increase in metamorphic grade towards the northeast as supported by metamorphic studies (e.g. Jacobs et al., 2002; Paulsson & Austrheim, 2003). Those samples that have highly elevated Cs, Rb, Nb and Ba concentrations (Fig 19c-f) also display strong negative Eu anomalies ($Eu/Eu^* = 0.31$-0.66, Fig. 22c) suggestive of metamorphic fluid alteration. Sample AB-13A displays the strongest negative Eu anomaly ($Eu/Eu^* = 0.24$; Fig. 22c) possibly also due to metasomatism. Some amphibolite samples (e.g. WB-34, ABA-37) show both pronounced negative Eu and Ce anomalies, which may be due to basalt-seawater alteration (Fig. 22b; e.g. Ludden and Thompson, 1979). Titanium appears to have been a relatively immobile element in the amphibolites. As can be seen in the Zr versus TiO_2 plot, even the highly altered sample WB-109 plots within the fractionation trend (Fig. 19a).

In summary, the geochemical data indicate that more than one secondary process has resulted in the mobility of elements including those that are generally considered to be immobile. While Ti has remained largely immobile, metamorphic fluid alteration resulted in the depletion of Zr and the LREEs, strong relative enrichment in Nb, Y, Cs, Rb, Ba, and large negative Eu anomalies.

Seawater alteration may account for both negative Eu and Ce anomalies observed in some of the amphibolite samples.

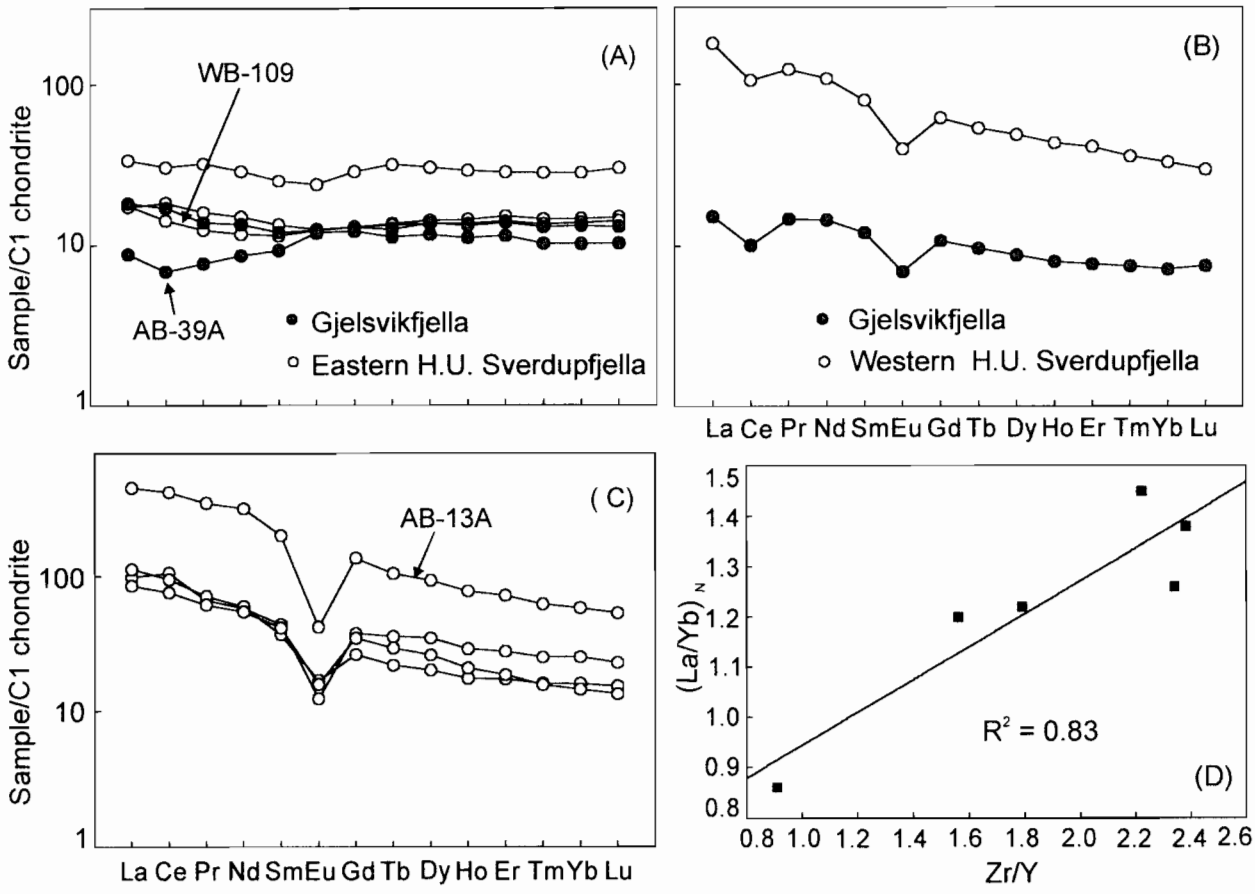

Fig. 22 REE patterns of amphibolite samples displaying evidence for secondary alteration (Gjelsvikfjella unpubl. data from A.Bisnath, 2005; eastern H.U. Sverdrupfjella data from Board, 2002; western H.U. Sverdrupfjella data from this study). Amphibolites showing concave-upward, LREE-depleted patterns due to metamorphic alteration correspond to those with severe depletion in Zr (a). Similarly, amphibolites showing pronounced negative Eu anomalies correspond to the samples also showing enrichment in 'immobile' trace elements due to metasomatism (c). The negative Ce and Eu anomalies in the REE patterns in some samples are attributed to interaction with sea-water (b). A positive correlation between Zr concentration and LREE depletion is observed in some amphibolites suggesting the mobility of these elements during high-grade metamorphism (d).

8.5 Trace element source characteristics and tectonic setting

8.5.1 Pre-tectonic mafic intrusions

Notwithstanding the effects of element mobility during metamorphism on the major and trace element geochemistry of mafic protolith rocks, an attempt is made to constrain, as far as possible, the source characteristics of the mafic rocks in this study, in particular with the help of relatively immobile trace elements and isotopic data. On an AFM diagram all the amphibolite data show considerable spread and overlap, indicating major element mobility during metamorphism (Fig. 17). Therefore, trace element binary and ternary plots, including the REE data, are used to compare amphibolites of unknown age to groups of amphibolites and mafic rocks for which reliable geochronological control is available. Amphibolites that have experienced metasomatism (Table 13) are shown separately in plots of all data in the trace element discrimination diagrams (e.g. Fig. 23b). Similarly, for the purpose of clarity, the Gjelsvikfjella amphibolite samples, distinguished from the majority by differences in their REE chemistry, are also shown separately on these diagrams.

The Nashornkalvane and other Borgmassivet Suite sills, as well as the Umkondo dolerites, form a tight cluster in the within-plate tholeiite and volcanic arc basalt field on the Nb-Zr-Y tectonic diagram of Meschede (1986; Fig. 23a). Most of the 1030 Ma amphibolite dykes from the Heimefrontfjella also plot into the same fields, but are distinguished from the Borgmassivet/ Umkondo dolerites by having higher Zr concentrations. Some of these dykes conform to a within-plate alkali basalt source. A more depleted source character is indicated by the c.590 Ma dykes from the Heimefrontfjella, which plot in the E-type MORB, N-type MORB and volcanic-arc basalt fields. Excluding strongly altered samples (Fig. 23c), amphibolites of unknown age from the western and eastern H.U. Sverdrupfjella and the Gjelsvikfjella are geochemically very similar to the Nashornkalvane, Borgmassivet and Umkondo dolerites (Fig. 23d). The Straumsvola western H.U. Sverdrupfjella and Gjelsvikfjella amphibolites overlap strongly with the Nashornkalvane and Umkondo dolerites, although some plot in the N-MORB and volcanic-arc field (Fig. 23d). Amphibolite sample EG-26 differs from all the other samples by having a particularly high Nb concentration. Those samples from the eastern H.U. Sverdrupfjella straddle the boundary between the within-plate and volcanic arc and N-type MORB and volcanic arc fields, with the majority plotting in the more depleted N-MORB and volcanic arc fields. A simi-

Table 13. Amphibolites in the Maud Belt which show evidence for open system chemical behaviour

Sample	LREE	Zr	Nb	Cs	Rb	Sr	Ba	Y	Ti	Eu/Eu*	Ce/Ce*
	Depletion	Depletion	Enrichment	Enrichment	Enrichment	Enrichment	Enrichment	Enrichment	Enriched	Strong	
ABA-63	Slight La										
ABA-62								(high)			
ABA-2								(high)	(low)		
AB-13A											
AB-14A											
AB-15A											
AB-31A											
AB-40A											
AB-41A											
AB-39A											
AB-16A											
ABA-27					(high)						
ABA-72									(low)		
ABA-13											
ABA-37											
ABA-70						(high)	(high)				
ABA-14A					(high)		(high)				
WBSV020											
WBSV064											
WBSV109											
WBSV034											

indicates alteration

lar situation is observed on the Ti-Zr-Y diagram of Pearce and Cann (1973; Fig. 24). With the exception of EG-26, distinguished as a high-Ti amphibolite, all the amphibolites of unknown age follow a trend away from the Borgmassivet and Umkondo sills in the calc-alkaline field to the more depleted MORB field. The strong within-plate to transitional MORB signature

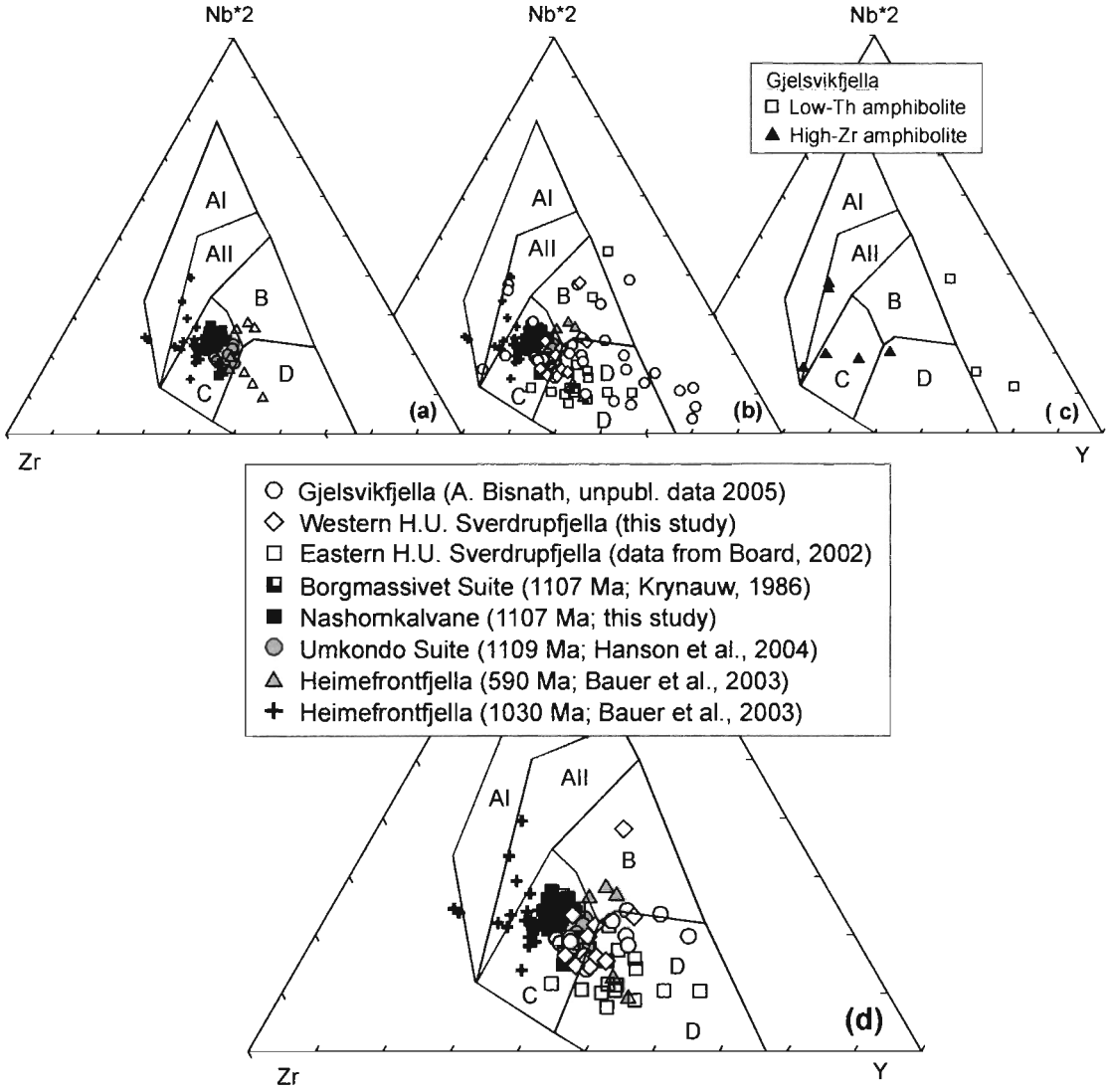

Fig. 23. Nb-Zr-Y diagram after Meschede (1986), data fields include: within-plate alkaline basalts (AI + AII), within-plate tholeiites (AII + C), P-MORB (B), N-MORB (D), volcanic arc basalts (C + D). Amphibolite dykes and mafic sills of known age are shown on this diagram (a). All data for amphibolites in this study of unknown age are compared (b, d). Samples of unknown age from the Gjelsvikfjella with differences in REE chemistry and those, which have been affected by metamorphism are shown separately of this diagram in (c) and (b), respectively.

and similarity in tectonic setting between the on-craton mafic sills and the amphibolites in the Maud Belt, particularly those in the western H.U. Sverdrupfjella, is also reflected in the Zr/Y versus Zr diagram of Pearce and Norry (1979), thereby suggesting the same active continental margin setting for these mafic rocks (Fig. 21).

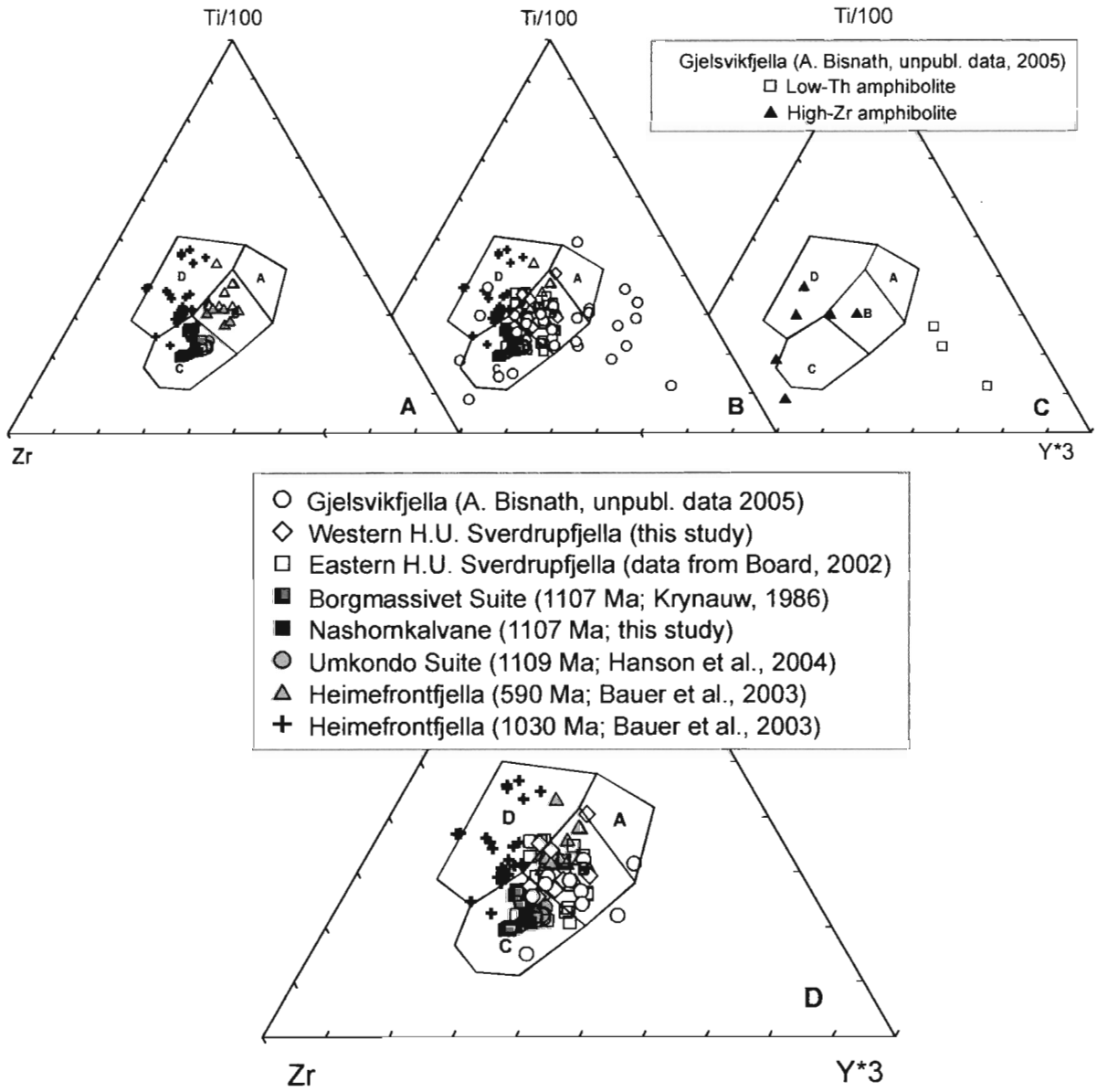

Fig. 24 Zr-Ti/100-Y*3 diagram after Pearce and Cann (1973), data fields include: island arc tholeiites (A), MORB, island arc tholeiites and calc-alkali basalts (B), calc-alkali basalts (C), within-plate basalts (D). As in Fig. 24, amphibolites of unknown age are compared to those, which have been dated (b, d). Samples with different REE patterns and those showing evidence for fluid remobilization are shown separately in (c) and (b), respectively.

Although the c.590 Ma amphibolite dykes in the Heimefrontfjella cannot be separated from some of the amphibolites in this study in the above tectonic discrimination diagrams, they differ by displaying flat REE patterns that are typical of E-type MORB (Fig. 20h; Bauer et al., 2003). The three Gjelsvikfjella amphibolite samples with the lowest $(La/Yb)_N$ ratios also share this flat REE pattern. Secondary enrichment in Y may have displaced these amphibolites, however, from the E-type MORB and MORB fields in the above tectonic discrimination diagrams (Fig. 23c and 24c).

The amphibolite samples from the Gjelsvikfjella with particularly high Zr concentrations and strongest overall REE-enrichment are distinguished on the Zr/Y versus Zr diagram from all other amphibolite samples with data points scattering near the within-plate basalt field (Fig. 21). A within-plate geochemistry is also indicated in the other diagrams mainly by samples AB-7A and AB-9A, however, some of these REE-enriched amphibolites plot outside the various fields, whereas others appear to have a possible subduction-related signature similar to the majority of the other amphibolite samples (e.g. Fig. 23c).

In the plot of Th (non-conservative element) versus Nb (conservative element) normalized to Yb (Pearce and Peate, 1995), the majority of amphibolites are displaced above the composition of the mantle array, with almost all samples plotting in the transitional zone between the continental and intra-oceanic arc subduction-related fields (Fig. 25). The on-craton Borgmassivet and Umkondo sills have slightly elevated Th concentrations compared to the amphibolites but an identical range in Nb concentrations. The three Gjelsvikfjella amphibiolite samples with the lowest $(La/Yb)_N$ ratios also display the lowest Th/Yb ratios on this diagram and are closely associated with data for the three Neoproterozoic amphibolites from the Heimefrontfjella. The position of these amphibolites plotting within and close to the enriched mantle field in this diagram is consistent with their flat, E-type MORB REE pattern.

In the MORB-normalized diagram of Pearce (1983) and Pearce and Peate (1995) it is observed that the majority of the amphibolites from the H.U. Sverdrupfjella and Gjelsvikfjella have similar N-type MORB-normalized patterns to those of the Borgmassivet intrusives, showing a strong enrichment in Sr, K, Rb, Ba and Th and depletion in Nb and Ta (Fig. 26a-e). This type of

pattern is indicative of a subduction-zone signature produced by melting of a mantle source previously metasomatized by fluids and melts derived from a subducted oceanic crustal slab (Pearce, 1983; Pearce and Peate, 1995). However, the same LILE-enriched signature and high Th/Yb ratios can also be produced by crustal contamination of the mafic magma (Pearce, 1983; Pearce and Peate, 1995).

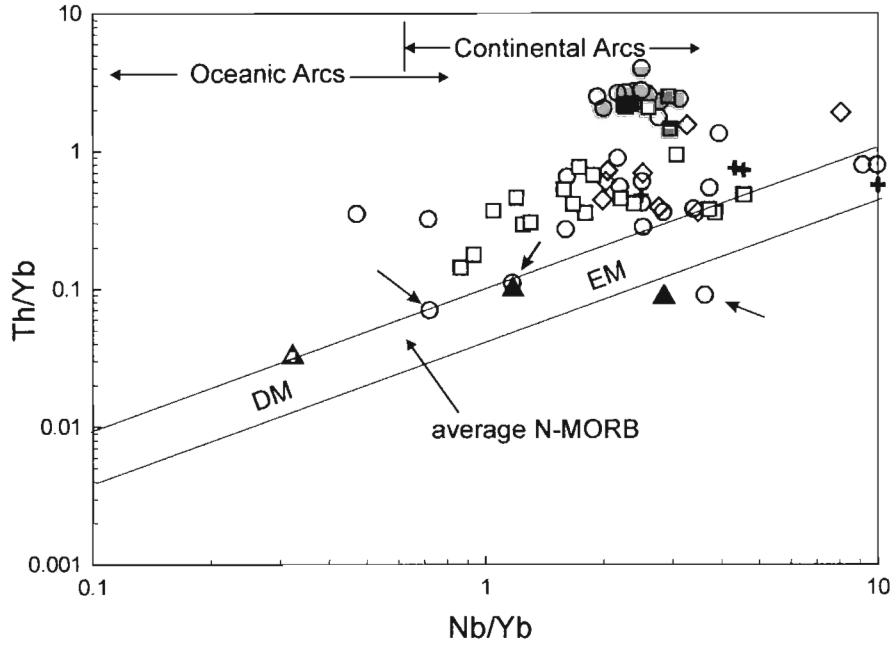

Fig. 25 Th/Yb versus Nb/Yb plot for the mafic rocks in Western Dronning Maud Land; EM = enriched mantle. DM = depleted mantle (after Pearce, 1983; Pearce and Peate, 1995). Note that most of the amphibolites in the Maud Belt and the on-craton mafic intrusives are displaced above the mantle array suggesting the influence of subduction zone metasomatism for these rocks. The three samples from the Gjelsvikfjella with the flat REE profiles plot close to the data for the c.590 Ma amphibolite dykes near the enriched mantle part of the array (For legend and data sources see Fig. 26).

A striking similarity between the Borgmassivet and Umkondo dolerites and these Maud Belt amphibolites is also reflected by the primitive mantle-normalized diagram of Sun and McDonough (1989; Fig. 27). Both the on-craton mafic sills and the amphibolites share a strong depletion in Nb, Sr, P, and Ti and enrichment in Pb (Fig. 27). These geochemical characteristics, together with a negative Eu anomaly, have been interpreted as reflecting the influence of subducted sediment in the mantle source region for mafic rocks (e.g. McLennan and Taylor, 1981; Sun and McDonough, 1989). In a Ba/Nb versus La/Nb diagram (Fig. 28; Sun and

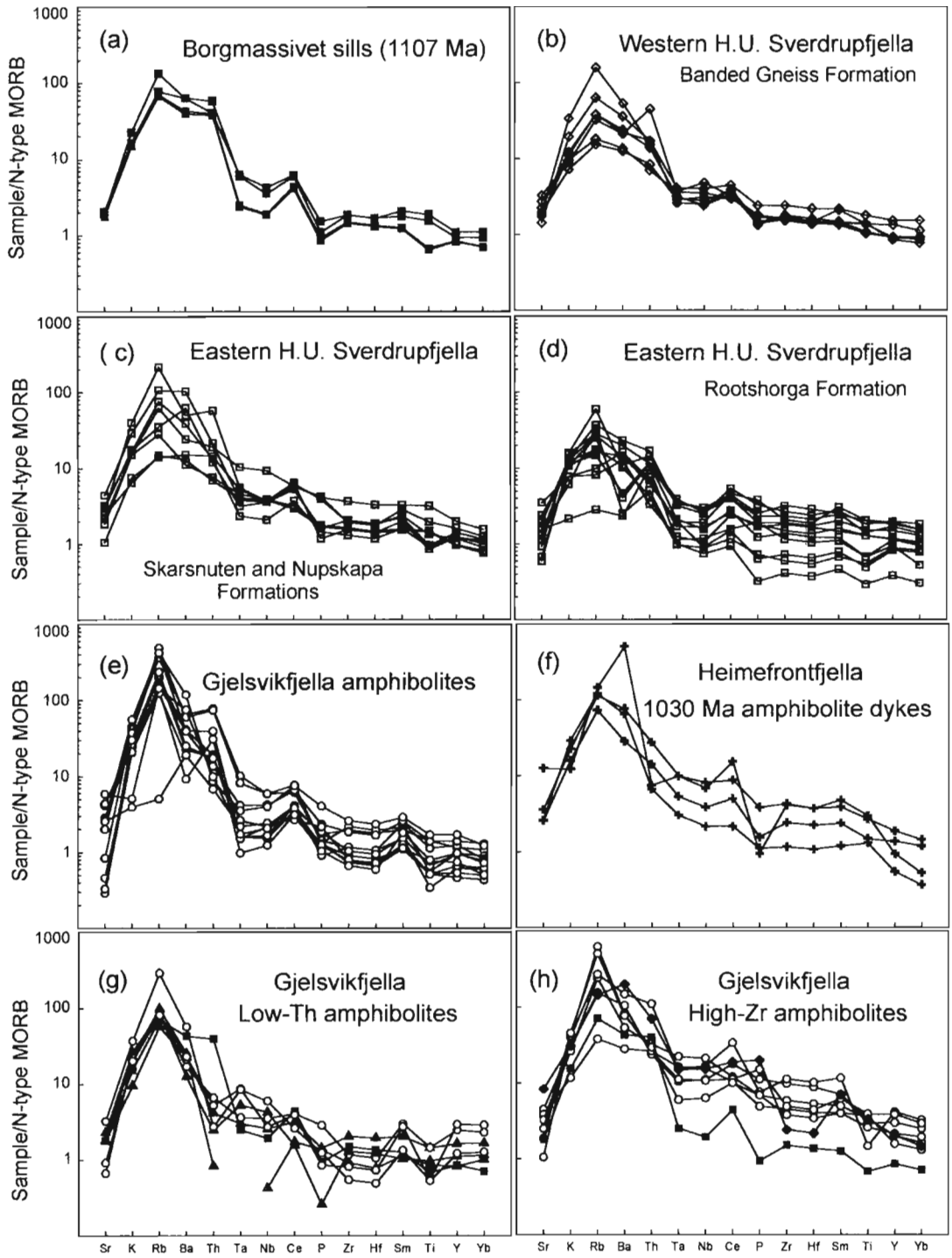

Fig. 26. N-type MORB-normalized trace element variation diagrams (after Pearce, 1983) for various amphibolites in the Maud Belt (Gjelsvikfjella unpubl. data from A. Bisnath 2005; eastern H.U. Sverdrupfjella data from Board, 2002; western H.U. Sverdrupfjella data from this study) in comparision to the Borgmassivet Suite mafic sills (this study and Krynauw, 1986) and the two groups of amphibolite dykes in the Heimefrontfjella dated at 1030 and 590 Ma (Bauer et al., 2003). Most of the amphibolites in the Maud Belt have very similar patterns to that of the Borgmassivet sills (e-f).

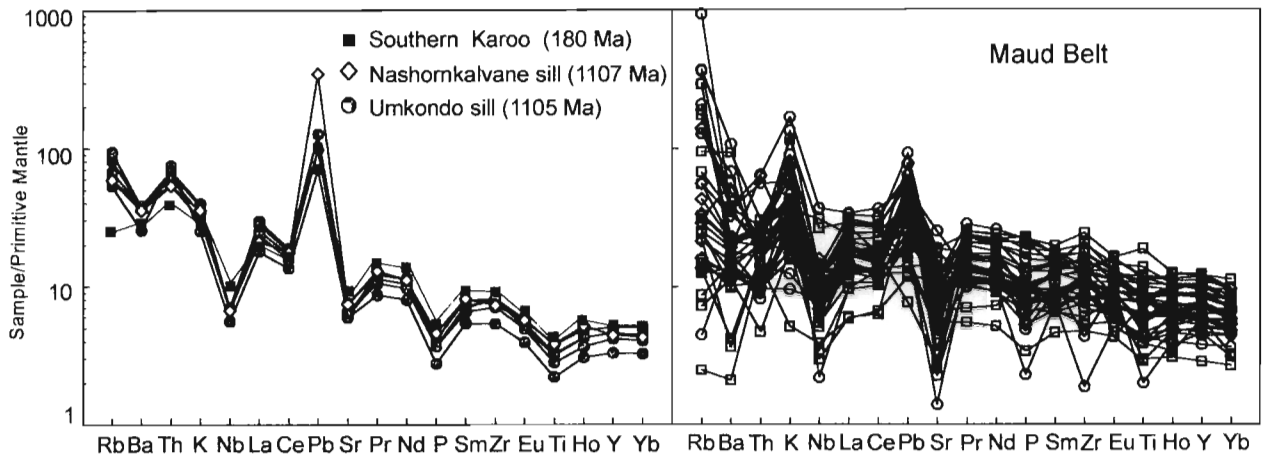

Fig. 27 Primitive mantle-normalized diagrams for the majority of the Maud Belt amphibolites (A. Bisnath, unpubl. data 2005; data from Board, 2002 and data from this study) in comparision to the Borgmassivet (this study) and Umkondo Suite (Munyanyiwa, 1999) mafic sills. Average southern Karoo basalt composition of southern Africa shown for comparision (Duncan et al., 1984).

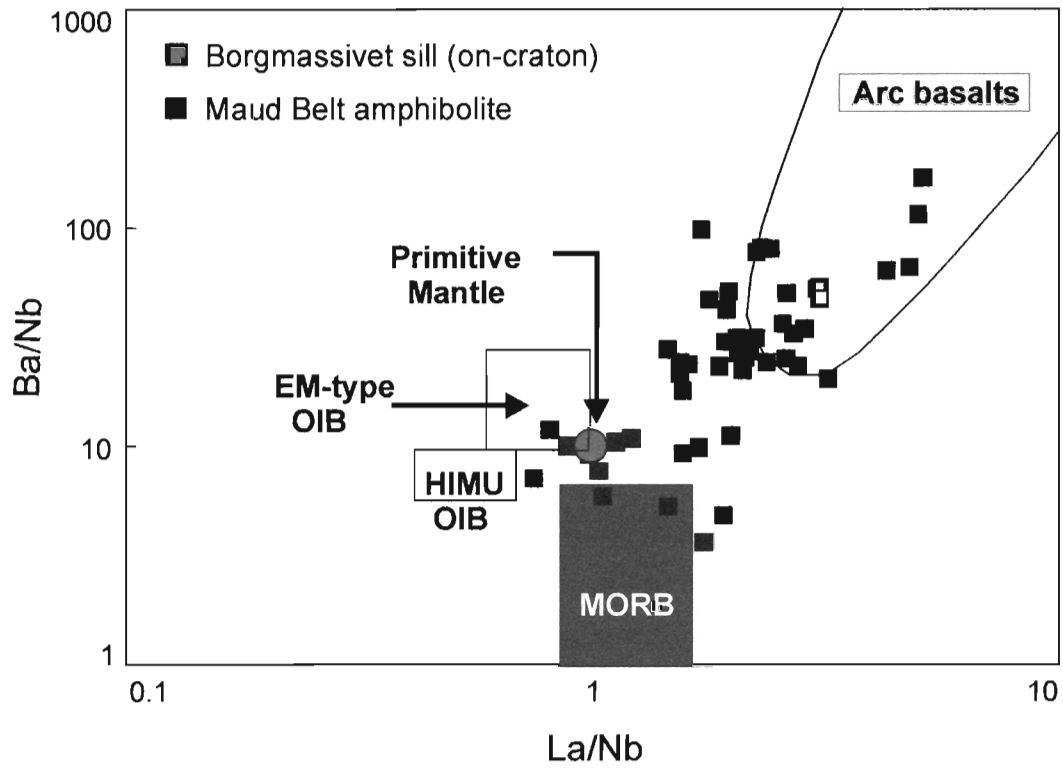

Fig. 28 Ba/Nb versus La/Nb diagram (after Sun and McDonough, 1989) for Nashornkalvane mafic sill and the amphibolites in the Maud Belt. Fields for primitive mantle, EM-type OIB = Enriched Mantle-type Ocean Island Basalt, HIMU OIB = HIMU Ocean Island Basalt, MORB = Mid-Ocean Ridge Basalt and Arc Basalts after Sun and McDonough (1989).

McDonough, 1989) a trend from the volcanic arc to the MORB field is noted. Except for a trend towards a more MORB-type chemistry for some of the amphibolites, the above analysis has shown that trace element geochemistry of the Borgmassivet Suite mafic sills and the majority of the Maud Belt amphibolites are equivocal. A true subduction-zone signature and a possible close tectonic relation between the mafic sills and amphibolites requires further investigation using isotope data. Some amphibolite samples show clear differences in trace element chemistry, such as the six samples from the Gjelsvikfjella with the highest overall REE and Zr enrichment and the three amphibolites showing the lowest $(La/Yb)_N$ and Th/Yb ratios. These amphibolites are hereafter referred to as the high-Zr and the low-Th amphibolites, respectively. Similarly, sample EG-26 from the western H.U. Sverdrupfjella with the highest $(La/Yb)_N$ ratio of 9 and highest TiO_2 concentration, is hereafter referred to as the high-Ti amphibolite.

8.5.2 Post-tectonic mafic intrusions

Major and trace element distributions of the post-tectonic mafic dykes in this study can best be best compared with volcanic arc rocks on the various tectonic discrimination diagrams (Fig. 29a-b). Stabben analyses do not conform to a typical basalt melt composition, thus precluding a meaningful comparision with the other mafic rocks studied. A very similar LREE–pattern as with the post-tectonic mafic dykes is noted, however (Fig. 20b).

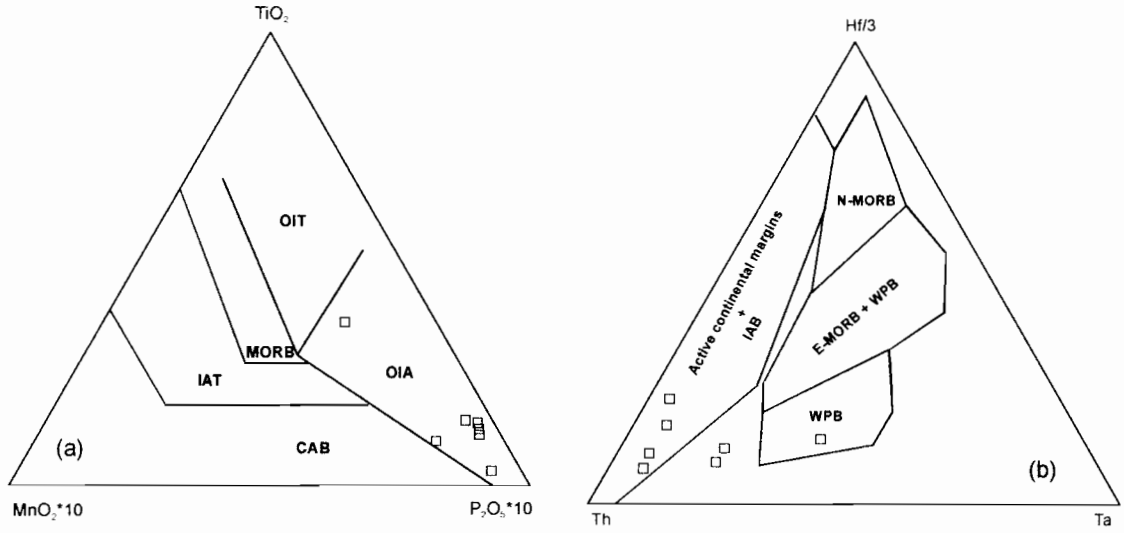

Fig. 29. Tectonic discrimination diagrams (after Mullen, 1983; Shervais, 1982; Wood, 1980) for the post-tectonic mafic dykes in the Gjelsvikfjella (A. Bisnath, unpubl. data 2005). (a) CAB = Calc-Alkaline Basalt, IAT = Island Arc Tholeiite, MORB = Mid-Ocean Ridge Basalt, OIA = Ocean Island Andesites, OIT = Ocean Island Tholeiites. (b) WPB = Within-Plate Basalt.

8.6 Influence of an 1109 Ma mantle plume in WDML?

A large-scale heat mechanism independent of crustal plate processes has been argued for to explain the widespread and short-lived on-craton magmatism between 1106 and 1112 Ma (Hanson et al., 1998; 2004). Frimmel (2004) suggested the possibility of a mantle plume interacting with the base of the sub-lithospheric mantle to have been responsible for this magmatism, with the lateral escape of heat away from the thicker roots of the Kalahari Craton leading to high-temperature, low-pressure metamorphism and extension in the surrounding mobile belts. This mantle anomaly may have interacted intermittently with the sub-cratonic mantle over a period of more than 200 myr and finally triggered the break-up of the late Meso-proterozoic supercontinent.

Although the role of a mantle plume in the generation of Large Igneous Provinces (LIP) is still a subject of debate, many workers have argued that the well-studied 180 Ma Karoo basalts on the Kalahari Craton were the result of a mantle plume that interacted with the sub-cratonic mantle leading to the break-up of Gondwana (e.g. Sweeney et al., 1991). Recently, a geochemical and geochronolgical study of an extensive suite of dolerites in the Ahlmannryggen region of the Grunehogna Craton were shown to be comtemparaneous with the Karoo dolerites of southern Africa as well as the other Mesozoic basalts in western Dronning Maud Land such as the Kirwanveggen and Vestfjell basalts (Riley et al., 2005). The data from this study supports the plume hypothesis for the generation of the Karoo-Antarctic LIP province as previously suggested (Riley et al., 2005). Given the link of the late Mesoproterozoic (1109 Ma) Borgmassivet mafic intrusions and the Mesozoic (~180 Ma) Karoo-Antarctic mafic intrusions on the Kaapvaal-Grunehogna Craton with a possible mantle plume, their geochemistry is compared in the discussion below.

To date, the source and petrogenesis of the Mesozoic Karoo basalts and its Antarctic equivalents remains problematic (e.g. Cox, 1978; Erlank et al., 1980; Cox et al., 1983; Erlank et al., 1984; Hawkesworth et al., 1984; Sweeney et al., 1991; 1994; Luttinen et al., 1998; Luttinen and Furnes, 2000; Riley et al., in press). Two fundamentally different end-member models have been suggested to explain the geochemical patterns of the Karoo basalts, which includes the

sub-lithospheric mantle source and the above mentioned mantle plume models. These two endmember models have been used to explain the occurrence of 'enriched' high-Ti-Zr basalts and the 'normal' low Ti-Zr basalts of the northern and southern Karoo Province, respectively. A heterogeneous, sub-lithospheric mantle source with two different mantle domains has been proposed for the chemical variation within the Karoo Igneous Province (Erlank et al., 1980; Cox et al., 1983; Erlank et al., 1984).

Sweeney et al. (1991; 1994), on the other hand, proposed the influence of a mantle plume to have been responsible for 'enriched' and 'normal' basalts. The high Ti-Zr basalts (and picrites) were interpreted to be derived from a depth of greater than 120-200 km (> 30-20 kbar) by mixing of two components, namely the hot, (>200°C above normal mantle temperatures) central stem of an asthenospheric plume and a thick metasomatized lithospheric 'keel'. The low Ti-Zr basalts were suggested to have been sourced from a shallower depth from depleted asthenospheric melts, which have equilibrated with thinned, sub-continental lithosphere with a similar thickness to that of continental crust (40-45 km, 13-15 kbar). Sub-lithospheric mantle regions peripheral to the thicker stable cratonic 'keel' were believed to be the source of the low-Ti-Zr southern Karoo basalts.

Furthermore, in the Ti-Y-Zr diagram of Pearce (1973), on-craton Karoo sills and basalts were found to plot firmly in the fields of calc-alkali basalts, ocean floor basalts and low-K tholeiites, rather than in the within-plate field, suggesting that their source chemistry was related to subduction zone processes (Cox, 1984). Cox (1978) suggested back-arc spreading and magmatism related to subduction beneath Gondwana along the Pacific margin as a tectonic setting required to produce the chemical characteristics of these basalts. The role of subduction zone processes in the genesis of the Karoo basalts is still not clear. This problem is exemplified in the case of the southern Karoo basalts (including the southern Lebombo and Lesotho basalts), which show high enrichment in Sr, K, Rb and Ba and low Ti. Whether this enrichment in LILE and depletion in Ti is a reflection of subduction-related metasomatism in the source or crustal contamination en route to the surface, or both, has remained an open question (e.g. Cox, 1983). Hawkesworth et al., (1984) suggested on the basis of Sm/Nd and Rb/Sr isotopic data, that the

Karoo basalts were derived from upper mantle regions that were previously enriched more than ~1.0 b.y. before the Karoo event. Such an enrichment event was interpreted to be related to subduction below the southern margin of the Kaapvaal Craton during the formation and accretion of the Proterozoic Namaqua-Natal Belt leading to the growth and stabilization of the lithospheric mantle within and around the craton. As subduction zone related magmas were considered to have negative Nb anomalies and high Sr contents (Pearce, 1983), some workers have argued that if subduction zone metasomatism has influenced the mantle source of the southern Karoo basalts, the processes responsible for the negative Nb anomalies and relatively low Sr contents of the Karoo basalts are required to be unrelated (e.g. Hawkesworth and Powell, 1980). The active subduction during the accretion of the former volcanic arcs related to the formation of the Namaqua-Natal Belt was considered a candidate responsible for the possible subduction zone metasomatism identified in the southern Karoo basalts (e.g. Hawkesworth et al., 1984). However, subsequent tectonic models for formation of the Natal Belt of southern Africa (as former oceanic island arcs) all envoked subduction directed away from the southern margin of the Kaapvaal Craton (e.g. Jacobs et al., 1993).

In a recent study, four geochemically distinct groups of Mesozoic mafic dykes were identified in the Ahlmannryggen region on the Grunehogna Craton of western Dronning Maud Land (Riley et al., 2005). Group 1 Mesozoic dykes are all low-Ti-Zr tholeiites, which is the predominant rock type throughout the Karoo-Dronning Maud Land flood basalt. Riley et al. (2005) has shown that these Ahlmannryggen dykes are geochemically similar in composition to the low Ti-Zr basalts of the Kirwanveggen (Harris et al., 1990), the chemical type 1 (CT1) basalts of Vestfjella in Antarctica (Luttinen and Furnes, 2000), and the southern Lebombo Sabie River Basalt Formation and Lesotho Basalts of southern Africa (e.g. Duncan et al., 1984). The Group 1 basalts have a characteristic negative Nb-Ta anomaly and are interpreted to represent 12% melting of the SCLM, mixed with Group 3 melts in the source,modified by assimilation of crustal material and post-magmatic alteration (Riley et al, 2005).

Group 2 dykes are low to moderate Ti-Zr rocks, which are described as being geochemically similar to the chemical type 2 or CT2 basalts of Luttinen et al. (1998) and the Rooi Rand dolerite dykes of South Africa. These basalts show very little evidence of crustal contamination.

Group 3 dykes are high Ti-Zr basalts relative to the other basalts in Ahlmannryggen area and are relatively depleted in LILE. They are regarded as an unusual magma type showing both N-MORB and E-MORB OIB type geochemical charateristics, that is from a depleted possibly plume related source. Three samples from this group are ferropicrites, which are intepreted as possible partial melts of Fe-rich mantle plume starting heads, with a melt component derived from the depleted convecting asthenosphere (Riley et al., 2005).

Group 4 dykes are characterized by very high Ti and Zr concentrations, that is the highest in the Karoo-Antarctic LIP. Half of the Group 4 dykes are low-K picrites and are noted to overlap with the picritic HTZ group of Sweeney et al. (1994) in the northern Lebombo lavas of South Africa and, in part, with the CT4 picrites of Luttinen et al., (1998). These dykes are noted to have an OIB-like (plume-related) chemistry (Riley et al., 2005).

Ar-Ar dating of these basalts indicate two stages of emplacement for the dykes. Groups 1 and 3 are dated at ~190 Ma, whereas Groups 2 and 4 are ~ 178 Ma in age (Riley et al., 2005). The new $^{40}Ar/^{39}Ar$ geochronological data indicates a long-lived magmatic event of greater than 10 Myr that generated the basalts of the Karoo-Dronning Maud Land LIP (Riley et al., 2005) consistent with the plume incubation model of Sweeney et al. (1991; 1994). This interpretation is also supported by the older ~190 Ma Group 3 ferropicrites, which have MORB and OIB-like (plume head) characteristics (Riley et al., 2005).

The Nashornkalvane sill of the 1090 Ma Borgmassivet Suite is more similar in composition to the most dominant basalt in the Karoo-Dronning Maud Land LIP, as seen in a primitive mantle plot (Fig 30). These include the low Ti-Zr Group1 basalts of the Mesozoic Ahlmannryggen dykes (Riley et al., 2005), the CT1 Vestfjella basalts, the Kirwanvegen lavas and the typical southern Karoo basalts (including Lesotho and southern Lebombo) that show a pronounced negative Nb-Ta anomaly and evidence for crustal contamination. The Nashornkalvane sill is geochemicllay distinct from the high Ti-Zr OIB (plume source) – type basalt of the Karoo-Antarctic Province (Fig. 30). As in the case of the Karoo basalts, it is not possible to distinguish between crustal contamination and/or subducted sediment in the mantle source for the Nashornkalvane sill.

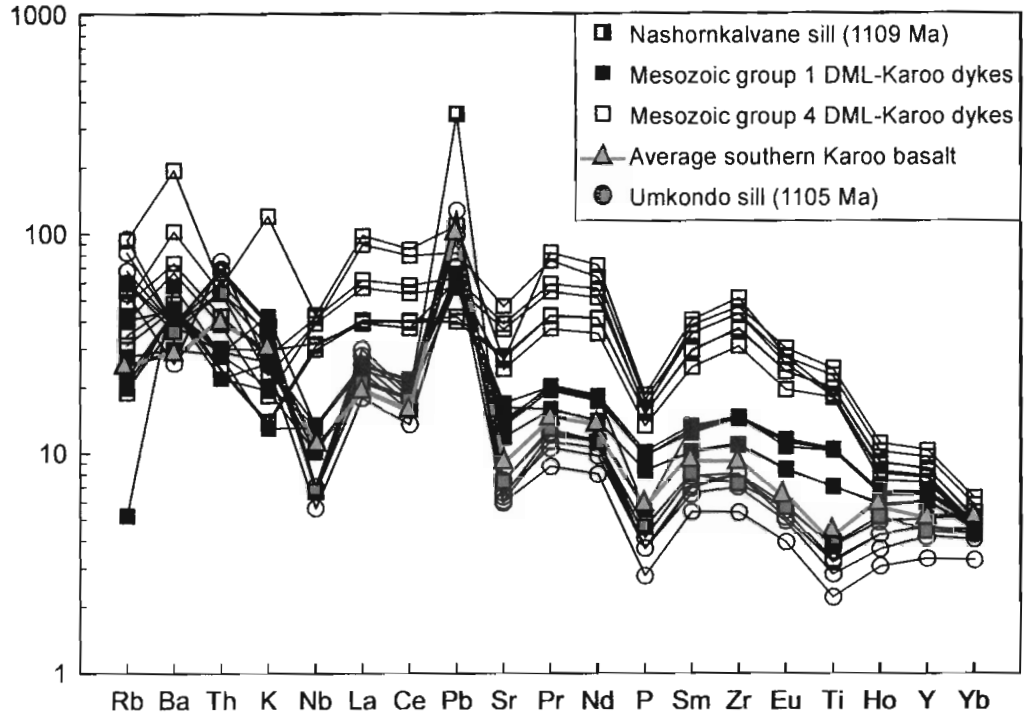

Fig. 30 The Nashornkalvane sill (this study) of the 1109 Ma Borgmassivet Suite and 1105 Umkondo mafic sills in comparision to various Mesozoic Karoo-Dronning Maud Land basalt groups of Riley et al. (2005). Data: Umkondo sills from Munyanyiwa (1999); Average composition of southern Karoo basalt from Duncan et al. (1984). Mesozoic Dronning Maud Land-Karoo (DML-Karoo) age Group 1 and 4 basalts from the Ahlmannryggen region, Antarctica from Riley et al. (2005).

The enrichment in Sr, K, Rb, Ba and Th and strong similarity in trace element geochemistry between the Nashornkalvane sill and the protoliths to the amphibolites in the Maud Belt points to possible subduction below the southeastern margin of the Kaapvaal Craton during formation of the former Maud volcanic arc (e.g. Fig 27). In the Th/Yb vs Nb/Yb diagram the Nashornkalvane sill is displaced above that of the continental arc mafics, suggesting that both processes of subduction metasomatism and crustal contamination may have played a role in their petrogenesis.

Following the model of Sweeney et al. (1991, 1994), asthenosphere-derived melts from a 1109 Ma Umkondo/Borgmassivet mantle plume may have melted and equilibrated with a shallow sub-lithospheric mantle that had been modified by subduction-related processes. Hence, as a

consequence of an ~1100 Ma Umkondo mantle plume, the Borgmassivet sills may have tapped the same subduction-related source below the southeastern margin of the Kaapvaal Craton as that of the later 180 Ma southern Lebombo, Lesotho, CT1, Kirwanveggen and Group 1 Ahlmanryggen dykes of Riley et al. (2005), only forming part of a much older Large Igneous Province. Such an interpretation would be in agreement with that of Hawkesworth et al. (1984) who suggested that the Karoo magmas tapped a source previously enriched by subduction ~1 byr before emplacement, however, in this case possibly due to formation of the late Mesoproterozoic Maud volcanic arc rather than the Namaqua-Natal Belt. In the following section, Nd-isotopic analyses for some of the amphibolite are presented which support a continental arc origin for the Maud Belt.

8.7 Four stages of mafic magmatism in WDML between 1160 Ma and 530 Ma

The age-corrected initial $^{87}Sr/^{86}Sr$ ratio for the Borgmassivet sill at 1110 Ma is 0.7117 (using an average of three samples; Table 14). Assuming a similar age for the emplacement of the protoliths to the amphibolites yields initial $^{87}Sr/^{86}Sr$ ratios for the western H.U. Sverdrupfjella amphibolites of between 0.70923 to 0.71603. Both, the high-Zr and the low-Th amphibolites from the Gjelsvikfjella have initial $^{87}Sr/^{86}Sr$ ratios that are unreasonably low at an assumed age of 1110 Ma (i.e. less than chondritic values) from which younger emplacement ages are deduced. Assuming an age of 600 Ma for the low-Th amphibolites yields more reasonable initial $^{87}Sr/^{86}Sr$ ratios that are comparable to typical ocean floor basalts ($\geq$ 0.7011). The maximum age required to obtain reasonable initial $^{87}Sr/^{86}Sr$ ratios for the high-Zr amphibolites as well as for AB-15A and AB-43A is about 530 Ma, which coincides with the age of high-grade Pan-African tectonism in the Gjelsvikfjella and with a phase of syn-tectonic mafic magmatism further east (Jacobs et al., 2003). These initial $^{87}Sr/^{86}Sr$ ratios ($\geq$ 0.7031) are similar or lower than those for the post-tectonic Stabben gabbro (0.7080), but are within the range of continental mafic rocks.

The initial $^{143}Nd/^{144}Nd$ ratios for the various mafic rocks were used in the calculation of ϵ_{Nd} values and Sm-Nd model ages (Table 15) in order to possibly distinguish between different mantle source regions. As both the Nashornkalvane sill on the craton and the amphibolites in the Maud Belt share possible supra-subduction-zone geochemical characteristics, their Sm-Nd

model ages are compared to assess their source characteristics and whether they were derived from similar mantle sources.

Sm-Nd model ages and ϵ_{Nd} for the mafic rocks in Western Dronning Maud Land show a wide spread (Fig. 31, Table 15), which speaks against melt-derivation from the same source. Strongly negative ϵ_{Nd} values between –14.7 and –6.0 were calculated for the Nashornkalvane sill and the western H.U. Sverdrupfjella amphibolites, using an initial $^{143}Nd/^{144}Nd$ ratio at 1110 Ma, which approximates the time of emplacement of the Borgmassivet mafic sills and the formation of the volcanic arc. The Sm-Nd model ages for three samples from the Nashornkalvane sill on the

Table 14. Rb-Sr isotopic data for mafic rocks in western Dronning Maud Land

Group (assumed age)	Sample	Rb (ppm)	Sr (ppm)	$^{87}Sr/^{86}Sr$	error (2-sigma)	$^{87}Rb/^{86}Sr$	$^{87}Sr/^{86}Sr$ (i)
Group 1	EG-032	21.26	203.55	0.71969	0.0017	0.30268	0.71488
(1110 Ma)	EG-030	21.24	159.18	0.71538	0.0016	0.38661	0.70923
	EG-021B	35.38	129.78	0.72859	0.0017	0.79072	0.71603
	EG-022	27.18	175.36	0.72303	0.0019	0.44938	0.71589
Group 2	EG-N1	39.56	165.40	0.72265	0.0029	0.69346	0.71163
(1110 Ma)	EG-N2	37.74	157.16	0.72315	0.0017	0.69627	0.71209
	EG-N3	38.66	157.39	0.72271	0.0025	0.71212	0.71140
	EG-026	80.68	753.63	0.71755	0.0020 0.0000	0.31022	0.71262
Group 3	ABA-2	48.60	60.30	0.73740	0.0019	2.33995	0.71738
(600 Ma)	ABA-62	45.50	82.40	0.71902	0.0019	1.60027	0.70533
	ABA-63	163.00	293.00	0.71493	0.0031	1.61159	0.70114
Group 4	AB-43A	232.03	246.38	0.72857	0.0016	2.73182	0.70793
(530 Ma)	AB-15A	187.31	47.49	0.80796	0.0018	11.52990	0.72086
	ABA-33A	86.31	404.41	0.71045	0.0017	0.61799	0.70578
	ABA-38A	283.75	225.31	0.73291	0.0019	3.65471	0.70530
	ABA-22A	349.00	94.40	0.78783	0.0019	10.78630	0.70634
	ABA-7A	134.58	294.00	0.71373	0.0019	1.32592	0.70371
	ABA-9A	21.29	347.63	0.70446	0.0017	0.17723	0.70312
Post-tectonic	ABA-65	13.00	2252	0.70818	0.0018	0.01671	0.70807
	ABA-58	64.00	2607	0.70849	0.0017	0.07107	0.70799

$^{87}Rb/^{86}Sr$ are calculated using the Rb and Sr abundances by ICP-MS.

AB# - data from A. Bisnath, 2005.

Grunehogna Craton are between 1810 and 1869 Ma. With the exception of the high-Ti amphibolite, EG-26, with a similar model age of ~1800 Ma, the remaining amphibolites from the

Table 15. Sm-Nd isotopic data for mafic rocks in western Dronning Maud Land

Group (assumed age)	Sample	Sm (ppm)	Nd (ppm)	$^{143}Nd/^{144}Nd$	error (2-sigma)	$^{147}Sm/^{144}Nd$	$^{143}Nd/^{144}Nd$ (i)	$\varepsilon_{Nd}(0)$	$\varepsilon_{Nd}(t)$	Nd Model age
Group 1	EG-032	3.52	14.34	0.51172	0.0009	0.14825	0.51064	-17.9	-11.1	2874
(1110 Ma)	EG-030	3.71	15.75	0.51173	0.0021	0.14212	0.51069	-17.8	-10.1	2533
	EG-021b	5.74	21.28	0.51208	0.0009	0.16291	0.51090	-10.8	-6.0	2488
	EG-022	3.92	16.46	0.51150	0.0010	0.14381	0.51045	-22.2	-14.7	3255
Group 2	EG-N1	3.35	15.86	0.51182	0.0009	0.12774	0.51089	-16.0	-6.2	1810
(1110 Ma)	EG-N2	3.24	15.09	0.51181	0.0008	0.12967	0.51087	-16.1	-6.6	1869
	EG-N3	3.10	14.48	0.51182	0.0009	0.12929	0.51088	-16.0	-6.4	1844
	EG-026	18.24	90.28	0.51175	0.0009	0.12202	0.51087	-17.2	-6.6	1799
Group 3	ABA/2	7.88	25.60	0.51260	0.0009	0.18593	0.51187	-0.8	0.0	584
(600 Ma)	ABA/62	7.21	23.00	0.51255	0.0011	0.18935	0.51180	-1.8	-1.2	1874
	ABA-63	3.53	14.00	0.51240	0.0025	0.15229	0.51180	-4.6	-1.2	814
Group 4	AB43A	6.81	29.10	0.51241	0.0009	0.14135	0.51192	-4.4	-0.6	621
(530 Ma)	AB-15A	3.37	13.50	0.51234	0.0011	0.15077	0.51182	-5.7	-2.6	974
	AB-33A	18.50	83.10	0.51226	0.0010	0.13446	0.51179	-7.4	-3.2	935
	AB-38A	10.40	44.80	0.51235	0.0009	0.14021	0.51187	-5.6	-1.8	772
	ABA/22	16.20	60.80	0.51240	0.0022	0.16093	0.51184	-4.6	-2.2	1007
	AB-7A	13.00	58.90	0.51253	0.0010	0.13331	0.51206	-2.2	2.1	986
	AB-9A	10.60	47.60	0.51253	0.0009	0.13451	0.51206	-2.2	2.0	999
Post-tectonic	ABA-65	15.60	92.80	0.51173	0.0010	0.10152	0.51141	-17.7	-11.7	1448
	ABA-58	17.20	113.00	0.51164	0.0011	0.09192	0.51135	-19.4	-12.9	1446

$^{147}Sm/^{144}Nd$ are calculated using the Sm and Nd abundances by ICP-MS. The initial isotopic ratios and are respectively corrected using an age of 1110 Ma for Groups 1 and 2, 600 Ma for Group 3 and 530 Ma for Group 4.

western H.U. Sverdrupfjella representative of the majority (possible subduction-related) amphibolite in the Maud Belt have distinctly older Sm-Nd model ages of between 2490 and 3300 Ma.

Calculated ϵ_{Nd} (600 Ma) values for the low-Th amphibolites, ABA-63 and ABA-62, are both -1.2. Sample ABA-2 has a ϵ_{Nd} (600 Ma) value of 0.0 and a Sm-Nd model of ~600 Ma, indicating direct extraction of the protolith melt of this amphibolite from CHUR at around that time. Assuming an initial $^{143}Nd/^{144}Nd$ at 530 Ma results in two high-Zr amphibolite samples having positive ϵ_{Nd} values (around 2.0), while the remainder, including other calc-alkaline samples, AB-15A and AB-43, have negative values. Sm-Nd model ages for these amphibolites (calculated on a depleted mantle and CHUR basis) are around 1000 Ma (Fig. 31), although two samples have significantly younger model ages of 771 Ma and 620 Ma. The Sm-Nd model age for the post-tectonic c. 490 Ma Stabben gabbro is around 1450 Ma.

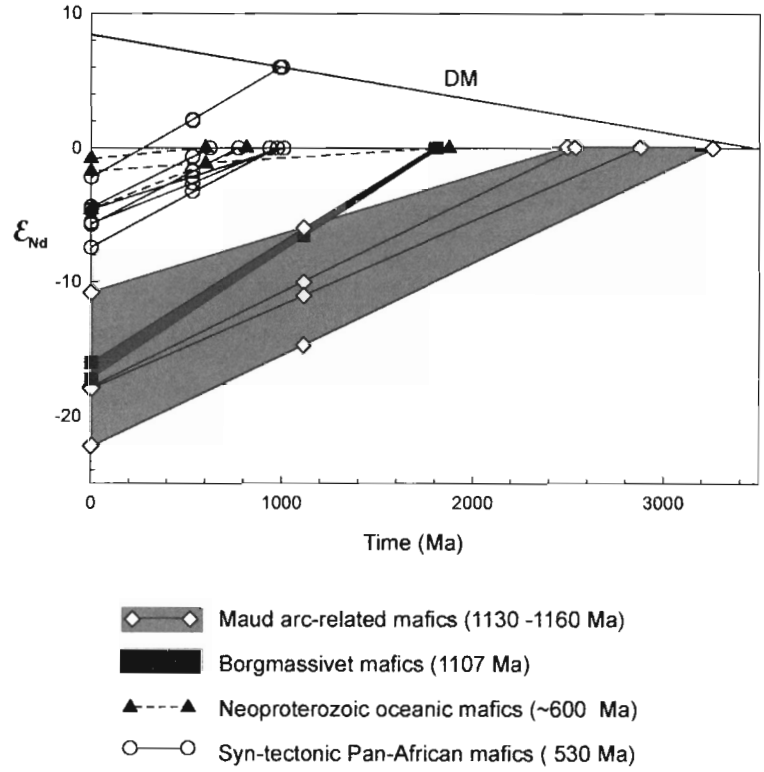

Fig. 31. Sm-Nd evolution diagram for pre- to syn-tectonic mafic rocks in Western Dronning Maud Land. (Group 2 = EG-N1 and EG-26).

The older Archaean to Proterozoic Nd model ages of the western H.U. Sverdrupfjella amphibolites are more characteristic of ancient sublithospheric mantle below Archaean cratons, which record a complex growth and stabilization history, rather than depleted mantle source regions below juvenile crust of a Mesoproterozoic island arc. The Sm-Nd isotope data indicate that the Maud Belt represents a former continental volcanic arc that formed on the margin of an Archaean craton, rather than as oceanic island arc. This Archaean craton is most likely the Grunehogna Craton. A close spatial relation between the Grunehogna Craton with its volcanosedimentary Ritcherflya Supergroup and an active volcanic arc is supported by the good agreement in U-Pb ages between the Ahlmannryggen Group (lowermost Ritcherflya Supergroup) and the oldest plutonic, arc-related rocks identified in the Maud Belt. Such a relationship would imply westward directed subduction below the craton margin in which case the basin for the Ritcherflya Supergroup would take a back-arc position. As the Grunehogna Craton is generally interpreted as a crustal fragment of the Kaapvaal Craton, the mafic protoliths to the amphibolites were probably sourced from within and below the sublithospheric mantle regions of the southeastern part of the Kaapvaal Craton. Pearson (1999) pointed out on the basis of thermobarometric and isotopic data from mantle xenoliths in the Kaapvaal Craton and surrounding Namaqua-Natal Belts that the sublithospheric mantle below southern Africa is very heterogeneous. Re-Os isotope data yielded model ages ranging from Archaean to Proterozoic with no systematic variation in these ages with depth or laterally in the mantle. Such heterogeneity could explain the Nd model ages obtained in this study.

From the high Rb/Sr ratio (0.24) and high initial $^{87}Sr/^{86}Sr$ (0.7117) significant crustal contamination is indicated for the Nashornkalvane sill. These values are very similar to some southern Karoo basalts interpreted to have assimilated Archaean crust (Hawkesworth et al., 1984). Assuming that this sill was located directly behind an active continental margin and emplaced in a continental back-arc setting, it is difficult to envisage that the source region of this Borgmassivet sill has escaped the influence of subduction-zone metasomatism. Therefore, the enrichment in LILE and LREE (slightly elevated above that of the amphibolites) and depletion in Nb and Ta could reflect a combination of subduction metasomatism in the source and enrichment due to assimilation of Archaean crustal material for this Borgmassivet Suite sill.

The four geochemically different groups of amphibolite in the Maud Belt can be ascribed to specific magmatic events between the end of the Mesoproterozoic and the Precambrian/ Cambrian boundary. Group 1 amphibolites are interpreted as continental volcanic arc-related mafic rocks, reflecting the oldest (1130-1160 Ma) mafic magmatism in the Maud Belt. They are characterized by Archaean Sm-Nd model ages (~2500-3300 Ma). The enrichment in LILE, moderate LREE-enrichment and depletions in Nb and Ta, indicated for the majority of amphibolites in the Maud Belt, are interpreted as subduction-related. ϵ_{Nd} (1110 Ma) values show a wide spread in negative values ranging between –6.0 and –15.0 from, which an ancient source may be inferred such as the sublithospheric mantle below the Kaapvaal-Grunehogna Craton.

Group 2 mafic rocks are represented by a high-Ti amphibolite (EG-26) in the Maud Belt and by the Nashalkvane sill of the Borgmassivet Suite on the craton. The source of high-Ti amphibolite is characterized by a Sm-Nd model age of ~1800 Ma, very similar to the Borgmassivet Suite sill on the eastern margin of the craton, indicating that protolith emplacement may have been contemporaneous with the Borgmassivet /Umkondo thermal event at c. 1109 Ma. Although this similarity in Sm-Nd model age may be a coincidence, it is possible that the protolith to the high-Ti amphibolite was emplaced during extension and mafic magmatism in a continental back-arc basin. The ϵ_{Nd} (1110 Ma) values of the Nashornkalvane sill (-6.4 to -6.6) and the high-Ti amphibolite (-6.2) are almost identical also indicating the involvement of an ancient source but, overlapping only with the uppermost values in the range for the Group 1 amphibolites. Considering the possible connection of the Borgmassivet/Umkondo thermal event with a c. 1109 Ma mantle plume (Frimmel, 2004; Hanson, 2004), this group of mafic rocks may have been the result of impingement of a mantle plume on the base of a sub-lithospheric mantle, which had been previously metasomatized by subduction-related processes a few tens of million of years prior to melting. This study has shown that the Nashornkalvane sill has a very similar geochemical signature to the most dominant basalt type of the 178-190 Ma possibly plume-related Karoo-Dronning Maud Land Large Igneous Province.

The presence of the high-Ti amphibolite with a similar mantle source to the Borgmassivet Suite sill indicates that many of the amphibolite protoliths in the Maud Belt with subduction zone signatures may have been the result of a mantle plume. The subduction-zone trace element enrich-

ment chemistry of the Nashornkalvane sill in this group as well as many of these plume-related amphibolites, however, is equivocal to the Group 1 amphibolite.

Group 3 amphibolites from the Gjelsvikfjella are distinguished by flat, E-type MORB REE patterns and low Th/Yb ratios similar to Neoproterozoic amphibolites dated at ~600 Ma in the Heimefronfjella. In contrast to Groups 1 and 2, their ϵ_{Nd} values, assuming an age of 600 Ma, define a narrow range between 0.0 and -1.2. This group probably represents oceanic basalts and mafic dykes that tapped a heterogeneous mantle during thinning of the crust and sub-lithospheric mantle in consequence of the opening of a Neoproterozoic ocean basin.

Group 4 amphibolites, also from the Gjelsvikfjella, are the most heterogeneous in composition. Rb-Sr data indicate an emplacement age of ~530 Ma, characterizing these amphibolites as syn-tectonic with respect to the final pulse of Pan-African tectonism. This group of amphibolites has late Mesoproterozoic Nd model ages and ϵ_{Nd} (530 Ma) values of between 2.1 and –3.2, which overlap with those of Group 3. However, they are distinguished from Group 3 and the other amphibolites by their overall REE-enrichment, rather than flat, E-type MORB REE patterns and as having the highest Zr concentrations. The 490 Ma post-tectonic Stabben gabbro has a similar but, somewhat higher late Mesoproterozoic Nd model age (1450 Ma). These syn-tectonic amphibolites and the post-tectonic mafic intrusives are therefore, interpreted as products of melting of arc-related Mesoproterozoic lower crust in response to orogenic collapse. Their calc-alkaline geochemical signature is thus an inherited feature probably due to mixing between mantle derived melts with a large component of melts derived from the lower crust of the former volcanic arc and has no bearing on the actual tectonic setting during emplacement.

9. GEODYNAMIC MODEL

In the current tectonic models suggested for the Maud Belt (Arndt et al., 1991; Jacobs, 1993; Grantham et al., 1995; Groenewald et al., 1995; Golynsky and Jacobs, 2001; Bauer et al, 2003; Paulsson and Austrheim, 2003; Basson et al., 2004) a rotation in the principal compressional tectonic stress by more than 90° around the south and southeastern margin of the Kaapvaal Craton would be required during the accretion of the Natal-Maud Belt island arc following the closure of the proposed Tugela Ocean. Contiguity of a volcanic arc stretching all around the southern Kaapvaal-Grunehogna Craton from the Namaqua sector to the Maud Belt is, however, not supported by more recent, precised U-Pb zircon age data from the Namaqua-Natal and Maud Belts (Frimmel, 2004). These data indicate arc formation in the Maud Belt to postdate that in the Namaqua-Natal Belt by at least ~200 myr.

A geochemical provenance study on metasedimentary rocks from the Mfongosi Valley in the Natal Belt (Basson et al., 2004) has shown that the southern Mfongosi Valley sediments have an active continental margin signature similar to the sediments of the Ahlmannryggen Group but distinct from the northern Mfongosi sediments for which an oceanic island arc source is indicated.

Limited Sm-Nd isotope data on felsic rocks from the Gjelsvikfjella including a homogeneous granodioritic arc-related migmatite with a protolith age of c. 1160 Ma and aplitic dykes dated at ~500 Ma yielded Proterozoic Nd model ages older than that of volcanic arc formation between 1390-1770 Ma and 1800-2220, respectively (Paulsson and Austrheim, 2003). The preferred model presented by Paulsson and Austrheim (2003) is the same as that of the above workers indicating that the Maud Belt was part of the Natal Belt island arc. They argue that the old (2220 Ma) Nd model ages probably reflect mixing of melts derived from Proterozoic island arc crust with another source from an unknown craton.

Discrepancies in the available tectonic models can be resolved if the Maud Belt is regarded as a former continental volcanic arc that formed in an independent and younger tectonic regime compared to island arc magmatism in the Natal Belt. By the time inboard subduction beneath

the eastern flank of the Kaapvaal-Grunehogna Craton took place, the island arc(s) of the Natal Belt would have already been obducted to the southern margin of the craton (Figs. 32 and 33). The geochemical trace and isotopic data therefore, indicate that the Pencksökket-Jutulstraumen Discontinuity (PJD) cannot represent a large-scale late Mesoproterozoic crustal suture that developed between an obducted oceanic island arc and the Kaapvaal-Grunehogna Craton, supporting the interpretation of the metamorphic hiatus between the Maud Belt and the Grunehogna Craton as a major Pan-African thrust rather than a Mesoproterozoic crustal discontinuity.

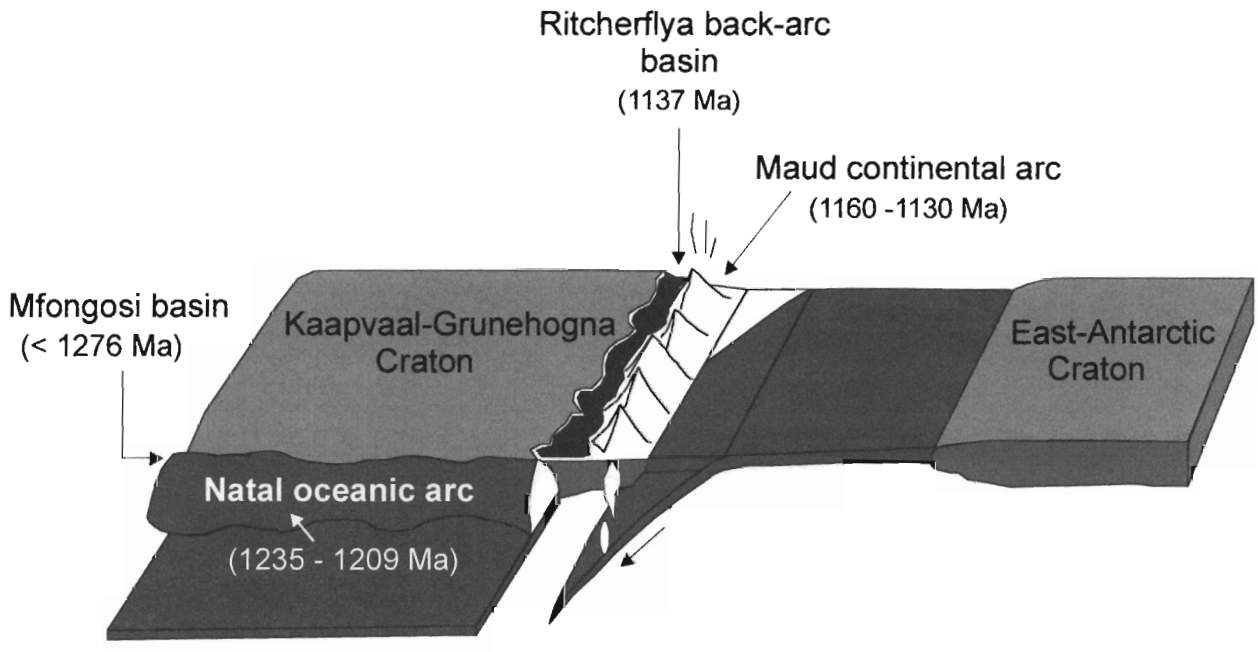

Fig. 32. Proposed model for the tectonic evolution along the southern and eastern margin of the Kaapvaal/ Grunehogna Craton during the late Mesoproterozoic showing the development of the Maud continental arc after accretion of the Natal oceanic island arc. Age data for the Ritcherflya basin from Frimmel (2004). Age data for the Maud Belt are from e.g. Arndt et al., 1991; Jacobs et al. 1999; Harris et al., 1995). Maximum age for the Mfongosi basin is from Johnston et al. (2001) and the age for the Natal oceanic arc is from Johnston et al. (2001) and (Thomas et al., 1999)

In the preferred model, subduction beneath the craton margin induced back-arc spreading, resulting in the Ritcherflya Supergroup being deposited in a cratonic back-arc basin with material derived from the craton and the Maud volcanic arc. Superimposed on the later stages of back-arc basin development was extension during to the Borgmassivet/Umkondo thermal event at c. 1107 Ma and emplacement of the Borgmassivet Suite sills into the Ritcherflya basin and also

into the adjacent continental volcanic arc. Early U-Pb metamorphic zircon overgrowth ages at 1104 ± 5 Ma (Arndt et al., 1991) and 1112 ± 29 Ma (Bauer et al., 2003) in the Heimefrontfjella, 1104 ± 8.3 Ma in the Gjelsvikfjella (Bisnath et al., in review) and leucosome development

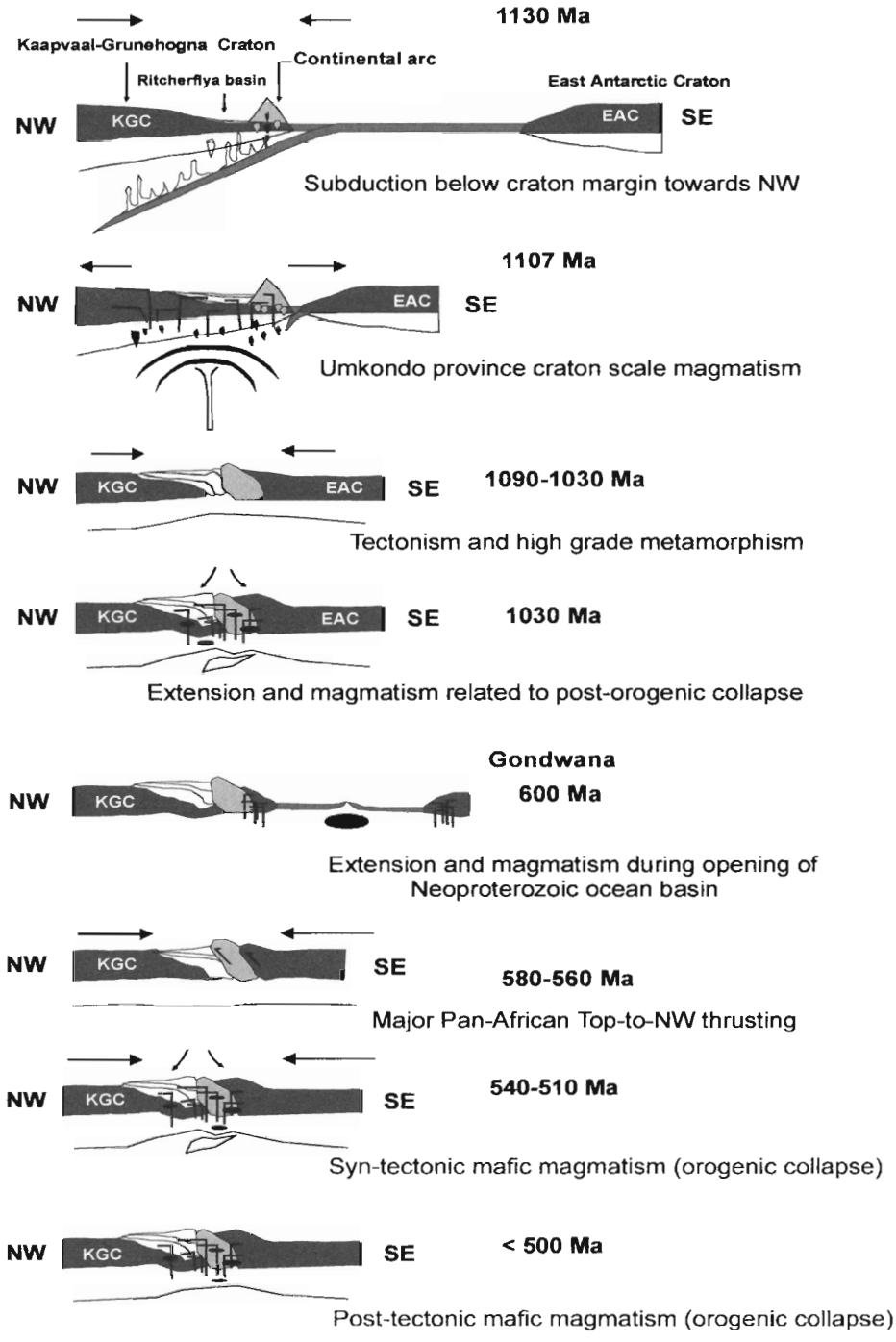

Fig. 33 Schematic geodynamic evolution of Western Dronning Maud Land.

dated at 1098 ± 5 Ma in the Kirwanveggen, probably record this event as high-grade thermal metamorphism throughout the Maud Belt.

Following arc formation, thermal metamorphism and back-arc basin extension, continental collision of the Kaapvaal craton with an unknown ("East Antarctic"?) craton is recorded in zircon overgrowths and zircon in anatectic leucosome throughout the Maud Belt with U-Pb ages of between 1030 and 1060 Ma. Post-orogenic collapse following crustal thickening during this continental collision was accompanied by intrusion of mafic dykes at c. 1030 Ma, so far recorded only from the Heimefrontfjella (Bauer et al., 2003).

Mafic dykes, approximately 600 Ma in age, were emplaced in the southwestern area of the belt (Bauer et al., 2003). Comparable dykes are now also indicated for the northeastern area of the belt. The timing and E-type MORB geochemical character of this magmatic event suggests that it was most likely related to the formation of oceanic basalts and mafic dykes during formation of a Neoproterozoic ocean basin, possibly the extension of the Mozambique Ocean. Considering a continuation of the Mozambique Ocean into East Antarctica implies that these mafic rocks record the latest stages of ocean basin formation. A period of major Pan-African tectonism followed in the form of two tectonic pulses, between ~570-560 Ma and 540-530 Ma resulting in the amalgamation of Gondwana. The latter phase of tectonism resulted in major top-to-NW thrusting and the development of the PJD as a large-scale Pan-African metamorphic discontinuity of T = 450°C and P = 6.5-8.7 kbar between the Maud Belt and the Grunehogna Craton. The second phase of tectonism was also associated with syn-tectonic mafic magmatism, whereas further, post-tectonic mafic magmatism is indicated for an orogenic collapse stage between 500 and 490 Ma. The composition of these rocks indicate their derivation from melting of Proterozoic arc-related lower crust, probably in response to sublithospheric mantle delamination and injection of asthenospheric-derived melts onto the base of the lower crust.

10. CONCLUSIONS

In the metamorphic study of mafic rocks on either side of the Pencksökket-Jutulstraumen Discontinuity (PJD), P-T conditions of 275°C and 2 kbars (lowermost greenschist facies) were calculated from a Borgmassivet Suite mafic sill on the eastern margin of the Grunehogna Craton, whereas metamorphic conditions of T = 713 – 748°C and P = 8.5 – 10.7 kbar (uppermost amphibolite facies) were calculated for the western part of the adjacent Maud Belt. These new P-T constraints indicate that the Pencksökket-Jutulstraumen Discontinuity represents a major metamorphic hiatus of T = 450°C and P = 6.5 - 8.7 kbar between the Grunehogna Craton and the Maud Belt and thus, a section of missing crust, estimated to be ~20 to 30 km thick.

Although a westward decreasing metamorphic field gradient has previously been reported in the Maud Belt, the similarity in P-T conditions between the western parts of the Maud Belt presented in this study and the Pan-African upper amphibolite metamorphic conditions recorded in the eastern Maud Belt, shows that a such a metamorphic field gradient does not exist. The similarity in P-T (upper amphibolite facies, M_{2b}) conditions recorded across the Maud Belt argues strongly in favour of major Pan-African tectonic reworking of the entire late Mesoproterozoic crust of the Maud Belt and the formation of the PJD as a large-scale Pan-African thrust. Granulite facies conditions (M_1) recorded as relic assemblages in anhydrous mafic boudin cores and in rocks to the west of the Pan-African Heimefront Shear Zone (HSZ), may be the only remaining evidence of late Mesoproterozoic metamorphism. A large-scale Pan-African thrust between the Grunehogna Craton and the Maud Belt could represent a continuation of the Mozambique Belt into East Antarctica forming a link with the exposed Heimefront Shear Zone in the south-eastern most part of the belt as the western tectonic front of the suture between East and West Gondwana.

As a late Mesoproterozoic P-T-t path and the early pre-Pan-African geological history of the Maud Belt have remained largely unknown due to intense Pan-African tectonism, various possible end-member tectonic models could be envisaged for the evolution of western Dronning Maud Land. For example, one possibility may have been that the Grunehogna Craton and the Maud Belt recorded two separate, independent geologic and metamorphic histories before being

tectonically juxtaposed. Despite major Pan-African reworking, complicating reconstruction of the early pre-tectonic history of the Maud Belt, combined trace and isotopic geochemical data on pre- to syn-tectonic and post-tectonic mafic rocks in western Dronning Maud Land has provided important insights into the late Mesoproterozoic to Pan-African geodynamic evolution of the Maud Belt. The variety of mafic rocks identified it this study include four groups of pre- to syn- tectonic amphibolite. The protoliths to the Group 1 amphibolite records early mafic magmatism during volcanic arc formation between 1160 and 1130 Ma. The Group 2 amphibolite represents mafic magmatism related to the Umkondo/Borgmassivet thermal event and may have been emplaced in response to a ~1110 Ma mantle plume. Amphibolite of Group 3 reflects oceanic basalts and dykes probably associated with the opening of a Neoproterozoic ocean basin to the east of the Maud Belt and as a possible continuation of the Mozambique Ocean basin into East Antarctica. Group 4 amphibolite indicates the presence of a syn- to post tectonic Pan-African mafic igneous province in the northeastern part of the belt, where Pan-African tectonothermal overprinting was most intense.

Sm-Nd isotope data for the earliest volcanic arc-related mafic group indicates that the Maud Belt represents a former continental volcanic arc and fixes the relative position of the arc the southeastern margin of the Kaapvaal-Grunehogna Craton. Although previous models all indicate outboard subduction directed away from the craton margin, in the preferred model presented in this study, subduction below the craton margin is favoured with the sediments of Ritcherflya Supergroup deposited in a cratonic back-arc basin. The new isotopic data indicates that the Maud Belt does not represent a simple continuation of the Namaqua-Natal Belt as an oceanic island arc into East Antarctica, as arc-related mafic magmatism was sourced from an inhomogeneous, Archaean mantle rather than from depleted mantle source regions below a late Mesoproterozoic juvenile island arc. Thus, the geochemical data on mafic rocks across the PJD in western Dronning Maud Land has fixed the relative position of the Maud Belt as a former continental volcanic arc to the margin of the Grunehogna Craton during the late Mesoproterozoic. This indicates that the geological and metamorphic history of the two crustal domains was coupled, arguing against their development in independent tectonic environments prior to tectonic juxtaposition. Consequently, the PJD does not represent a large-scale crustal suture that developed by accretion of an oceanic island arc onto the Grunehogna Craton margin. Rather,

the P-T data presented supports the interpretation of the metamorphic discontinuity between Maud Belt and the Grunehogna Craton as a major Pan-African thrust and as a possible extension of the East African Orogen into East Antarctica.

The youngest mafic group identified is syn-tectonic with respect to the Pan-African orogeny. Together with post-tectonic mafic intrusions, it shows typical subduction-related geochemical signatures. The calc-alkaline, subduction-related geochemical signature was probably inherited by mantle derived magmas that melted and assimilated significant quantities of lower crust, that consisted largely of Mesoproterozoic volcanic arc material, during orogenic collapse. This highlights the limitations of conventional tectonic discrimination diagrams.

REFERENCES

Apted, M.J., Liou, J.G., 1983. Phase relations among greenschist, epidote-amphibolite, and amphibolite in a basaltic system. Am. J. Sci. 283-A, 328-354.

Arima, M., Tani, K., Kawate, S., Johnston, S.T., 2001. Geochemical characteristics and tectonic setting of metamorphosed rocks in the Tugela terrane, Natal Belt, South Africa. Mem. Nat. Inst. Polar Res. 55, 1-39

Arndt, N.T., Todt, W., Chauvel, C., Tapfer, M., Weber, K., 1991. U-Pb zircon age and Nd isotopic composition of granitoids, charnockites and supracrustal rocks from Heimefrontfjella, Antarctica. Geol. Rundsch. 80, 759-777.

Basson, I.J., Perrit, S., Watkeys, M.K., Menzies, A.H., 2004. Geochemical correlation between metasediments of the Mfongosi Group of the Natal Sector of the Namaqua-Natal Metamorphic Province, South Africa and the Ahlmannryggen Group of the Grunehogna Province, Antarctica. Gondwana Res. 7(1), 57-73.

Bauer, W., Fielitz, W., Jacobs, J., Fanning, C.M., Spaeth, G., 2003. Mafic dykes from Heimefrontfjella and implications for the post-Grenvillian to pre-Pan-African geological evolution of western Dronning Maud Land, Antarctica. Antarc. Sci. 15(3), 379-391.

Bevins, R.E., Robinson, D., Rowbotham, G., 1991. Compositional variations in mafic phyllosilicates from regional low-grade metabasites and application of the chlorite geothermometer. J. Metamorphic Geol. 9, 711-721.

Bingen, B., Demaiffe, D., Hertogen, J., 1996. Redistrubution of rare earth elements, thorium, and uranium over accessory minerals in the course of amphibolite to granulite facies metamorphism: the role of apatite and monazite in orthogneisses from southwestern Norway. Geochim. Cosmochim. Acta 60, 1341-1354.

Bird, D.K., Schiffman, P., Elders, W.A., Williams, A.E., McDowell, S.D., 1984. Calc-silicate mineralization of active systems. Econ. Geol. 79, 671-695.

Bisnath, A.B., Frimmel, H.E., Armstrong, R.A., Board, W.S., in review. Tectono-thermal evolution of the Maud Belt: New SHRIMP U-Pb zircon data from the Gjelsvikfjella, Dronning Maud Land, East Antarctica. Precambrian Res.

Board, W.S., 2002. Tectonothermal evolution of the southern H.U. Sverdrupfjella, western Dronning Maud Land, Antartica. PhD Thesis, University of Cape Town, unpublished, 174p.

Board, W.S., Frimmel, H.E., Armstrong, R.A., 2005. Pan-African tectonism in the western Maud Belt: P-T-t path for high-grade gneisses in the H.U. Sverdrufjella, East Antarctica. J. of Petrol.

Boger, S.D., Wilson, C.J.L., Fanning, C.M., 2001. Early Palaeozoic tectonism within the East Antarctic craton: the final suture between east and west Gondwana? Geology 29, 463-466.

Boger, S.D., Miller, J. McL., 2004. Terminal suturing of Gondwana and the onset of the Ross-Delamerian Orogeny: the cause and effect of an Early Cambrian reconfiguration of plate motions. Earth Planet. Sci. Lett. 219, 35-48.

Bohlen, S.R., Montana, A., Kerrick, D.M., 1991. Precise determinations of the equilibria kyanite = sillimanite and kyanite = andalusite and a revised triple point for Al_2SiO_5 polymorphs. Am. Miner. 76, 677-680.

Carswell, D.A., Harley, S.L., 1989. Mineral barometry and thermometry. In: D.A.Carswell (Ed). Eclogites and related rocks. Blackie, Glasglow, pp. 83-110.

Cathelineau, M., 1987. U-Th-REE mobility during albitization and quartz dissolution in granitoids: evidence from southeast French Massif Central. Bull. Mineral. 110, 249-259.

Cathelineau, M., 1988. Cation site occupancy in chlorites and illites as a function of temperature. Clay Minerals, 23, 471-485.

Cathelineau, M., Nieva, D., 1985. A chlorite solid solution geothermometer. The Los Azufres geothermal system (Mexico). Contrib. Mineral. Petrol. 91, 235-244.

Cho, M., Maruyama, S., Liou, J.G., 1986. Transition from the zeolite to prehnite-pumpellyite facies in the Karmutsen metabasites, Vancouver Island, B.C. J. Petrol. 27, 467-494.

Cox, K.G., 1978. Flood basalts, subduction and the break-up of Gondwanaland. Nature 274, 47-49.

Cox, K.G., 1983. The Karoo Province of southern Africa: origin of trace element enrichment patterns. In: Hawkesworth, C.J., Norry, M.J. (Eds.), Continental Flood Basalts and Mantle Xenoliths. Shiva Publ., Nantwhich, UK, p.139-157.

Cullers, R.L., Medaris, L.G., Haskin, L.A., 1973. Experimental studies of the distribution of rare earths as trace elements among silicate minerals and liquids and water. Geochim. Cosmochim. Acta. 37, 1499-1512.

Dale, J., Holland, T.J.B., Powell, R., 2000. Hornblende-garnet-plagioclase thermobarometry: a natural assemblage calibration of the thermodynamics of hornblende. Contrib. Mineral. Petrol. 140, 353-362.

Decleir, H., Van Autenboer, T., 1982. Gravity and magnetic anomalies across Jutulstraumen, a major geologic feature in western Dronning Maud Land. In: C. Cradock (Ed), Antarctic Geoscience. The University of Wisconsin Press, Madison, pp. 941-948.

De Caritat, P., Hutcheon, I., Walshe, J.L., 1993. Chlorite geothermometry: a review. Clay minerals 41, 219-239.

DePaolo, D.J., 1981. Neodymium isotopes in the Colorado Front Range and crustal-mantle evolution in the Proterozoic. Nature 291, 193-196.

Dirks, P.H.G.M., Carson, C.J., Wilson, C.J.L., 1993. The deformation history of the Larsemann Hills, Prydz Bay: the importance of the Pan-African (500 Ma) in East Antarctica. Antarc. Sci. 5, 179-193.

Droop, G.T.R., 1987. A general equation for estimating Fe^{3+} concentrations in ferromagnesian silicates and oxides from microprobe analyses, using stoichiometric criteria. Mineral. Mag. 51, 431-435.

Duncan, A.R., Erlank, A.J., Betton, P.J., 1984. Analytical techniques and database descriptions. Geol. Soc. S. Afr. Spec. Publ. 13, 389-395.

Duncan, A.R., Erlank, A.J., Marsh, J.S., 1984. Regional geochemistry of the Karoo Igneous Province. Geol. Soc. S. Afr. Spec. Publ. 13, 355-388.

Erlank, A.J. (Ed.), 1984. Petrogenesis of the volcanic rocks of the Karoo Province. Geol. Soc. S. Afr. Spec. Publ. 13, p. 395.

Erlank, A.J., Allsop, H. L., Duncan, A.R., Bristow, J.W., 1980. Mantle heterogeneity beneath southern Africa: evidence from the volcanic record. Phil. Trans. R.Soc. Lond. A297, 295-307.

Ferreira, E.P., 1988. The sedimentology and stratigraphy of the Ahlmannryggen Group, Antarctica. Unpubl. MSc Thesis, University of Stellenbosch, p. 193.

Fitzsimons, I.C.W., 2000a. A review of tectonic events in the East Antarctic Shield and their implications for Gondwana and earlier supercontinents. J. Afri. Earth Sci. 31, 3-23.

Fitzsimons, I.C.W., 2000b. Grenville-age basement provinces in East Antarctica: evidence for three separate collisional orogens. Geology 28, 879-882.

Fitzsimons, I.C.W., Kinny, P.D., Harley, S.L., 1997. Two stages of zircon and monazite growth in anatectic leucogneiss: SHRIMP constraints on the duration and intensity of Pan-African metamorphism in Prydz Bay, East Antarctica. Terra Nova 9, 47-51.

Frey, F.A., 1983. Rare earth element abundances in upper mantle rocks. In: Henderson, P. (Eds.), Rare Earth Element Geochemistry. Elservier, Amsterdam, p. 256-259.

Frey, M., de Capitani, C., Liou, J.G. 1991. A new petrogenetic grid for low-grade metabasites. J. Metamorphic Geol. 9, 497-509.

Frimmel, H.E., 1997. Chlorite Thermometry in the Witwatersrand Basin: Constraints on the Paleoproterozoic Geotherm in the Kaapvaal Craton, South Africa. J. Geol. 105, 601-615.

Frimmel, E.F., Zartman, R.E., Späth, A., 2001. The Richtersveld Igneous Complex, South Africa: U-Pb Zircon and Geochemical Evidence for the Beginning of Neoproterozoic Continental Breakup. J. Geol. 109, 493-508.

Frimmel, H.E., 2004. Formation of a late Mesoproterozoic supercontinent: The South Africa–East Antarctica connection. In: P.G. Eriksson, W. Altermann, D.R. Nelson, W.U. Mueller and O. Catuneau (Eds.), The Precambrian Earth: Tempos and Events. Elsevier, Amsterdam, p. 240-255.

Grantham, G.H., Groenewald, P.B., Hunter, D.R., 1988. Geology of the northern H.U. Sverdrupfjella, western Dronning Maud Land and implications for Gondwana reconstructions. S. Afri. J. Antarc. Res. 18, 2-10.

Grantham, G.H., Hunter, D.R., 1991. The timing and nature of faulting and jointing adjacent to the Pencksökket, western Dronning Maud Land and implications for Gondwana reconstructions. In: M.R.A. Thomson, J.A. Crame and J.W. Thomson (Eds.), Geological Evolution of Antarctica. Cambridge University Press, Cambridge, p. 47-51.

Grantham, .H., Jackson, C., Moyes, A.B., Groenewald, P.B., Harris, P.B., Ferrar, G., Krynauw, J.R., 1995. The tectonothermal evolution of the Kirwanveggen-H.U.

Sverdrupfjella areas, Dronning Maud Land, Antarctica. Precambrian Res. 75, 209-229.

Grauch, R.I., 1989. Rare earth elements in metamorphic rocks. In: B.R. Lipin and G.A. McKay (Eds.), Geochemistry and mineralogy of rare earth elements. Rev. Mineral. 21, 147 - 167.

Groenewald, P.B., Hunter, D.R., 1991. Granulites of northern Sverdrufjella, western Dronning Maud Land: metamorphic history from garnet-pyroxene assemblages, coronas and rehydration reactions. In: M.R.A. Thomson, J.A. Crame, and J.W. Thomson (Eds.), Geological Evolution of Antarctica, Cambridge University Press, Cambridge, pp. 61-66.

Groenewald, P. B., Moyes, A.B., Grantham, G.H., Krynauw, J.R., 1995. East Antarctic crustal evolution: geological constraints and modeling in western Dronning Maud Land. Precambrian Res. 75, 231-250.

Grosch, E.G., Frimmel, H.E., in review. Metamorphic evidence for a major Pan-African thrust between the Grunehogna Craton and the Maud Belt, East Antarctica. Antarc. Sci.

Golynsky, A.V., Grikurov, G.E, Kamenev, E.N, 1997. Geologic significance of regional magnetic anomalies in Coats Land, western Dronning Maud Land. Polarforsch. 67(3), 91-99.

Golynsky, A., Jacobs, J., 2001. Grenville-age versus Pan-African magnetic anomaly imprints in western Dronning Maud Land, East Antarctica. J. Geol. 109, 136-142.

Gose, W.A., Helper, M.A., Connelly, J.N., Hutson, F.E., Dalziel, I.W.D., 1997. Paleomagnetic data and U-Pb isotopic age determinations from Coats Land, Antarctica: Implications for late Proterozoic plate reconstructions. J. Geophys. Res. 102, 7887-7902.

Gieré, R., 1986. Zirconolite, allanite and hoegbomite in a marble skarn from the Begell contact aureole: implications for the mobility of Ti, Zr and REE. Contrib. Miner. Petrol. 93, 459-470.

Gieré, R., 1989. Hydrothermal mobility of Ti, Zr and REE: examples from the Bergell and Ademello contact aureoles (Italy). Terra Nova. 2, 60-67.

Grunow, A., Henson, R., Wilson, T., 1996. Were aspects of Pan-African deformation linked to Iapetus opening? Geology 24, 1063-1066.

Hanson, R.E. Martin, M.W., Bowring, S.A., Munyanyiwa, H., 1998. U- Pb zircon age for the Umkondo dolerites, eastern Zimbabwe: 1.1 Ga large igneous province in southern Africa-East Antarctica and possible Rodinia correlations. Geology 26, 1143-1146.

Hanson, R.E., James, C.L., Bowring, S.A., Ramezani, J., Gose, W.A., Dalziel, I.W.D., Pancake, J.A., Seidel. E.K., Blenkinsop, T.G., Mukwakwami, J., 2004. Coeval large-scale magmatism in the Kalahari and Laurentian cratons during Rodinia assembly. Science 304, 1126-1129.

Harris, C., Grantham, G.H., 1993. Geology and petrogenesis of the Straumsvola nepheline syenite complex, Dronning Maud Land, Antarctica. Geol. Mag. 130, 513-532.

Harris, C., Marsh, J.S., Duncan, A.R., Erlank, A.J., 1990. The petrogenesis of the Kirwan Basalts of Dronning Maud Land, Antarctica. J. of Petrol. 31, 341-369.

Harris, C., Johnstone, W.P., Phillips, D., 2002. Petrogenesis of the Mesozoic Sistefjell syenite intrusion, Dronning Maud Land, Antarctica and surrounding low-$\delta^{18}O$ lavas. S. Afr. J. Geol. 105, 205-226.

Harris, P.D., Moyes, A.B., Fanning, C.M., Armstrong, R.A., 1995. Zircon ion microprobe results from the Maudheim high-grade gneiss terrane, western Dronning Maud Land, Antarctica. In: J.M. Barton and Y.E. Copperthwaite (Eds.), Centennial Geocongress, 3-7 April 1995, Johannesburg, Geological Society of South Africa 1, 240-243.

Hawkesworth, C.J., Marsh, J.S., Duncan, A.R., Erlank, A.J., Norry, M.J., 1984. The role of continental lithosphere in the generation of the Karoo volcanic rocks: Evidence from combined Nd and Sr isotope studies. Spec. Publ. geol. Soc. S. Afr. 13, 341-354.

Hawkesworth, C.J., Powell, B.M. 1980. Magma genesis in the Lesser Antilles island arc. Earth. Planet. Sci. Lett. 51, 297-308.

Hekinian, R., 1982. Petrology of the Ocean Floor. Elsevier, Amsterdam, 393 pp.

Holland, T.J.B., Blundy, J., 1994. Non-ideal interactions in calcic amphiboles and their bearing on amphibole-plagioclase thermometry. Contrib. Mineral. Petrol. 116, 433-447.

Holland, T.J.B., Powell, R., 1998. An internally-consistent thermodynamic dataset for phases of petrological interest. J. Metamorphic Geol. 16, 309-344.

Jackson, C., 1999. Characterization of the Mesoproterozoic to Palaeozoic crustal evolution of western Dronning Maud Land. Study 3: Deformational history and thermochonology of the Kirwanveggen. Unpubl. report, Department of Environmental Affairs and Tourism, Pretoria, p. 80.

Jacobs, J., Ahrendt, H., Kreutzer, H., Weber, K., 1995. K-Ar, 40Ar-39Ar and apatite fission-track evidence for Neoproterozoic and Mesozoic basement rejuvenation events in the Heimefrontfjella and Mannefallknausane (East Antarctica). Precambrian Res. 75, 251-262.

Jacobs. J., Bauer, W., Spaeth, G., Thomas, R.J., Weber, K., 1996. Lithology and structure of the Grenville-aged (~1.1 Ga) basement of the Heimefrontfjella, East Antarctica. Geol. Rundsch. 85, 800-821.

Jacobs, J., Fanning, C.M., Henjes-Kunst, F., Olesch, M, Paech, H. -J., 1998. Continuation of the Mozambique Belt into East Antarctica: Grenville-age metamorphism and polyphase Pan-African high-grade events in central Dronning Maud Land. J. Geol. 106, 385-406.

Jacobs, J., Fanning, C.M., Bauer, W., 2003. Timing of Grenville-age vs. Pan-African medium- to high-grade metamorphism in western Dronning Maud Land (East Antarctica) and significance for correlations in Rodinia and Gondwana. Precambrian Res. 125, 1-20.

Jacobs, J., Hansen, B.T., Henjes-Kunst, F., Thomas, R.J., Bauer, W., Weber, K., Armstrong, R.A., Cornell, D.H., 1999. New age constraints on the Proterozoic/lower Palaeozoic evolution of the Heimefrontfjella, East Antarctica, and its bearing on Rodinia/Gondwana correlations. Terra Antarc. 6, 377-389.

Jacobs, J., Klemd, R., Fanning, C.M., Bauer, W., Colombo, F., 2003. Extensional collapse of the late Neoproterozoic-early Palaeozoic East African-Antarctic Orogen in central Dronning Maud Land, East Antarctica. In: M. Yoshida, B.F. Windley and S. Dasgupta (Eds.), Proterozoic East Gondwana: Supercontinent Assembly and Breakup, Geological Society, London, Special Publications 206, 271-287.

Jacobs, J., Thomas, R.J., Weber, K., 1993. Accretion and indentation tectonics at the southern edge of the Kaapvaal craton during the Kibaran (Grenville) orogeny. Geology 21, 203-206

Jacobs, J., Thomas, R.J., 2002. The Mozambique Belt from an East Antarctic perspective. In: Gamble, J.A., Skinner, D.N.B., Henrys, S. (Editors), Antarctica at the close of a millennium, Proceedings of the 8th International Symposium on Antarctic Earth Sciences. R. Soc. N. Zealand Bull. 35, 3-18.

Jacobsen, S.B., Wasserburg, G.J., 1980. Sm-Nd isotopic evolution of chondrites. Earth Planetary Sci. Lett. 50, 139-155.

Jiang, W.T., Peacor, D.R., Buseck, P.R., 1994. Chlorite geothermometry –contamination and apparent octahedral vacancies. Clay Minerals 42, 593-605.

Johannes, W., 1978. Loss of iron to the platinum-container in melting experiments with basalts and a method to reduce it. Contrib. Mineral. Petrol. 67, 221-225.

Johnston, S.T., Armstrong, R., Heaman, L., McCourt, S., Mitchell, A., Bisnath, A., Arima, M., 2001. Preliminary U-Pb geochronology of the Tugela terrane, Natal Belt, eastern South Africa: Mem. Nat. Inst. Polar Res. 55, 40-58.

Kranidiotis, P., MacLean, W.H., 1987. Systematics of Chlorite Alteration at the Phelps Dodge Massive Sulphide Deposit, Matagami, Quebec. Econ. Geol. 82, 1898-1911.

Kretz, R., 1994. Petrology of veined gneisses of the Otter complex, southern Grenville Province. Can. J. Earth Sci. 31, 835-851.

Kristmannsdóttir, H., 1979. Alteration of basaltic rocks by hydrothermal activity at 100-300°C. In: International Clay Conference, (1978). M.M. Morland and V.C. Farmer (Eds.). Elsevier, New York, 410 pp.

Krynauw, J.R., 1986. The petrology and geochemistry of intrusions at selected nunataks in the Ahlmannryggen and Gaeverryggen, western Dronning Maud Land, Antarctica. PhD Thesis, University of Natal, Durban, unpublished.

Krynauw, J.R., Hunter, D.R., Wilson, A.H., 1988. Emplacement of sills into wet sediments at Grunehogna, western Dronning Maud Land, Antarctica. J. Geol. Soc. Lond. 145, 1019-1032.

Krynauw, J.R., Watters, B.R., Hunter, D.R., Wilson, A.H., 1991. A review of the field relations, petrology and geochemistry of the Borgmassivet intrusions in the Grunehogna Province, western Dronning Maud Land, Antarctica. In: M.R.A. Thomson, J.A. Crame and J.A. Thomson (Eds.), Geological Evolution of Antarctica. Cambridge University Press, Cambridge, pp.33-39.

Krynauw, J.R., 1996. A review of the geology of east Antarctica, with special reference to the ca. 1000 Ma and ca. 500 Ma events. Terra Antarc. 3, 77-89.

Leake, B.E., Woolley, A.R., Arps, C.E.S., Birch, W.D., Gilbert, M.C., Grice, J.D., Hawthorne, F.C., Kato, A., Kisch, H.J., Krivovichev, V.G., Linthout, K., Laird, J., Mandarino, J.A., Maresch, W.V., Nickel, E.H., Rock, N.M.S., Schumacher, J.C., Smith, D.C., Stephenson, N.C.N., Ungaretti, L., Whittaker, E.J.W. and Youzhi, G., 1997. Nomenclature of amphiboles: Report of the Subcommittee on Amphiboles of the International Mineralogical Association, Commission on New Minerals and Mineral Names. Am. Miner. 82, 1019-1037.

le Roex, A.P., 1985. Geochemistry, mineralogy and magmatic evolution of the basaltic and trachytic lavas from Gough Island, South Atlantic. J. of Petrol 26, 149-186.

le Roex, A.P., Lanyon, R. 1998. Isotope and trace element geochemistry of Cretaceous Damaraland lamprophyres and carbonatites, northwestern Namibia: evidence for plume-lithosphere interactions. J. of Petrol. 39, 1117-1146.

Liou, J.G., Maruyama, S., Cho, M., 1987. Very low-grade metamorphism of volcanic and volcaniclastic rocks – mineral assemblages and mineral facies. In: M. Frey (Editor), Low temperature metamorphism. Blackie, Glasgow, pp 63-80.

Liou, J.G., Maruyama, S., Cho, M., 1985a. Phase equilibria and mineral paragenesis of metabasites in low-grade metamorphism. Mineral. Mag. 49, 321-333.

Liou, J.G., Seki, Y., Guillemette, R., Sakai, H., 1985b. Compositions and paragenesis of secondary minerals in the Onikobe geothermal system, Japan. Chem. Geol. 49, 1-20.

Ludden, J.N., Thompson, G., 1979. An evaluation of the behaviour of the rare earth elements during the weathering of sea-floor basalt. Earth Planet. Sci. Lett. 43, 85-92.

Lugmair, G.W., Marti, K., 1978. Lunar initial 143Nd/144Nd; differential evolution of the lunar crust and mantle. Earth Planetary Sci. Lett. 39, 349-357.

Luttinen, A. V., Furnes, H. 2000. Flood basalts of the Vestfjella: Jurassic magmatism across an Archaean Proterozoic lithospheric boundary in Dronning Maud Land, Antarctic. J. of Petrol. 41, 1271-1305.

McLennan, S.M., Taylor, S.R., 1981. Role of subducted sediments in island-arc magmatism: constraints from REE patterns. Earth Planet. Sci. Lett. 54, 423-430.

Mengel, F.C., Rivers, T., 1991. Decompression reactions and P-T conditions in high grade rocks, northern Labrador: P-T-t paths from individual samples and implications for early Proterozoic tectonic evolution. J. Petrol. 32, 139 – 167.

Meschede, M., 1986. A method of discriminating between different types of mid-ocean ridge basalts and continental tholeiites with the Nb-Zr-Y diagram. Chem. Geol. 56, 207-218.

Michard, A., Gurriet, P., Soudant, M., Albarede, F., 1985. Nd isotopes in French Phanerozoic shales: external vs. internal aspects of crustal evolution. Geochim. Cosmochim. Acta. 49, 601-610.

Middlemost, E.A.K., 1991. Towards a comprehensive classification of igneous rocks and magmas. Earth Sci. Rev. 31, 73-87.

Moyes, A.B., Barton, J.M. Groenewald, P.B., 1993a. Late Proterozoic to Early Palaeozoic tectonism in Dronning Maud Land, Antarctica: supercontinental fragmentation and amalgamation. J. Geol. Soc. Lond. 150, 833-842.

Moyes, A.B., Harris, P.D., 1996. Final project report of the radiogenic isotopes project on the geological evolution of Western Dronning Maud Land within a Gondwana framework. Final report submitted to the South African National Antarctic Programme, Department of Environment and Tourism Directorate: Antarctica and Islands, South Africa, p. 38.

Mullen, E.D., 1983. MnO-TiO_2-P_2O_5: A minor element discriminant for basaltic rocks of oceanic environments and its implications for petrogenesis. Earth Planet. Sci. Lett. 62, 1, 53-62.

Munyanyiwa, H., 1999. Geochemical study of the Umkondo dolerites and lavas in the Chimanimani and Chipinge Districts (eastern Zimbabwe) and their regional implications. J. Afri. Earth. Sci. 28(2), 349-365.

Mikhalsky, E.V., Beliatsky, B.V., Savva, E.V., Wetzel, H.-U., Fedorov, L.V., Weiser, T. and Hahne, K., 1997. Reconnaissance geochronologic data on polymetamorphic and igneous rocks of the Humboldt Mountains, Central Queen Maud Land, East Antarctica. In: Ricci, C.A. (Eds.), The Antarctic Region: Geological Evolution and Processes. Terra Antarc. Publication, Siena, p. 45-54.

Mysen, B.O., 1979. Trace-element partitioning between garnet peridotite minerals and water-rich vapour: experimental data from 5 to 30 kbar. Am. Miner. 64, 274-287.

Nedelec, A., Ralison, B., Bouchez, J.L., Gregoire, V., 2000. Structure and metamorphism of the granite basement around Antananarivo: A key to the Pan-African history of central Madagascar and its Gondwana connections. Tectonics 19(5), 997-1020.

Norrish, K., Hutton, J.T., 1969. An accurate X-ray spectrographic method for the analysis of a wide range of gological samples. Geochim et Cosm. Acta 33, 431-453.

Pattison, D.R.M., 2003. Petrogenetic significance of orthopyroxene-free garnet + clinopyroxene + plagioclase ± quartz-bearing metabasites with respect to the amphibolite and granulite facies. J. Metamorphic Geol. 21, 21-34.

Paulsonn, O., Austrheim, H., 2003. A geochronological and geochemical study of rocks from the Gjelsvikfjella, Dronning Maud Land, Antarctica – implications for Mesoproterozoic correlations and assembly of Gondwana. Precambrian Res. 125, 113-138.

Pearce, J.A., 1975. Basalt geochemistry to investigate past tectonic environments on Cyprus. Tectonophysics 25, 41-67.

Pearce, J.A., 1976. Statistical analysis of major element patterns in basalts. J. Petrol. 17, 15-43.

Pearce, J.A., 1983. Role of the sub-continental lithosphere in magma genesis at active continental margins. In: Hawkesworth, C.J., Norry, M.J. (Eds.), Continental Basalts and Mantle Xenoliths. Shiva Publ., Nantwhich, UK, p.230-249.

Pearce, J.A., Norry, M.J., 1979. Petrogenetic implications of Ti, Zr, Y, and Nb variations in volcanic rocks. Contrib. Mineral. Petrol. 69, 33-47.

Pearce, J.A., Cann, J.R., 1973. Tectonic setting of basic volcanic rocks determined using trace element analyses. Earth Planet. Sci. Lett. 19, 290-300.

Pearce, J.A., Peate, D.W., 1995. Tectonic implications of the composition of volcanic arc magmas. Ann. Rev. Earth. Planet. Sci. 23, 251-85.

Pearson, D.G., 1999. The age of continental roots. Lithos 48, 171-194.

Pinna, P., Jourde, G., Calvez, J.Y., Mroz, J.P., Marques, J.M., 1993. The Mozambique Belt in northern Mozambique: Neo-Proterozoic (1100-850 Ma) crustal growth and

tectogenesis and superimposed Pan-African (800-550 Ma) tectonism. Precambrian Res. 62, 1-59.

Piwinskii, A.J., 1968. Experimental studies of igneous rock series, central Sierra Nevada Batholith, California. J. Geol. 76(5), 548 – 570.

Pouchou, J.L., Pichoir, F., 1984. A new model for quantitative X-ray microanalysis. Recherches Aéospatial, 3, 13-37.

Ravich, M.G., Solo'vev, D.S., 1966. Geology and petrology of the mountains of central Queen Maud Land (East Antarctica). Trans. Sci. Res. Inst. Arct. Geol., 348 pp. Ministry of Geology of the U.S.S.R. (Israel Program for Scientific Translations, Jerusalem, 1969).

Richardson, S.H., Gurney, J.J., Erlank, A.J., Harris, J.W., 1984. Origin of diamonds in old enriched mantle. Nature 310, 198-202.

Riley, R.T., Leat, P.T., Curtis, M.L., Millar, I.L., Duncan, R.A., Fazel, A., 2005. Early-Middle Jurassic dolerite dykes from Western Dronning Maud Land (Antarctica): Identifying mantle sources in the Karoo Large Igneous Province. J. of Petrol. 46(7), 1489-1524.

Robinson, D., Bevins, R.E., Rowbotham, G., 1993. The characterization of mafic phyllosilicates in low-grade metabasalts from eastern North Greenland. Am. Miner. 78, 377-390.

Roots, E.F., 1969. Geology of western Dronning Maud Land. Explanation of plate VI, Folio 12, Antarctic Map Series, American Geophysical Union.

Rudashevskiy, N.S., 1969. Epidote-orthite from the metasomatites of southern Siberia, Vses. Mineral. Obshchest. Zap. 98/6, 739-749 (in Russian).

Sawyer, E.W., 1991. Disequilibrium melting and the rate of melt residuum separation during migmatisation of mafic rocks from the Grenville Front, Quebec. J. Petrol. 32, 701-738.

Schiffman, P., Fridleifsson, G.O., 1991. The smectite to chlorite transition in drillhole NJ-15, Nesjavellir Geothermal Field, Iceland: XRD, BSE, and electron microprobe investigation. J. Metamorphic Geol. 9, 679-696.

Shackelton, R.M., 1996. The final collision zone between East and West Gondwana: where is it? J. Afri. Earth Sci. 23, 271-287.

Shervais, J.W., 1982. Ti-Y plots, the petrogenesis of modern, ophiolitic lavas. Earth Planet. Sci. Lett. 59, 101-118.

Shiraishi, K., Hiroi, Y., Ellis, D.J., Fanning, C.M., Motoyoshi, Y., Nakai, Y., 1992. The first report of a Cambrian Orogenic belt in East Antarctica – An Ion Microprobe Study of the Lutzow-Holm Complex. In: Y. Yoshida, K. Kaminuma and K. Shiraishi (Eds.), Recent Progress in Antarctic Earth Science, Terra Sci. Pub., Tokyo, p. 67-74.

Spear, F.S. 1993. Metamorphic Phase Equilibria and Pressure-Temperature-Time Paths. Mineralogical Society of America Monograph, Washington, DC., 799 pp.

Steiger, R.H., Laeger, E., 1977. Subcommission on geochronology; convention on the use of decay constants in geo- and cosmochronology. Earth Planetary Sci. Lett. 36 (3), 359-362.

Sun, -s, McDonough, W.F., 1989. Chemical and isotopic systems of oceanic basalts: implications for mantle composition and processes. In: Saunders, A.D., Norry, M.J. (Eds.), Magmatism in the Ocean Basins, Geological Society Special Publication No. 42, p.313-345.

Sweeney, R.J., Duncan, A.R., Erlank, A.J., 1994. Geochemistry and petrogenesis of Central Lebombo Basalts of the Karoo Igneous Province. J. Petrol. 35, 95-125.

Sweeney, R.J., Falloon, T.J., Green, D.H., Tatsumi, Y., 1991. The mantle origins of Karoo picrites. Earth Planet. Sci. Lett. 107, 256-271.

Thomas, R.J., Cornell, D.H., Armstrong, R.A., 1999. Provenance age and metamorphic history of the Quha Formation, Natal Metamorphic Province: a U-Th-Pb zircon SHRIMP study. S. Afr. J. of Geol. 102, 83-88.

Tingey, R.J., 1991. The regional geology of Archaean and Proterozoic rocks in Antarctica. In: Craddock, C. (Ed.), Antarctic Geoscience. Univ. Wisconsin Press, Madison, p. 455-464.

Walshe, J.L., 1986. A six-component chlorite solid solution model and the conditions of chlorite formation in hydrothermal and geothermal systems. Econ. Geol. 81, 681-703.

Watters, B.R., Krynauw, J.R., Hunter, D.R., 1991. Volcanic rocks of the Proterozoic Jutulstraumen Group in western Dronning Maud Land, Antarctica. In: Thomson,

M.R.A., Crame, J.A., Thomson, J.W. (Eds.), Geological Evolution of Antarctica. Cambridge Univ.Press, Cambridge, p. 41-46.

Wendlandt, R.F., Harrison, W.J., 1979. Rare earth partitioning between immiscible carbonate and silicate liquids and CO_2 vapour: results and implications for the formation of light rare earth-enriched rocks. Contrib. Miner. Petrol. 69, 409-419.

Wincherster, J.A., Floyd, P.A., 1977. Geochemical discrimination of different magma series and their differentiation products using immobile elements. Chem. Geol. 20, 325-343.

Wolmarans, L.G., Kent, L.E, 1982. Geological investigations in western Dronning Maud Land, Antarctica – a synthesis. S. Afri. J. Antarc. Res. Supplement, 2, 93 pp.

Wood, D.A., 1980. The application of a Th-Hf-Ta diagram to problems of tectonomagmatic classification and to establish the nature of crustal contamination of basaltic lavas of the British Tertiary volcanic province. Earth Planet. Sci. Lett. 50, 11-30.

Wyllie, P.J., Wolf, M.B., 1993. Amphibolite dehydration-melting: sorting out the solidus. In: H. M. Prichard, T. Alabaster, N.B.W. Harris and C.R. Neary (Eds.), Magmatic Processes and Plate Tectonics, Special publication, 76, 405-416. Geological Society, London.

Yoshida, M., 1992. Late Proterozoic to early Palaeozoic events in the East Gondwanaian crustal fragments. Abstracts, 29th International Geological Congress, Kyoto, Japan, vol.2/3, p. 265.

Zaleski, E., Pattison, D.R.M., 1993. Metamorphism in the generation of granulite veins: mass balance, mass transfer, and reference frames. J. Petrol. 34, 1303-1323.

Zang, W., Fyfe, W.S., 1995. Chloritisation of the hydrothermally altered bedrock at the Igarape Bahia gold deposit, Carajas, Brazil. Mineralium Deposita 30, 30-38.

Zhao, Y., Song, B., Wang, Y., Ren, L., Li, J., Chen, T., 1992. Geochronology of the late granite in the Larsemann Hills, East Antarctica. In: Y. Yoshida, K. Kaminuma and K. Shiraishi (Eds.), Recent Progress in Antarctic Earth Science, Terra Sci. Pub., Tokyo, p.155-161.

APPENDICES

APPENDIX 1:

Published abstracts:

1. Grosch, E., Frimmel, H.E., 2004. Metamorphic evidence for a major Pan-African thrust between the Archaean Grunehogna Craton and the Mesoproterozoic Maud Belt, western Dronning Maud Land, East Antarctica, Abstract, In: L.D. Ashwal (Ed.) Geoscience Africa 2004, 12-16 July 2004, University of the Witwatersrand, Johannesburg, vol. 1, pp. 227.

2. Grosch, E., Bisnath, A., Frimmel, H.E., 2004. Geochemistry and tectonic setting of Proterozoic mafic rocks in western Dronning Maud Land, Antarctica, Abstract, In: L.D. Ashwal (Ed.) Geoscience Africa 2004, 12-16 July 2004, University of the Witwatersrand, Johannesburg, vol. 1, pp. 229.

APPENDIX 1 (continued):

Manuscripts submitted to peer-reviewed international journals:

1. Grosch, E.G., Frimmel, H.E., 2005. P-T constraints on a large-scale crustal discontinuity between the Grunehogna Craton and the Maud Belt, East Antarctica: Evidence for a major Pan-African thrust in western Dronning Maud Land? *Antarctic Science.*

2. Grosch, E.G., Bisnath, A., Frimmel, H.E., Board, W.S., 2005. Geochemistry and tectonic setting of mafic rocks in western Dronning Maud Land, East Antarctica: Implications for the geodynamic evolution of the Proterozoic Maud Belt. *Chemical Geology.*

The contents of these manuscripts overlap largely with chapters of this thesis and, therefore, only the respective abstracts are appended here.

METAMORPHIC EVIDENCE FOR A MAJOR PAN-AFRICAN THRUST BETWEEN THE ARCHAEAN GRUNEHOGNA CRATON AND THE MESOPROTEROZOIC MAUD BELT, WESTERN DRONNING MAUD LAND, EAST ANTARCTICA.

E. Grosch* and H. E. Frimmel, Department of Geological Sciences, University of Cape Town, Rondeboch 7701, South Africa. *corresponding author, email: egrosch@geology.uct.ac.za, ph +27 – 21 – 650 2933 or 705 9708, fax +27 – 21 – 650 3783.

Introduction: Western Dronning Maud Land of Antarctica consists of two distinct lithotectonic provinces, the Grunehogna Craton, interpreted as an Archaean fragment possibly connected with the Kaapvaal Craton, and the high-grade metamorphic Maud Belt. These two provinces are tectonically juxtaposed along an inferred sub-glacial large-scale structure known as the Pencksökket-Jutulstraumen Discontinuity (PJD). To test the significance of this discontinuity, the metamorphic grade was established for metabasic rocks on either side, namely at Nashalkalvane on the eastern edge of the Grunehogna Craton and at Straumsvola in the northwestern extreme of the Maud Belt.

Petrographic examination of the Nashalkalvane metabasites reveals the presence of minerals diagnostic of the greenschist facies confined to local microdomains within a former dolerite sill. Actinolite (after the uralitization of clinopyroxene) and chlorite, typically forming the metamorphic mineral assemblage with or without epidote, albite and secondary quartz, occurs scattered between dominant relic igneous phases. Calculated activities from electron microprobe data for the various greenschist facies minerals were used in the construction of a petrogenetic grid for the system NCMASH using the program THERMOCALC v. 2.75 [1]. The results confirm a temperature of ~300°C for the location of the reactions defining the subgreenschist-greenschist facies boundary. A systematic increase in modal proportion of hydrous metamorphic phases and temperatures calculated using chlorite geothermometry suggests that variations in fluid/rock ratio on a microscale are an important control on chlorite temperature estimates. This metamorphic effect may be one of the factors responsible for the large uncertainty known to be associated with chlorite geothermometry. A temperature of 259°C is a minimum estimate for the metamorphic conditions at Nashalkalvane with more hydrated microdomains yielding higher temperatures (as much as 285°C) that are closer to the constraint derived from the P-T grid. The metamorphic grade at Nashalkalvane is, therefore, assigned to the lowermost greenschist facies with a peak metamorphic temperature estimate of 300°C.

Application of hornblende-plagioclase geothermometry to the Straumsvola metabasites yields temperatures of between 700 and 800°C. Although pressure is only poorly constrained at 2.5-11.3 kbar, this upper amphibolite facies temperature estimate is in perfect agreement with that obtained in the eastern Maud Belt [2]. This new data does not support the concept of a westward decreasing Mesoproterozoic metamorphic field gradient in the H.U. Sverdrupfjella as previously proposed [3,4]. The PJD is, therefore, interpreted to represent a major metamorphic hiatus of 500-400°C, thus implying a large-scale crustal discontinuity along which most parts of the middle crust are missing.

Recently, pervasive top-to-NW thrusting in the H.U. Sverdrupfjella has been shown to be Pan-African (c.540 Ma) in age [2]. Although geochronological control on an early eclogite facies (M1) metamorphism is not available to date, [2] interpreted major decompression from M1 to M2, evidenced by upper amphibolite facies hornblende-plagioclase symplectitic textures (M2) surrounding clinopyroxene and garnet of the eclogite facies assemblage to have developed during Pan-African top-to-NW thrusting. Metamorphic temperatures recorded at Straumsvola are identical to the M2 conditions (T=687-758°C, P=9.2-11.3 kbar) reported for the eastern part of the belt. One amphibolite sample collected from a less hydrated, strain protected boudin core at Straumsvola displayed evidence of recrystallization showing poikiloblastic amphibole cores surrounded by a second generation of smaller, euhedral amphibole. Both generations of amphibole yielded upper amphibolite temperatures of 700-800°C. As only two tectonothermal episodes are known to be recorded in the Maud Belt, the temperatures yielded by the second generation of amphibole is interpreted to record the latest Pan-African metamorphic conditions. Hence, the intense foliated amphibolite zones surrounding boudin cores and the

pervasive penetrative fabric observed throughout the country rock at Straumsvola is considered Pan-African in age. A 540 Ma age for the metamorphism at Straumsvola directly adjacent to the PJD suggests that the entire H.U. Sverdrupfjella experienced major Pan-African deformation and metamorphism. High-grade granulite assemblages in pre-tectonic mafic dykes [3] from the eastern part of the belt are regarded as representing relics of the older Grenvillian metamorphism that is indicated by U-Pb zircon ages [5] in early anatectic leucosome and zircon overgrowths.

A metamorphic hiatus of 500-400 °C, the similarity in M2 upper amphibolite facies conditions across the Maud Belt, and the geographical orientation of the PJD, which is consistent with the pervasive 540 Ma top-to-the-NW planar fabric in the belt, suggests that the PJD represents a major Pan-African thrust that developed in a compressional tectonic setting. Such an inferred Pan-African thrust could represent an extension of the orogenic front from the Mozambique Belt into East Antarctica. This suture was subsequently reactivated during the Mesozoic extension forming a graben-type structure during the break-up of Gondwana and facilitated alkaline magmatic activity along its flank.

References:

[1] Powell R. and Holland T.J.B. (1988). An internally consistent thermodynamic dataset with uncertainties and correlations: 3: application methods, worked examples and a computer program. *J. Metamorph. Geol, 6,* 173-204.

[2] Board W.S. (2002). Tectonothermal evolution of the southern H.U. Sverdrupfjella, western Dronning Maud Land, Antarctica, Unpubl. PhD thesis, University of Cape Town, 174 p.

[2]* Board W.S. Frimmel H.E. and Armstrong R.A. (2004). Pan-African tectonism in the western Maud Belt: P-T-t path for high-grade gneisses in the H.U. Sverdrupfjella, East Antarctica. *J. Petrol.*, in review.

[3] Groenewald P. B., Moyes A.B., Grantham G.H., Krynauw J.R. (1995). East Antarctic crustal evolution: geological constraints and modelling in western Dronning Maud Land. *Precambrian Res., 75,* 231-250.

[4] Grantham G.H., Jackson C., Moyes A.B., Groenewald P.B., Harris P.B., Ferrar G., Krynauw J.R. (1995). The tectonothermal evolution of the Kirwanveggen-H.U. Sverdrupfjella areas, Dronning Maud Land, Antarctica. *Precambrian Res., 75,* 209-229.

[5] Frimmel H.E. (2004). Formation of a late Mesoproterozoic supercontinent: The South Africa - East Antarctica connection. In: P. Eriksson and O. Catuneanu (Editors), The Precambrian Earth: Tempos and Events. Elsevier, Amsterdam.

GEOCHEMISTRY AND TECTONIC SETTING OF PROTEROZOIC MAFIC ROCKS IN WESTERN DRONNING MAUD LAND, ANTARCTICA.

E. G. Grosch*, A. Bisnath and H. E. Frimmel, Department of Geological Sciences, University of Cape Town, Rondebosch 7701, South Africa. *corresponding author, email: egrosch@geology.uct.ac.za, ph +27 – 21 – 650 2933 or 705 9708, fax +27 – 21 – 650 3783.

Mafic amphibolite sills, dykes and boudins are extensive throughout the Maud Belt of Western Dronning Maud Land, East Antarctica. In the light of limited U-Pb age data for mafic rocks in the Maud Belt, the geochemistry of amphibolites from the western and eastern H.U. Sverdrupfjella and the Gjelsvikfjella areas of the belt are compared to that in the south-westernmost Heimefrontfjella and mafic dolerite sills of the 1107 Ma Borgmassivet Suite on the adjacent Grunehogna Craton. In this study, three groups of pre-Pan African amphibolites are distinguished based on systematic geochemical differences in particular with regard to (Nb+Ta)-Th-Ce. The recognition of three different mafic events each recording a specific tectonic setting, allows for a model reconstruction of the tectonic evolution of the Maud Belt.

Group I amphibolites identified in the H.U. Sverdrupfjella are genetically equivalent to the mafic diabase Borgmassivet sills on the Grunehogna Craton and are interpreted to represent an early phase of mafic magmatic activity affecting Western Dronning Maud Land. An emplacement age for these mafic sills is established at c.1107 Ma (Knoper unpub. data, in [1]). The striking similarity in N-type MORB- and primitive mantle-normalized patterns between Group I pretectonic amphibolite boudins and the Borgmassivet intrusions, therefore, implies emplacement of mafic sills into both, the Grunehogna Craton and the island-arc (Maud Belt). Intrusion of the sills must have occurred prior to Grevillian orogenesis bracketed between 1090-1030 Ma by U-Pb zircon ages from early anatectic leucosome and zircon overgrowths [1]. Although the Borgmassivet sills are characterized as typical continental tholeiites and the mafic rocks from the H.U. Sverdrupfjella show a transitional but mostly depleted N-type MORB chemistry, they both record a strong superimposed subduction zone signature indicated by high concentrations of large ion lithophile elements, depletions in Nb and Ta, and enrichment in Ce and Sm. The contemporaneous Umkondo dolerites in eastern Zimbabwe dated at 1105±2 Ma [2] have identical REE profiles, N-type MORB- and primitive mantle-normalized signatures and also classify as a Group I magma type on a Nb-Th-Ce ternary diagram. The Ce/Yb vs Ta/Yb binary plot of [3] indicates that the Group I mafic rocks are displaced from the MORB + within-plate basalt array into the subduction zone enriched arc-related basalt and crustal contamination field. However, due to petrological and geochemical evidence for the Maud Belt as a former island-arc, a sublithospheric mantle source modified by subduction zone processes is favoured, rather than crustal contamination, to explain the geochemistry of Group I. The geochemical characteristics of this group are strikingly similar to those of the Mesozoic southern Karoo basalts, Ferrar dolerites of the Trans-Antarctic mountains and the Tasmanian dolerites for which a lithospheric source affected by subduction zone processes below Gondwana has been suggested [4]. The primitive mantle-normalized patterns of these dolerites are indistinguishable from terrigenous sediments showing low Sr, P, Ti, Nb and high Pb concentrations as well as typical crustal Sr, Nd and Pb isotopic compositions suggesting the involvement of sediment in their source (Hergt, J.M. unpubl. thesis, reported in [5]). The first order interpretation of the subduction zone signature shared by both the Borgmassivet dolerites and the amphibolites of Group I is that the Grunehogna Craton was in close proximity to a volcanically active island-arc with subduction and related metasomatism occurring beneath the arc and the craton. Subsequent c.1107 Ma extension and mafic magmatism affected both lithotectonic units of western Dronning Maud Land before collision of the arc with the craton during Grenvillian orogenesis. This interpretation is compatible with the similarity in U-Pb zircon ages from two tuff layers in the lowermost Ahlmannryggen Formation of the Ritchersflya Supergroup (1130±7 Ma) on the craton and the oldest plutonic (arc) rocks in the Maud Belt [1]. The geochemical data for the Group I magma-type indicates inversion from a compressional to extensional setting and the deposition of the Ritchersflya sediments in a back-arc basin prior to Grenvillian tectonism.

Two geochemically distinct groups of mafic dykes have been identified in the south-westernmost Heimefrontfjella area of the Maud Belt [6]. The first group of dykes was found to have a within-plate, continental tholeiite composition with a U-Pb SHRIMP age of 1033±7 Ma, whereas the second group was reported to have an E-type MORB chemistry and yielded a U-Pb age of 586±7 Ma. Amphibolite samples collected in the north-eastern Gjelsvikfjella area of the Maud Belt were found in this study to be geochemically similar to these two groups and are classified as Group II and Group III, respectively, based on their (Nb + Ta)-Th-Ce distributions. Group II amphibolites are the most heterogeneous in composition and display the highest Th concentrations. Their strong within-plate signature indicates the existence of a sub-lithospheric mantle at that time. The heterogeneous nature displayed by primitive mantle-normalized diagrams of this group may be explained by a period of post-Grenvillian orogenic collapse [6]. Although a dominant within-plate chemistry is present, a remnant subduction zone component is still recorded in these rocks. The high and variable Th concentrations of this group are most likely the result of crustal contamination of mafic magma reservoirs undergoing different degrees of crystal fractionation at various levels in the crust. The chemical heterogeneity can also be explained by larger variations in partial melting as well as differences in the timing and conditions of post-orogenic collapse throughout the Maud Belt.

Group III pre-Pan African mafic rocks display the lowest Th and Ce concentrations, and are the most enriched in Nb and Ta. They have low Zr/Y ratios and relatively flat REE patterns strongly resembling that of typical enriched MOR basalts. The mantle-normalized diagrams are similar to those for Group I indicating the influence of terrigenous sediment in the mantle source. Relative to N-type MORB, Group III shows enrichment in Nb and Ta, and depletion in Th, which points to a mantle source that contained a large proportion of re-worked oceanic crust. Such crustal reworking via dehydration and partial melting would be most readily achieved by subduction. The age of these dykes is compatible with emplacement during the waning stages of Neoproterozoic ocean opening (possibly as a continuation of the Mozambique Ocean further north). A peripheral subduction zone that existed along the entire southern margin of Gondwana since about 650 Ma may explain the perculiar geochemistry of Group III dykes in the Maud Belt.

References:

[1] Frimmel, H.E. (2004) In: P. Eriksson and O. Catuneanu (Editors), The Precambrian Earth: Tempos and Events. Elsevier, Amsterdam.

[2] Hanson R.E., Martin M.W., Bowring S.A. and Munyanyiwa H. (1998) *Geol., 26,* 1143-1146.

[3] Pearce J.A. (1983) In: Continental Basalts and Mantle Xenoliths. Hawkesworth, C.J., and Norry, M.J. (Editors). Shiva Publishing Limited, Cheshire, UK. p. 230-249.

[4] Cox K.G. (1978) *Nature, 274,* 47-49.

[5] Sun S.-s and McDonough W.F. (1989) In: Magmatism in the Ocean Basins. Geological Society Special Publication No. 42. Saunders, A.D. and Norry, M.J. (Editors). Blackwell Scientific Publications. London.

[6] Bauer W., Fielitz W, Jacobs J, Fanning C.M. and Spaeth G. (2003) *Antarc. Sci, 15(3),* 379-391.

P-T CONSTRAINTS ON A LARGE-SCALE CRUSTAL DISCONTINUITY BETWEEN THE GRUNEHOGNA CRATON AND THE MAUD BELT, EAST ANTARCTICA: EVIDENCE FOR A MAJOR PAN-AFRICAN THRUST IN WESTERN DRONNING MAUD LAND?

E.G. GROSCH* AND H.E. FRIMMEL**

Department of Geological Sciences, University of Cape Town, Rondebosch 7701, South Africa.

*corresponding author, email: egrosch@geology.uct.ac.za, ph +27 – 21 – 650 2933, fax +27 – 21 – 650 3783

** current address: Institute of Mineralogy, University of Würzburg, Am Hubland, D-97074 Würzburg, Germany

Submitted to: Antarctic Science

Abstract

A petrological and metamorphic comparison of Mesoproterozoic metabasic rocks on the eastern margin of the Archaean Grunehogna Craton and the adjacent Maud Belt in western Dronning Maud Land, East Antarctica, revealed a difference in peak metamorphic conditions from T = ~275°C to 730°C and P = 2 to 10.7 kbar over a distance of only 30 km across a major glacial valley. The lower grade constraints were derived from average P-T calculations using THERMOCALC and thermodynamic modeling of phase equilibria together with chlorite geothermometry. The high-grade P-T constraint for the western extreme of the Maud Belt, derived from hornblende-plagioclase thermometry and geobarometric calculations with a garnet amphibolite assemblage, is very similar to that reported for the eastern Maud Belt and, therefore, does not support the concept of a westward decreasing metamorphic field gradient as previously proposed. In conjunction with a recent geochronological study on the eastern Maud Belt, this study suggests that the inferred sub-glacial boundary between the Grunehogna Craton and the Maud Belt, known as the Pencksökket-Jutulstraumen Discontinuity, may represent a major thrust that developed during Pan-African orogenesis (possibly as the continuation of the East African Mozambique Belt into East Antarctica) prior to extension and its possible development as a normal listric fault or succession of fault slices during the Mesozoic break-up of Gondwana.

GEOCHEMISTRY AND TECTONIC SETTING OF MAFIC ROCKS IN WESTERN DRONNING MAUD LAND, EAST ANTARCTICA: IMPLICATIONS FOR THE GEODYNAMIC EVOLUTION OF THE PROTEROZOIC MAUD BELT

EUGENE G. GROSCH*, AVINASH BISNATH, HARTWIG E. FRIMMEL**, WARWICK S. BOARD

Department of Geological Sciences, University of Cape Town, Rondebosch 7701, South Africa.

*corresponding author, email: egrosch@geology.uct.ac.za, ph + 27 –27 – 6502933, fax +27 – 21 – 650 37 87

** current address: Institute of Mineralogy, University of Würzburg, Am Hubland, D-97074 Würzburg, Germany

Submitted to: Chemical Geology

Abstract

Bulk major-, trace- (including rare earth) element and isotopic data of variably metamorphosed mafic rocks in the polymetamorphic Maud Belt of western Dronning Maud Land, East Antarctica, in conjunction with limited geochronological data, indicate that the Maud Belt was once an active continental volcanic arc that formed on the southeastern margin of the Kaapvaal-Grunehogna Craton during the late Mesoproterozoic (1160-1130 Ma). This is in contrast to models of an oceanic island arc that was obducted onto the craton margin in analogy with the evolution of the Natal Belt in southern Africa. Four groups of amphibolite are distinguished on the basis of new lithogeochemical and Rb-Sr as well as Sm-Nd isotope data. Group 1 is the oldest and is interpreted as representing volcanic arc-related mafic protoliths in the Maud Belt. It is characterized by Archaean Sm-Nd model ages (2500 to 3300 Ma), depletion in Nb and Ta, and strong enrichment in light rare earth and large ion lithophile elements. Its ϵ_{Nd} (1110 Ma) values show a wide spread ranging between –6.0 and –15.0. The mafic protoliths to the Group 2 amphibolites are ascribed to the 1107 Ma Umkondo/Borgmassivet thermal event on the basis of comparable Sm-Nd model ages (~1800 Ma) and trace element distributions. Group 3 amphibolites are distinguished by flat, E-type MORB-like rare earth element patterns and low Th/Yb ratios. They are interpreted to represent largely juvenile oceanic basalts/dykes that were emplaced during opening of a Neoproterozoic ocean basin. Group

4 amphibolites show overall enrichment in rare earth elements and elevated Zr concentrations. They are interpreted to be related to a phase of c. 530 Ma syn-tectonic mafic magmatism that is derived from partial melting of late Mesoproterozoic lithosphere. Post-tectonic, c. 490 Ma gabbro and mafic dykes have a geochemical signature with subduction-zone characteristics. From their chronometric, isotopic and field relationships it is evident, however, that they are related to partial melting of lower calc-alkaline, arc-related Mesoproterozoic crust during orogenic collapse and not to melt formation in an active supra-subduction-zone setting. This demonstrates the limitations and problems of conventional tectonic discrimination diagrams.

APPENDIX 2: Sample description and petrography of selected metabasites from Straumsvola and Nashornkalvane South

A: Nashornkalvane metabasite (Borgmassivet Suite sill, eastern Grunehogna Craton: 072°19.06S/001°57.46W)

Sample: EG-N1

Rock Type: Mafic diabase/dolerite sill

This is a highly altered rock. Most of the thin section consists of altered primary igneous phases such as corroded clinopyroxene (augite) and sericitized plagioclase. Metamorphic minerals such as actinolite, chlorite and epidote are scattered randomly and are present in variable proportions in local domains between the igneous phases. Clinopyroxene is uralitized to fine actinolite needles and chlorite along grain boundaries. Chlorite is the most abundant metamorphic phase. The replacement of ilmenite by skeletal grains of metamorphic sphene is common throughout the section. The above observations suggests possible limited infiltration of a fluid phase during low-grade, greenschist facies metamorphic conditions (most likely an aqueous fluid since no carbonate minerals can be identified).

Sample: EG-N2

Rock-Type: Mafic diabase/dolerite sill

The mineralogy and texture of this sample is very similar to EG-N1, however, the thin section of this metabasite consists of a larger greenschist facies metamorphic microdomain. In this local domain metamorphic albite is present and coexists with actinolite, chlorite, epidote, and quartz. The albite is unaltered and differs from the highly sericitized, almost unrecognizable relic igneous plagioclase grains, which constitute most of the thin section. Clinopyroxene is also completely replaced by actinolite in these domains but chlorite is the still the most abundant metamorphic mineral (possibly also after actinolite). Sphene occurs as a reaction rim around opaque ilmenite.

B: Straumsvola metabasites (western Maud Belt: 072°09.775/000°14.52W)

Sample: EG-021b

Rock description: Amphibolite boudin (core)

This is a fine- to medium-grained, inequigranular rock, displaying a granoblastic and moderately interlobate texture. Triple junction grain boundaries between amphibole grains are common. The mineralogy consists essentially of syn-kinematic green-yellow to blue-green amphibole, plagioclase and quartz. Accessory metamorphic sphene and/or rutile have replaced relic igneous ilmenite. The modal proportions of minerals are: amphibole, 45%; plagioclase, 35%; quartz, 7%; biotite, 5%; sphene, 5% and trace amounts of opaque ilmenite. Prominent amphibole cleavages are at times disrupted by holes and inclusions of minerals such as plagioclase giving the amphiboles a poikiloblastic appearance. The small plagioclase grains are only slightly saussurritized. Minor brown biotite appears to have grown as randomly oriented laths, indicating post-kinematic growth. (Minerals are not particularly well aligned in the thin section since the sample represents the core of a mafic amphibolite boudin).

Sample: EG-026

Rock description: Amphibolite boudin

A strong planar fabric is displayed by this particularly well-foliated amphibolite sample defined by the alignment of syn-kinematic pale-green amphibole, bioitite, quartz and opaque oxide (ilmenite). It displays a moderately equigranular texture. Triple junction grain boundaries are absent. Mineral proportions include amphibole, 35%; plagioclase, 30%; bioitite, 15%; quartz, 10%; and opaque phase, 10%. The amphibole is extensively replaced by biotite, particularly along grain boundaries, cleavage planes and fractures. Plagioclase is moderately saussuritized. Opaque oxides are abundant in this sample, however, no replacement by metamorphic sphene is indicated. K-rich fluid infiltration appears to have been far more pervasive possibly due to the smaller size of the boudin.

Sample: EG-023

Rock description: Amphibolite boudin (outer foliation zone)

This amphibolite displays an inequigranular, granoblastic and interlobate texture. Individual amphibole grains coarser-grained, more uniform in habit and are aligned to define a strong planar fabric. Minerals present in this rock include pale green-brown, syn-kinematic amphibole (45%), plagioclase (40%), quartz (10%), biotite (3%) and accessory opaque ilmenite, sphene and rutile (~ 2%). Inclusions commonly occur in amphibole and sphene. Sphene is restricted to the grain-boundaries of ilmenite and forms a reaction rim around the small grains. Sphene is also less abundant in this sample than in other amphibolites. A good example of the late growth of biotite (i.e. fabric development) is indicated by the thin, randomly oriented bioitite laths truncating amphibole, which defines the foliation.

Sample: EG-016

Rock description: Garnet bearing amphibolite boudin

A granoblastic, inequigranular texture, similar to the above samples, is displayed by this rock, although the moderate interlobate texture is mainly due to plagioclase and quartz grain boundaries. The amphibolitic mineral assemblage consists of syn-kinematic brown-green amphibole (35%), garnet (30%), plagioclase (10%), quartz (5%) and accessory ilmenite, sphene and rutile. Amphibole is fresh in appearance with irregular grain boundaries. Garnet grains (~ 1-1.5 mm in size) are poikiloblastic with poorly developed and irregular grain boundaries. Metamorphic sphene occurs as small elongate grains in trail-like clusters associated with opaque ilmenite. Post-kinematic biotite is absent in this sample.

Sample: EG-028

Rock description: Mafic amphibolite boudin (core)

This is a very fine-grained, equigranular amphibolite comprising amphibole and plagioclase with minor opaque ilmenite. Overall texture is one, which indicates that the original amphibolitic assemblage experienced recrystallization during a second metamorphic event. Amphibole, plagioclase and opaques are present in mineral clusters. Two generations of amphibole appear to be present in this sample, namely core and rim amphibole. Poikiloblastic relic cores of first

generation amphibole are mantled by rims of small, subhedral second-generation amphibole grains, most likely indicating to two metamorphic episodes. No biotite is present in this rock.

Sample: EG-030

Rock Type: Mafic amphibolite boudin (core)

This relatively fresh rock has a similar texture and mineralogy to the amphibolites described above. Mineral phases include syn-kinematic brown-green amphibole (40%), plagioclase (40%), quartz (10%), biotite (5%) and with accessory sphene replacing opaque ilmenite. Accessory metamorphic sphene is associated with trains/trails of ilmenite. Plagioclase displays an unusual internal structure with apparent inclusions of quartz. The amphibole grains are slightly more equigranular in nature in comparision to the other amphibolites. Post-kinematic biotite crosscuts amphibole grains.

APPENDIX 3: Electron microprobe analyses for individual minerals

A: Nashornkalvane metabasites

EG-N3

Chlorite	chl 1	chl 2	chl 3	chl 4	chl 5	chl 6	chl 7	chl 8
F	0.000	0	0.069	0.045	0.018	0	0	0.075
Na2O	0.038	0.048	0.05	0.033	0.022	0.008	0.016	0.019
K2O	0.005	0.006	0.008	0.016	0.007	0.019	0.002	0.009
Al2O3	21.049	21.084	19.769	20.04	20.785	20.73	20.705	19.779
FeO	28.613	29.398	29.602	29.649	28.748	28.949	28.107	28.921
MnO	0.382	0.39	0.437	0.409	0.419	0.434	0.428	0.483
MgO	13.68	12.749	13.28	12.39	12.256	12.7	13.131	12.451
SiO2	25.462	26.002	26.572	25.918	25.933	26.846	26.479	25.991
TiO2	0.02	0.023	0.02	0.009	0.035	0.017	0.003	0.021
CaO	0.007	0	0.017	0.061	0.031	0.023	0.017	0.012
Total	89.256	89.7	89.824	88.571	88.253	89.726	88.887	87.761

	chl 9	chl 10	chl 11	chl 12	chl 13	chl 14	chl 15	chl 16
F	0.117	0	0	0.053	0	0	0.139	0
Na2O	0.019	0.012	0.029	0	0.045	0.014	0.036	0.027
K2O	0.002	0	0.027	0	0.003	0.004	0.013	0
Al2O3	20.005	20.872	19.212	20.415	20.342	20.217	20.217	20.534
FeO	28.301	29.007	28.332	28.39	28.467	28.758	28.571	29.34
MnO	0.417	0.435	0.397	0.466	0.46	0.419	0.394	0.444
MgO	12.855	12.645	13.294	13.205	12.284	13.183	12.574	11.915
SiO2	27.005	26.61	27.76	26.725	26.594	27.124	27.551	26.292
TiO2	0.026	0.025	0.053	0.001	0.016	0.028	0.018	0.041
CaO	0.041	0.049	0.048	0.045	0.06	0.038	0.075	0.054
Total	88.787	89.656	89.152	89.3	88.271	89.784	89.588	88.648

Actinolite	Act 1	Act 2	Act 3	Act 4	Act 5	Act 6	Act 7	Act 8
F	0.124	0.02	0	0.008	0	0	0.223	0
Na2O	0.217	0.313	0.278	0.27	0.379	0.221	0.285	0.231
K2O	0.102	0.116	0.087	0.109	0.177	0.107	0.134	0.118
Al2O3	2.259	3.181	2.864	2.555	3.932	2.507	2.766	2.625
FeO	15.726	16.201	16.248	16.124	16.409	15.802	16.101	15.835
MnO	0.367	0.361	0.296	0.359	0.338	0.253	0.327	0.263
MgO	12.688	11.706	12.538	12.288	11.101	12.441	11.911	12.649
SiO2	54.529	53.717	53.816	53.466	52.943	54.809	54.464	54.564
TiO2	0.014	0.082	0.141	0.016	0.035	0.009	0.049	0.012
CaO	12.62	12.372	11.907	12.515	12.124	12.516	12.291	12.586
Total	98.646	98.071	98.175	97.711	97.437	98.664	98.55	98.882

EG-N14a

Chlorite	chl 1	chl 2	chl 3	chl 4	chl 5	chl 6	chl 7	chl 8
F	0	0	0	0	0.017	0.065	0	0
Na2O	0.017	0	0.058	0.01	0.045	0.043	0.027	0.065
K2O	0.002	0.006	0	0.011	0.037	0.004	0.012	0.028
Al2O3	21.678	21.159	21.54	21.783	21.557	21.53	21.696	20.695
FeO	30.134	29.784	29.991	30.091	29.825	29.841	29.918	29.691
MnO	0.471	0.43	0.494	0.483	0.413	0.468	0.43	0.444
MgO	10.948	10.957	11.007	11.21	11.025	10.485	11.084	11.171
SiO2	26.514	26.692	26.754	26.308	26.165	25.819	26.233	26.328
TiO2	0.042	0.017	0.019	0.013	0.024	0.015	0.016	0.023
CaO	0.033	0.043	0.023	0.051	0.047	0.047	0.033	0.007
Total	89.838	89.088	89.886	89.961	89.156	88.316	89.45	88.452

	chl 9	chl 10	chl 11	chl 12	chl 13	chl 14	chl 15
F	0	0.22	0.014	0	0	0.136	0
Na2O	0.038	0	0.006	0.068	0.019	0.041	0
K2O	0.021	0.007	0.01	0.044	0.003	0.013	0.007
Al2O3	21.545	20.965	21.421	21.505	21.718	21.843	20.972
FeO	29.768	30.199	30.157	30.016	29.568	29.628	30.379
MnO	0.447	0.49	0.396	0.494	0.47	0.456	0.479
MgO	11.346	10.946	10.785	11.241	11.488	11.051	10.666
SiO2	25.991	26.937	26.103	26.356	26.56	25.264	26.418
TiO2	0.016	0.016	0.055	0.055	0	0.017	0.045
CaO	0.037	0.03	0.035	0.031	0.034	0.029	0.037
Total	89.208	89.811	88.983	89.812	89.86	88.476	89.003

Actinolite	Act 1	Act 2	Act 3	Act 4	Act 5	Act 6
F	0.153	0.319	0	0.109	0	0
Na2O	0.378	0.217	0.584	0.552	0.55	0.216
K2O	0.098	0.105	0.103	0.099	0.095	0.098
Al2O3	4.019	2.404	4.129	3.986	4.229	2.458
FeO	18.794	18.731	18.66	18.977	18.05	18.354
MnO	0.356	0.421	0.346	0.332	0.375	0.477
MgO	10.873	9.823	10.237	9.623	10.488	10.072
SiO2	51.57	53.872	51.88	52.347	52.792	54.397
TiO2	0.036	0.201	0.038	0.039	0.146	0.113
CaO	11.27	12.2	12.138	12.216	12.205	12.045
Total	97.546	98.293	98.113	98.279	98.931	98.23

EG-N2

Chlorite	chl 1	chl 2	chl 3	chl 4	chl 5	chl 6	chl 7	chl 8
F	0.128	0.000	0.064	0.000	0.000	0.000	0.000	0.270
Na2O	0.022	0.025	0.088	0.013	0.000	0.033	0.000	0.08
K2O	0.001	0.005	0.014	0.018	0.017	0.028	0.011	0.006
Al2O3	21.036	20.484	21.261	20.19	20.500	20.655	20.564	20.402
FeO	30.359	30.271	30.458	29.964	29.755	30.019	30.398	29.877
MnO	0.393	0.472	0.486	0.436	0.453	0.408	0.467	0.391
MgO	12.328	12.513	12.345	12.906	12.529	11.845	12.099	12.448
SiO2	25.375	25.533	25.18	26.336	25.695	25.573	25.884	26.003
TiO2	0.015	0.000	0.028	0.024	0.036	0.02	0.000	0.011
CaO	0.018	0.020	0.047	0.011	0.018	0.045	0.053	0.03
Total	89.676	89.323	89.97	89.899	89.001	88.626	89.476	89.518

	chl 9	chl 10	chl 11	chl 12	chl 13	chl 14	chl 15	chl 16
F	0.022	0.096	0.000	0.000	0.000	0.024	0.141	0.000
Na2O	0.024	0.019	0.050	0.020	0.000	0.032	0.032	0.009
K2O	0.000	0.021	0.002	0.011	0.008	0.012	0.017	0.012
Al2O3	19.859	20.693	20.199	20.968	22.27	21.161	21.558	21.536
FeO	29.171	29.744	29.713	30.363	28.932	29.615	29.488	29.459
MnO	0.420	0.488	0.407	0.418	0.457	0.422	0.417	0.445
MgO	13.154	12.92	13.147	12.458	10.69	11.26	12.172	10.885
SiO2	26.188	25.496	24.841	25.513	26.063	26.669	25.597	25.757
TiO2	0.010	0.028	0.01	0.027	0.025	0.012	0.02	0.034
CaO	0.033	0.03	0.000	0.036	0.021	0.085	0.232	0.074
Total	88.880	89.536	88.369	89.813	88.466	89.291	89.674	88.21

Albite	Alb 1	Alb 2	Alb 3	Alb 4	Alb 5	Alb 6	Alb 7	Alb 8
Na2O	10.585	10.974	11.084	11.781	11.378	11.908	11.407	10.85
K2O	0.085	0.088	0.078	0.087	0.071	0.083	0.077	0.064
SiO2	67.765	67.409	68.785	67.12	68.249	67.415	68.791	68.971
FeO	0.077	0.182	0.418	0.172	0.181	0.491	0.096	0.568
Al2O3	20.75	20.573	19.915	19.685	20.006	20.009	19.767	19.637
MgO	0	0.004	0.086	0	0.008	0.007	0	0.225
CaO	1.185	1.047	0.344	0.298	0.498	0.422	0.311	0.49
Total	100.447	100.276	100.71	99.142	100.39	100.335	100.449	100.805

	Alb 9	Alb 10	Alb 11
Na2O	11.557	11.776	10.762
K2O	0.069	0.09	0.057
SiO2	68.582	68.92	67.87
FeO	0.096	0.096	0.217
Al2O3	19.914	19.773	20.293
MgO	0.003	0	0
CaO	0.336	0.242	0.747
Total	100.559	100.898	99.946

Actinl.	Act 1	Act 2	Act 3	Act 4
F	0.012	0	0.051	0
Na2O	0.162	0.333	0.299	0.203
K2O	0.158	0.147	0.178	0.109
Al2O3	3.926	3.663	4.396	2.516
FeO	17.154	17.373	18.018	17.356
MnO	0.298	0.336	0.399	0.339
MgO	11.375	10.934	11.134	12.269
SiO2	54.378	53.672	51.626	52.273
TiO2	0.033	0.047	0.054	0.01
CaO	11.403	12.36	11.729	11.721
Total	98.9	98.864	97.883	96.796

Epidote	Epi 1	Epi 2	Epi 3	Epi 4	Epi 5	Epi 6
Na2O	0.022	0.017	0.039	0	0.039	0.032
K2O	0	0.016	0.02	0	0.005	0
SiO2	39.107	38.77	38.175	37.072	37.591	36.902
Al2O3	29.628	28.779	29.012	23.708	23.774	28.504
FeO	5.44	6.27	5.719	12.324	12.376	5.855
MgO	0.023	0.017	0.007	0	0.139	0
CaO	24.256	24.375	24.252	23.326	23.245	22.88
Total	98.475	98.245	97.764	96.43	97.169	94.173

EG-14c

Chlorite	chl 1	chl 2	chl 3	chl 4	chl 5	chl 6	chl 7	chl 8
F	0	0	0	0	0	0	0	0
Na2O	0.027	0.042	0.054	0	0	0.086	0	0.037
K2O	0	0.019	0.028	0.006	0.014	0.009	0.018	0.011
Al2O3	20.39	19.948	18.693	19.299	20.171	20.605	20.917	21.461
FeO	30.769	30.495	29.827	29.971	30.12	30.146	30.463	30.443
MnO	0.464	0.493	0.408	0.464	0.472	0.534	0.497	0.539
MgO	12.735	13.564	14.01	13.481	13.881	12.808	12.757	12.726
SiO2	23.744	25.226	25.889	24.965	24.635	23.808	24.349	23.773
TiO2	0.004	0.025	0.016	0.018	0.017	0.01	0.028	0.024
CaO	0.061	0.11	0.092	0.051	0.011	0.056	0.013	0.056
Total	88.194	89.922	89.018	88.254	89.32	88.063	89.041	89.07

	chl 9	chl 10	chl 11	chl 12	chl 13	chl 14	chl 15	chl 16
F	0	0	0.137	0.294	0	0.052	0.035	0.063
Na2O	0.021	0.052	0.058	0.041	0.051	0	0.057	0.02
K2O	0.018	0.042	0.039	0.032	0.018	0.032	0.007	0.029
Al2O3	20.913	20.769	19.1	19.961	18.846	19.169	19.973	21.227
FeO	30.708	30.755	30.177	30.651	29.862	29.488	30.34	30.182
MnO	0.483	0.529	0.481	0.44	0.464	0.403	0.479	0.529
MgO	12.912	12.644	13.775	13.212	14.302	14.256	13.386	13.193
SiO2	23.016	24.412	26.015	24.913	26.199	25.848	24.983	24.228
TiO2	0.034	0.023	0.034	0.037	0.022	0.049	0.036	0.028
CaO	0.059	0.05	0.143	0.114	0.098	0.083	0.101	0.046
Total	88.164	89.275	89.96	89.695	89.862	89.38	89.398	89.545

Actinolite	Act 1	Act 2	Act 3	Act 4	Act 5	Act 6	Act 7	Act 8
F	0.035	0.052	0.051	0	0.173	0.192	0	0
Na2O	0.552	0.35	0.217	0.596	0.501	0.472	0.644	0.588
K2O	0.109	0.115	0.06	0.173	0.098	0.116	0.141	0.1
Al2O3	3.799	3.218	1.98	5.541	4.361	3.908	4.867	4.216
FeO	18.492	17.748	19.134	19.019	18.749	18.766	19.307	18.984
MnO	0.39	0.297	0.414	0.39	0.398	0.388	0.437	0.425
MgO	12.488	13.193	13.088	11.487	12.494	12.334	11.868	11.89
SiO2	49.76	49.817	51.234	48.944	49.27	49.586	47.76	49.336
TiO2	0.131	0.089	0.097	0.139	0.132	0.099	0.208	0.189
CaO	12.747	12.848	12.579	12.565	12.414	12.306	12.101	12.382
Total	98.504	97.727	98.854	98.853	98.589	98.167	97.332	98.109

	Act 9	Act 10	Act 11	Act 12	**Epidote**	1	2	3
F	0.008	0.04	0	0.024	F	0.341	0	0
Na2O	0.167	0.803	0.732	0.5	Na2O	0.014	0	0.105
K2O	0.054	0.1	0.121	0.089	K2O	0.013	0.007	0.035
Al2O3	1.382	4.402	4.063	3.057	Al2O3	24.112	25.554	24.458
FeO	18.857	20.537	20.051	19.113	FeO	12.44	11.183	9.096
MnO	0.469	0.382	0.461	0.557	MnO	0.052	0.016	0.145
MgO	12.544	11.051	11.877	12.535	MgO	0.026	0	2.693
SiO2	51.822	48.699	47.623	50.314	SiO2	36.667	37.134	41.241
TiO2	0.104	0.14	0.064	0.075	TiO2	0.029	0	0.041
CaO	12.764	12.246	12.063	11.786	CaO	24.107	24.2	21.623
Total	98.171	98.398	97.055	98.05	Total	97.801	98.095	99.438

Epidote	4	5	6	7	8	9	10
F	0.013	0.04	0	0.027	0	0.066	0
Na2O	0.057	0.006	0.048	0	0.044	0.024	0
K2O	0.01	0.019	0.01	0.011	0	0.016	0
Al2O3	22.839	28.828	29.789	29.448	28.655	24.911	29.525
FeO	13.569	7.449	6.474	6.456	6.603	11.557	6.162
MnO	0.031	0.052	0.105	0.076	0.055	0.06	0.085
MgO	0.005	0.002	0.036	0.025	0.001	0.031	0.018
SiO2	36.846	37.506	38.263	38.382	37.716	37.444	38.223
TiO2	0.032	0.036	0.032	0.019	0.072	0.016	0.106
CaO	24.029	24.444	24.421	24.738	25.111	24.122	24.855
Total	97.431	98.382	99.179	99.181	98.256	98.246	98.974

EG-10

Actinolite	Act 1	Act 2	Act 3	Act 4	Act 5	Act 6	Act 7	Act 8
F	0.091	0	0.17	0.138	0.056	0	0.056	0.04
Na2O	0.207	0.394	0.158	0.336	0.262	0.202	0.333	0.196
K2O	0.092	0.138	0.078	0.127	0.111	0.081	0.123	0.131
Al2O3	2.109	3.559	1.904	3.133	2.973	3.772	3.264	2.57
FeO	17.036	17.491	16.439	17.052	16.72	18.103	17.386	17.116
MnO	0.324	0.416	0.281	0.423	0.341	0.261	0.319	0.389
MgO	13.664	12.292	13.644	12.872	13.133	13.52	12.39	13.034
SiO2	52.015	50.679	53.264	52.021	52.339	50.745	51.893	51.892
TiO2	0.153	0.163	0.051	0.173	0.086	0.021	0.05	0.064
CaO	12.751	12.396	12.946	12.611	12.828	11.897	12.568	12.718
Total	98.444	97.528	98.935	98.886	98.849	98.603	98.382	98.151

Actinolite	Act 9	Act 10	Act 11	Act 12	Act 13	Act 14
F	0.068	0	0	0	0.158	0.091
Na2O	0.375	0.283	0.219	0.204	0.207	0.489
K2O	0.062	0.137	0.112	0.129	0.103	0.132
Al2O3	3.01	2.557	2.315	2.167	2.937	3.864
FeO	18.176	17.187	16.804	16.169	17.61	20.59
MnO	0.455	0.32	0.281	0.302	0.422	0.509
MgO	12.421	12.742	13.502	12.855	12.96	10.535
SiO2	51.838	52.043	52.152	52.499	51.502	50.262
TiO2	0.101	0.028	0.03	0.05	0.069	0.065
CaO	12.248	12.871	12.9	12.748	12.42	12.288
Total	98.753	98.167	98.315	97.121	98.389	98.824

EG-14b

Chlorite	chl 1	chl 2	chl 3	chl 4	chl 5	chl 6	chl 7	chl 8
F	0	0.03	0	0	0	0	0	0.091
Na2O	0.081	0.054	0	0	0	0	0	0.022
K2O	0.035	0.04	0.024	0.001	0	0.004	0	0
Al2O3	20.176	19.104	19.381	19.987	19.677	21.356	19.927	20.408
FeO	29.598	28.577	29.281	29.774	29.93	30.915	30.181	30.81
MnO	0.369	0.467	0.427	0.425	0.459	0.467	0.449	0.49
MgO	12.296	13.015	12.947	13.013	13.036	11.651	12.938	12.202
SiO2	26.213	26.799	27.161	26.014	25.807	24.853	26.066	24.991
TiO2	0.008	0.036	0.019	0.025	0.035	0.015	0.051	0.041
CaO	0.07	0.12	0.161	0.102	0.062	0.057	0.03	0.032
Total	88.846	88.242	89.4	89.341	89.006	89.318	89.644	89.087

Chlorite	chl 9	chl 10	chl 11	chl 12	chl 13	chl 14	chl 15
F	0.039	0.153	0	0	0	0.022	0
Na2O	0.014	0.017	0.023	0.051	0.005	0.047	0
K2O	0	0.001	0.002	0	0.002	0.04	0.009
Al2O3	20.504	19.267	21.035	20.883	21.087	18.132	20.789
FeO	30.302	29.782	30.203	29.969	30.506	28.908	30.79
MnO	0.462	0.447	0.521	0.433	0.484	0.423	0.443
MgO	12.501	13.102	12.541	12.836	12.721	13.697	12.296
SiO2	24.959	26.831	25.197	24.92	24.81	27.814	25.05
TiO2	0.014	0	0.013	0.02	0.014	0.018	0.042
CaO	0.06	0.229	0.023	0.063	0.023	0.046	0.065
Total	88.855	89.829	89.558	89.175	89.654	89.146	89.485

Actinolite	Act 1	Act 2	Act 3	Act 4	Act 5	Act 6	Act 7	Act 8
F	0	0.033	0.035	0	0	0.043	0.202	0
Na2O	0.588	0.41	0.392	0.684	0.481	0.708	0.41	0.588
K2O	0.113	0.056	0.113	0.171	0.103	0.1	0.102	0.138
Al2O3	3.919	3.381	3.867	5.506	4.397	5.042	4.415	4.822
FeO	18.086	17.969	18.97	18.802	18.395	20.398	18.534	19.018
MnO	0.419	0.36	0.412	0.316	0.373	0.392	0.375	0.414
MgO	11.282	10.972	9.982	10.536	11.865	10.492	11.642	10.915
SiO2	51.863	52.624	50.338	48.86	50.412	49.275	50.579	49.814
TiO2	0.122	0.058	0.129	0.174	0.107	0.046	0.068	0.152
CaO	12.308	12.457	12.111	12.602	12.018	12.229	12.605	12.541
Total	98.702	98.319	96.349	97.651	98.152	98.725	98.932	98.402

Actinolite	Act 9
F	0.06
Na2O	0.222
K2O	0.118
Al2O3	2.566
FeO	17.904
MnO	0.401
MgO	12.045
SiO2	52.239
TiO2	0.028
CaO	12.723
Total	98.308

Epidote	Epi 1
Na2O	0
K2O	0.001
SiO2	40.915
Al2O3	31.05
FeO	5.695
MgO	0.02
CaO	24.285
Total	101.967

B: Straumsvola metabasites

EG-024

Amphibole	1	2	3	4	5	6	7	8	9	10	11	12	13	14
F	0.012	0	0	0.203	0	0.121	0.097	0.144	0	0.063	0.115	0.016	0.179	0.44
Na2O	1.556	1.555	1.325	1.593	1.473	1.466	1.456	1.463	1.573	1.484	1.451	1.555	1.42	1.475
K2O	1.037	1.086	1.06	0.961	0.979	1.093	1.041	1.015	1.074	1.059	0.978	1.003	1.047	1.069
Al2O3	12.229	11.766	11.468	11.267	11.205	11.907	11.393	10.945	11.886	11.465	11.434	11.264	11.307	11.681
FeO	18.81	18.744	17.821	17.857	17.922	18.045	18.202	17.681	18.403	17.952	17.825	17.587	17.858	18.107
MnO	0.318	0.28	0.208	0.206	0.25	0.294	0.337	0.259	0.276	0.303	0.248	0.284	0.32	0.275
MgO	9.7	9.602	9.867	10.405	10.047	9.519	10.007	10.154	9.775	9.649	9.884	9.893	9.995	9.753
SiO2	42.222	42.13	42.731	42.837	43.225	42.437	42.733	43.577	42.358	42.376	42.886	43.419	43.346	42.539
TiO2	1.06	0.984	1.055	0.861	1.003	0.954	0.808	0.803	0.95	0.788	0.991	0.971	0.772	1.045
CaO	12.035	11.909	12.018	12.064	12.116	12.05	12.011	12.012	12.033	12.137	12.202	12.023	12.111	12.172
Total	98.978	98.056	97.553	98.253	98.219	97.887	98.084	98.052	98.328	97.277	98.013	98.014	98.355	98.554

Plagioclase	1	2	3	4	5	6	7	8	9	10	11	12	13	14
Na2O	7.754	8.035	8.493	7.604	7.452	7.329	7.44	7.721	7.638	8.615	8.288	8.43	7.71	7.862
K2O	0.166	0.149	0.159	0.177	0.122	0.126	0.093	0.114	0.1	0.111	0.147	0.157	0.132	0.127
SiO2	58.194	58.862	59.689	58.54	58.838	58.95	57.798	58.562	58.165	59.363	59.508	59.535	58.415	59.529
Al2O3	25.923	25.936	25.762	26.404	26.357	26.007	26.869	26.495	26.815	25.744	25.703	26.017	26.444	26.129
FeO	0.087	0.138	0.117	0.194	0.086	0.131	0.113	0.121	0.106	0.097	0.127	0.119	0.148	0.078
MgO	0.021	0	0	0	0.011	0	0.013	0.026	0.003	0	0.014	0	0.013	0
CaO	7.147	7.193	6.617	7.426	7.567	7.241	8.043	7.683	7.965	6.888	6.786	6.848	7.667	7.138
Total	99.292	100.313	100.837	100.345	100.431	99.785	100.369	100.722	100.792	100.818	100.573	101.107	100.529	100.863

EG-022

Amphibole	1	2	3	4	5	6	7	8	9	10	11	12	13	14
F	0	0.178	0.341	0.16	0.133	0.136	0.268	0.251	0	0.322	0.145	0.025	0.359	0.23
Na2O	1.502	1.433	1.319	1.405	1.487	1.457	1.419	1.383	1.477	1.413	1.565	1.445	1.434	1.546
K2O	1.624	1.422	1.381	1.433	1.531	1.525	1.549	1.492	1.54	1.404	1.412	1.481	1.42	1.525
Al2O3	12.663	12.332	12.282	11.931	12.557	12.676	12.205	12.5	12.48	12.27	12.193	12.251	12.621	12.551
FeO	20.944	20.615	20.626	20.379	21.034	20.971	20.905	20.687	20.785	20.728	20.672	20.753	20.431	20.881
MnO	0.375	0.406	0.399	0.417	0.431	0.427	0.391	0.428	0.406	0.412	0.364	0.404	0.369	0.36
MgO	7.208	7.745	7.749	7.826	7.491	7.705	7.692	7.725	7.401	7.314	7.65	7.543	7.791	7.642
SiO2	40.038	41.327	41.24	41.16	40.585	41.008	40.842	40.608	41.086	41.65	41.219	40.449	41.509	40.845
TiO2	1.314	1.195	1.157	1.232	1.319	1.33	1.181	1.247	1.407	1.207	1.281	1.285	1.131	1.272
CaO	11.524	11.905	11.785	11.641	11.709	11.672	11.886	11.711	11.771	11.655	11.67	11.685	11.8	11.801
Total	97.191	98.559	98.281	97.587	98.278	98.908	98.337	98.031	98.352	98.376	98.17	97.321	98.865	98.652

Plagioclase	1	2	3	4	5	6	7	8	9	10	11	12	13	14
Na2O	9.125	8.964	8.795	8.626	4.891	8.848	8.612	6.102	8.198	8.763	7.573	8.353	8.356	8.622
K2O	0.202	0.213	0.225	0.169	0.167	0.165	0.187	0.173	0.203	0.159	0.15	0.142	0.098	0.164
SiO2	62.47	62.972	62.796	61.159	63.735	61.588	61.017	61.695	62.12	61.89	61.12	63.261	61.472	61.049
Al2O3	23.747	24.129	24.154	24.679	25.221	23.89	24.674	25.305	24.783	24.293	25.151	24.643	24.964	24.357
FeO	0.097	0.156	0.071	0.058	0.076	0.122	0.079	0.104	0.085	0.112	0.054	0.091	0.061	0.091
MgO	0.006	0.039	0.01	0	0.009	0	0.006	0	0	0.004	0	0	0	0
CaO	4.783	4.448	4.939	5.716	5.491	4.786	5.606	5.925	5.461	4.934	5.852	5.114	5.963	5.384
Total	100.429	100.921	100.99	100.406	99.59	99.399	100.182	99.304	100.85	100.154	99.9	101.605	100.914	99.668

EG-031

Amphibole	1	2	3	4	5	6	7	8	9	10	11
F	0	0.228	0.263	0	0.076	0	0	0	0	0.214	0.083
Na2O	1.634	1.473	1.592	1.533	1.509	1.619	1.6	1.551	1.699	1.466	1.456
K2O	0.842	0.787	0.824	0.847	0.81	0.785	0.84	0.859	0.873	0.832	0.754
Al2O3	11.882	11.806	12.025	12.561	12.183	12.119	12.18	12.335	12.624	12.148	12.033
FeO	18.236	17.917	18.16	17.936	18.042	17.753	17.879	17.944	18.543	18.333	17.79
MnO	0.274	0.263	0.314	0.293	0.328	0.267	0.282	0.245	0.305	0.215	0.271
MgO	9.328	9.338	9.154	9.239	9.407	9.339	9.389	9.516	9.263	9.362	9.257
SiO2	42.323	42.734	42.444	42.873	42.613	42.701	42.628	42.62	42.569	43.225	42.718
TiO2	1.036	0.973	1.004	1.033	1.026	0.976	0.995	0.977	1.039	0.979	1.058
CaO	11.965	11.63	11.805	11.77	11.751	11.721	11.771	11.87	11.762	11.871	11.834
Total	97.519	97.149	97.586	98.086	97.744	97.28	97.564	97.917	98.677	98.645	97.255

Plagioclase	1	2	3	4	5	6	7	8	9	10	11
Na2O	7.06	6.955	7.509	7.278	6.957	7.052	6.875	7.089	7.15	7.571	7.463
K2O	0.149	0.164	0.166	0.174	0.15	0.141	0.131	0.142	0.124	0.188	0.193
SiO2	58.092	56.362	59.223	58.085	57.837	57.55	57.76	58.22	57.319	59.522	58.96
Al2O3	27.143	26.995	26.306	26.121	26.414	26.986	27.187	26.75	26.546	25.879	26.196
FeO	0.145	0.202	0.139	0.039	0.205	0.077	0.08	0.12	0.213	0.099	0.113
MgO	0	0	0	0.001	0	0.018	0.018	0.013	0.039	0.02	0
CaO	8.198	8.542	7.499	7.469	7.903	8.54	8.55	8.194	8.273	7.005	7.486
Total	100.787	99.22	100.842	99.167	99.466	100.364	100.602	100.529	99.664	100.283	100.412

EG-028

Amphibole	rim1	core1	rim2	core2	rim3	core3	rim4	core4	rim5	core5	rim6	core6
F	0	0	0	0	0	0	0	0	0.055	0	0.13	0
Na2O	1.384	1.269	1.166	1.139	1.235	1.337	1.361	1.149	1.205	0.905	1.349	1.34
K2O	0.863	0.638	0.459	0.545	0.555	0.588	0.626	0.516	0.466	0.422	0.616	0.464
Al2O3	12.779	11.366	10.679	10.902	11.168	11.707	11.935	10.879	10.623	9.39	11.559	11.168
FeO	19.729	18.613	18.419	18.688	18.742	18.91	19.41	18.566	18.017	17.744	18.545	18.43
MnO	0.263	0.279	0.298	0.264	0.294	0.295	0.295	0.248	0.248	0.273	0.268	0.284
MgO	8.774	9.751	10.477	9.954	10.074	9.778	9.442	10.25	10.633	10.972	10.238	10.466
SiO2	40.976	42.308	44.583	43.376	43.789	42.596	42.392	43.654	44.297	44.827	43.316	43.349
TiO2	1.249	0.94	0.68	0.794	0.776	0.786	0.808	0.746	0.752	0.64	0.871	0.768
CaO	11.959	11.877	11.897	11.939	12.121	11.862	12.063	11.991	11.964	12.196	12.093	12.164
Total	97.976	97.039	98.659	97.601	98.755	97.86	98.333	98	98.26	97.37	98.986	98.433

Plag	1	2	3	4	5	6
Na2O	8.013	6.745	7.392	7.215	7.994	7.821
K2O	0.174	0.121	0.313	0.163	0.192	0.207
SiO2	62.537	59.27	61.254	60.349	62.561	61.515
FeO	0.111	0.087	0.444	0.104	0.114	0.166
Al2O3	23.035	25.135	23.983	24.696	23.05	23.245
MgO	0	0.009	0.12	0	0	0.02
CaO	5.553	7.869	6.579	7.487	5.653	6.125
Total	99.423	99.237	100.085	100.015	99.563	99.1

EG-032

Amphibole	1	2	3	4	5
F	0	0	0	0	0.203
Na2O	1.679	1.638	1.53	1.618	1.76
K2O	0.918	0.861	0.856	0.944	0.934
Al2O3	12.565	11.689	12.153	12.369	12.626
FeO	19.904	19.286	20.144	20.26	20.474
MnO	0.339	0.273	0.242	0.277	0.27
MgO	8.493	8.842	8.347	8.336	8.321
SiO2	41.997	42.694	42.405	41.577	41.865
TiO2	1.01	0.984	0.844	1.082	1.079
CaO	11.506	11.685	11.651	11.516	11.415
Total	98.41	97.95	98.171	97.978	98.948

Plagioclase	1	2	3	4	5
Na2O	8.472	8.937	9.047	8.952	8.596
K2O	0.127	0.11	0.083	0.118	0.109
SiO2	60.482	60.967	60.332	60.124	59.858
Al2O3	25.224	25.207	25.353	25.006	25.796
FeO	0.172	0.204	0.12	0.145	0.044
MgO	0.004	0	0.017	0	0
CaO	5.492	5.32	5.971	5.773	6.295
Total	99.974	100.747	100.923	100.118	100.699

EG-023

Amphibole	1	2	3	4	5	6	7	8	9	10	11	12	13	14	15	Average	Stdev
F	0	0.13	0	0.238	0	0	0.045	0.091	0.007	0.114	0.018	0	0	0.095	0.209	0.063	0.080
Na2O	1.431	1.516	1.412	1.48	1.425	1.45	1.271	1.421	1.477	1.423	1.349	1.407	1.436	1.229	1.380	1.407	0.076
K2O	1.075	1.138	1.154	1.166	1.15	1.059	1.055	1.044	1.072	1.063	1.039	1.122	1.155	1.004	1.076	1.091	0.051
Al2O3	11.607	11.634	11.58	12.116	12.169	11.94	11.823	11.9	12.283	12.304	11.701	12.586	12.367	11.726	12.288	12.002	0.322
FeO	20.85	20.569	20.927	20.781	20.819	20.254	20.195	20.178	19.531	20.113	20.082	20.42	20.266	20.442	20.145	20.371	0.374
MnO	0.369	0.294	0.308	0.313	0.297	0.318	0.286	0.27	0.351	0.302	0.284	0.267	0.289	0.317	0.281	0.303	0.028
MgO	8.184	8.292	7.916	8.36	7.84	7.942	7.978	8.303	8.316	7.892	8.253	7.914	8.035	8.259	8.234	8.115	0.186
SiO2	41.664	41.08	40.952	40.964	40.895	41.687	42.055	42.378	41.422	41.754	41.938	41.46	41.310	41.915	42.102	41.572	0.465
TiO2	1.408	1.433	1.49	1.407	1.404	1.37	1.45	1.314	1.338	1.329	1.338	1.428	1.563	1.250	1.253	1.385	0.085
CaO	11.318	11.517	11.711	11.246	11.27	11.538	11.649	11.657	11.762	11.622	11.702	11.8	11.808	11.736	11.834	11.611	0.195
Total	97.906	97.603	97.45	98.071	97.269	97.558	97.807	98.556	97.559	97.916	97.704	98.404	98.229	97.973	98.802	97.920	0.431

Plagioclase	1	2	3	4	5	6	7	8	9	10	11	12	13.000	14.000	15.000	Average	Stdev
Na2O	8.739	8.714	8.976	9.271	8.653	8.767	8.356	8.54	8.75	8.531	8.69	8.456	8.739	8.986	8.973	8.743	0.235
K2O	0.148	0.138	0.139	0.143	0.142	0.151	0.144	0.112	0.105	0.108	0.165	0.068	0.154	0.150	0.140	0.134	0.025
SiO2	61.87	62.495	62.513	63.319	61.879	61.955	61.45	61.537	62.136	60.641	61.694	61.485	62.008	62.121	63.264	62.024	0.688
FeO	0.107	0.067	0.106	0.099	0.149	0.056	0.066	0.146	0.217	0.2	0.095	0.042	0.205	0.117	0.091	0.118	0.055
Al2O3	23.404	23.618	23.744	22.865	23.458	23.861	24.077	23.722	23.977	23.899	23.556	24.224	23.324	23.384	23.271	23.626	0.356
MgO	0	0.021	0.004	0	0	0.006	0	0	0	0.005	0.017	0	0	0.020	0	0.005	0.008
CaO	5.337	5.305	5.224	4.458	5.362	5.405	5.96	5.464	5.435	5.701	5.399	5.807	5.237	4.985	4.697	5.318	0.387
Total	99.605	100.322	100.706	100.155	99.643	100.201	100.053	99.521	100.619	99.085	99.616	100.082	99.666	99.762	100.435	99.965	0.455

EG-030

Amphibole	1	2	3	4	5		7	8	9	10	Average	Stdev
F	0	0.08	0	0.106	0.2	0	0	0	0	0.079	0.047	0.069
Na2O	1.477	1.344	1.198	1.377	1.303	1.34	1.394	1.36	1.384	1.365	1.354	0.071
K2O	1.014	0.966	1.036	1.1	1.048	0.961	0.983	0.951	0.974	1.117	1.015	0.059
Al2O3	10.91	10.696	11.136	11.722	11.194	11.018	11.177	11.062	11.366	11.863	11.214	0.355
FeO	20.677	20.781	21.077	21.2	20.954	20.703	20.606	20.833	20.973	20.947	20.875	0.188
MnO	0.324	0.327	0.276	0.261	0.263	0.293	0.286	0.309	0.296	0.275	0.291	0.023
MgO	8.489	8.707	8.524	7.974	7.997	8.644	8.365	8.773	8.665	8.278	8.442	0.285
SiO2	41.567	41.566	41.494	40.866	41.05	42.116	41.476	42.3	42.019	40.864	41.532	0.505
TiO2	1.339	1.006	1.14	1.175	1.326	1.133	1.041	0.754	1.074	1.013	1.100	0.169
CaO	11.439	11.56	11.744	11.729	11.694	11.636	11.701	11.701	11.746	11.789	11.674	0.104
Total	97.236	97.033	97.625	97.51	97.029	97.844	97.029	98.043	98.497	97.59	97.544	0.488

Plagioclase	1	2	3	4	5	6	7	8	9	10	Average	Stdev
Na2O	8.879	8.648	8.22	8.019	8.251	7.88	8.016	7.775	7.341	8.131	8.036	0.433
K2O	0.148	0.144	0.094	0.202	0.194	0.158	0.122	0.1	0.15	0.172	0.163	0.028
SiO2	60.022	63.241	62.017	61.216	62.783	61.392	61.565	61.087	59.453	61.902	61.455	1.053
FeO	0.132	0.104	0.102	0.106	0.04	0.09	0.091	0.103	0.074	0.098	0.114	0.056
Al2O3	24.026	23.495	24.099	24.476	22.694	23.986	24.251	24.162	25.025	23.599	24.082	0.610
MgO	0.011	0	0	0.016	0.107	0	0.002	0.009	0.003	0.01	0.009	0.022
CaO	6.906	5.178	6.211	6.367	5.007	5.99	6.241	6.225	7.311	5.519	6.102	0.713
Total	100.123	100.809	100.745	100.401	99.076	99.495	100.288	99.461	99.356	99.431	99.961	0.546

EG-016

Amphibole	1	2	3	4	5	6	7	8	9	10	11	12	13	14	15 Average		STDEV
F	0	0	0	0	0	0	0	0.195	0.093	0.267	0.083	0	0	0	0.248	0.057	0.093
Na2O	1.639	1.562	1.622	1.632	1.616	1.603	1.462	1.612	1.581	1.666	1.751	1.415	1.632	1.658	1.742	1.629	0.090
K2O	0.798	0.757	0.818	0.813	0.833	0.8	0.753	0.773	0.751	0.782	0.852	0.775	0.857	0.769	0.796	0.797	0.031
Al2O3	13.195	13.255	13.205	12.408	12.751	12.733	12.892	13.382	13.202	13.138	13.274	13.191	13.163	13.273	13.397	13.136	0.266
FeO	18.591	18.123	19.478	18.978	19.527	18.449	19.224	19.124	19.378	18.817	19.089	18.828	19.125	18.605	18.542	19.034	0.424
MnO	0.126	0.112	0.088	0.148	0.111	0.125	0.123	0.161	0.155	0.101	0.11	0.129	0.091	0.114	0.102	0.117	0.020
MgO	8.739	9.046	8.427	8.756	8.515	8.597	8.604	8.454	7.954	8.613	8.441	8.447	8.662	8.509	9.153	8.611	0.257
SiO2	41.71	42.077	41.387	41.136	42.081	42.161	41.799	41.935	41.923	42.183	41.606	41.945	41.905	41.694	41.763	41.830	0.264
TiO2	1.279	1.279	1.209	1.559	1.606	1.533	1.124	1.028	1.303	1.327	1.643	1.16	1.36	1.218	1.089	1.289	0.177
CaO	11.806	11.673	11.569	11.646	11.932	11.777	11.648	11.538	11.385	11.589	11.555	11.742	11.674	11.546	11.725	11.639	0.122
Total	97.882	97.883	97.803	97.077	98.972	97.778	97.629	98.201	97.725	98.483	98.404	97.63	98.469	97.386	98.557	98.140	0.545

Plagioclase	1	2	3	4	5	6	7	8	9	10	11	12	13	14	15 Average		STDEV
Na2O	7.95	7.827	6.221	7.769	7.289	8.192	7.886	7.4	7.201	7.075	8.64	7.532	8.224	8.166	7.973	7.738	0.520
K2O	0.144	0.125	0.096	0.173	0.081	0.227	0.103	0.109	0.075	0.156	0.177	0.144	0.232	0.173	0.167	0.152	0.049
SiO2	61.338	60.589	58.358	61.793	60.119	63.108	62.015	60.476	59.402	59.735	63.604	60.585	62.853	62.56	61.823	61.327	1.304
FeO	0.098	0.119	0.126	0.036	0.143	0.05	0.028	0.138	0.281	0.117	0.111	0.092	0.127	0.115	0.082	0.120	0.058
Al2O3	23.605	24.119	26.707	24.515	25.41	23.234	24.319	24.918	25.222	25.305	23.246	24.205	23.252	23.938	24.066	24.267	0.879
MgO	0.003	0	0.022	0.007	0	0	0.004	0	0	0.01	0	0	0.003	0.003	0	0.004	0.006
CaO	6.105	6.424	9.105	6.203	7.401	5.132	6.276	6.977	7.536	7.45	4.826	6.599	5.173	5.722	6.072	6.333	0.980
Total	99.242	99.218	100.635	100.496	100.443	99.944	100.631	100.017	99.716	99.847	100.605	99.156	99.865	100.677	100.182	99.943	0.568

EG-016

Garnet	1	2	3	4	5	6	7	8	9	10	11	12	13	14	15 Average		Stdev
SiO2	37.834	37.104	37.578	37.235	37.319	37.712	37.653	38.19	37.371	37.751	37.501	37.778	37.842	37.901	38.21	37.676	0.345
TiO2	0.162	0.222	0.156	0.11	0.192	0.205	0.061	0.391	0.15	0.158	0.123	0.138	0.081	0.097	0.168	0.153	0.069
Al2O3	21.291	21.437	21.551	21.726	21.194	21.711	20.917	20.85	21.186	20.984	21.159	21.23	21.3	21.263	21.177	21.223	0.243
Cr2O3	0	0.011	0.028	0.008	0.063	0	0.025	0.067	0.119	0.088	0.125	0.029	0	0	0	0.030	0.039
FeO	26.31	26.323	26.36	26.29	26.357	25.901	26.256	26.764	25.998	26.339	25.622	26.427	26.488	25.583	26.527	26.224	0.309
MnO	0.892	1.472	1.009	0.892	1.114	1.388	1.358	1.071	1.09	1.084	1.063	1.159	1.159	0.652	1.1	1.072	0.220
MgO	2.671	2.877	2.73	2.637	2.79	2.795	2.772	2.717	2.745	2.822	2.707	2.791	2.855	2.529	2.732	2.719	0.126
CaO	11.563	10.683	11.243	11.673	10.784	11.002	10.4	10.887	11.178	10.907	11.43	10.93	10.732	11.698	10.84	11.089	0.393
Na2O	0	0.051	0	0	0.045	0.098	0.045	0.056	0.04	0.062	0.021	0.069	0.055	0.05	0.044	0.037	0.029
Total	100.723	100.181	100.655	100.57	99.858	100.812	99.488	100.991	99.878	100.196	99.751	100.551	100.511	99.774	100.798	100.223	0.499

EG-021a

Amphibole	1	2	3	4	5	6	7	8	9	10	11	Average	Stdev
F	0.117	0	0	0	0	0	0	0	0.062	0.209	0	0.035	0.069
Na2O	1.401	1.387	1.487	1.449	1.249	1.272	1.313	1.293	1.318	1.272	1.361	1.346	0.078
K2O	1.549	1.552	1.238	1.339	1.598	1.585	1.524	1.522	1.418	1.29	1.595	1.474	0.130
Al2O3	12.74	12.767	12.419	12.737	12.582	12.755	12.747	12.986	12.578	12.66	12.862	12.712	0.151
FeO	23.048	22.241	22.417	22.307	22.736	23.214	22.77	22.742	22.295	22.561	22.723	22.641	0.314
MnO	0.339	0.318	0.332	0.399	0.375	0.347	0.346	0.361	0.351	0.415	0.386	0.361	0.030
MgO	6.24	6.678	6.744	6.877	6.591	6.537	6.603	6.495	6.878	6.592	6.476	6.610	0.184
SiO2	39.399	39.842	40.345	40.584	40.024	39.575	40.442	40.422	40.593	40.568	39.839	40.148	0.431
TiO2	1.199	1.447	1.246	1.271	1.624	1.48	1.349	1.428	1.294	1.127	1.561	1.366	0.156
CaO	11.694	11.669	11.632	11.572	11.687	11.707	11.645	11.656	11.714	11.796	11.69	11.678	0.056
Total	97.726	97.901	97.86	98.535	98.466	98.472	98.739	98.905	98.501	98.49	98.493	98.372	0.376

Plagioclase	1	2	3	4	5	6	7	8	9	10	11	Average	Stdev
Na2O	8.235	8.058	8.198	8.742	8.576	8.695	8.701	8.605	8.558	8.523	8.738	8.588	0.266
K2O	0.157	0.162	0.156	0.134	0.102	0.13	0.144	0.141	0.138	0.15	0.155	0.142	0.015
SiO2	61.322	62.128	61.704	61.344	61.401	61.103	61.65	61.591	61.717	60.885	61.577	61.568	0.372
FeO	0.053	0.087	0.152	0.094	0.049	0.069	0.182	0.035	0.202	0.204	0.103	0.117	0.057
Al2O3	24.295	23.863	23.818	24.044	24.386	23.633	24.077	23.54	23.839	23.617	23.851	23.840	0.287
MgO	0	0.004	0	0.001	0	0	0	0	0	0.007	0	0.002	0.003
CaO	5.988	5.862	5.783	6.044	6.283	5.893	5.99	5.464	5.789	5.898	5.8	5.825	0.245
Total	100.05	100.164	99.804	100.402	100.798	99.524	100.744	99.376	100.245	99.285	100.224	100.082	0.476

EG-026

Amphibole	1	2	3	4	5	6	7	8	9	Average	Stdev
F	0.12	0.431	0	0.178	0.07	0.106	0.207	0	0.107	0.135	0.131
Na2O	1.721	1.753	1.635	1.434	1.661	1.504	1.432	1.596	1.487	1.580	0.121
K2O	0.953	0.995	1.04	1.206	1.02	0.977	0.824	1.018	0.945	0.998	0.101
Al2O3	12.391	12.141	12.332	13.045	12.342	12.498	12.345	13.472	12.435	12.556	0.424
FeO	21.992	22.054	21.984	21.906	21.631	22.007	21.35	21.778	22.205	21.879	0.257
MnO	0.491	0.436	0.442	0.435	0.505	0.422	0.489	0.493	0.507	0.469	0.034
MgO	8.436	8.554	8.21	8.656	8.233	7.649	8.519	7.6	8.187	8.227	0.379
SiO2	39.751	39.609	39.274	40.088	39.396	40.75	40.248	40.013	40.313	39.938	0.475
TiO2	0.933	1.005	0.947	1.01	1.133	1.083	0.649	1.101	1.008	0.985	0.143
CaO	11.477	11.513	11.524	10.157	11.707	11.395	11.589	10.96	11.708	11.337	0.495
Total	98.264	98.489	97.388	98.116	97.7	98.392	97.652	98.031	98.903	98.104	0.472

Appendix 4: Analytical Techniques

A. X-Ray Fluorescence (XRF) Spectrometey

Major and some trace element concentrations, excluding the REE, were determined by conventional x-ray fluorescence spectrometry (XRF) on a Philips X'Unique II PW1480 spectrometer in the Department of Geological Sciences at the University of Cape Town following the techniques described by Duncan et al. (1984) and le Roex (1985). The lithium tetraborate fusion method of Norrish and Hutton (1969) was used to determine all major and some minor elements, whereas pressed powder briquettes were used for the determination of the trace elements. A loss-on-ignition (LOI) value was obtained for each sample by heating in a furnace for at least 12 hours at ~950°C. The disks were analyzed using XRF with a dual target Mo/Sc X-ray tube. Fe, Mn, Ni, Cr and Ti are measured with the tube at 50 kV, 50 mA. The other elements were determined with the tube at 40 kV, 65 mA. Peak only measurements were made on the elements Ni through Mg. Sodium was determined using powder briquettes at 40 kV, 65 mA, and with background measured at –2.00 and +2.00°2 θ from the peak.

Typical detection limits are below 0.01 wt% and 2 ppm for the major and trace elements, respectively.

B. Inductively coupled plasma mass spectrometry

ICP-MS analyses were determined on a Perkin Elmer ELAN 6000 ICP-MS in the Department of Geological Sciences at the University of Cape Town. Fifty milligram of sample powder were dissolved in a 4:1 HF-HNO_3 acid mixture in sealed Teflon® beakersfor 48 hours on a hot plate. This step was followed by evaporation to dryness. An aliquot of 2ml concentrated HNO_3 was added and the sample was heated to dry. This step was then repeated.

The final dry product was taken up in 5% HNO_3 solution containing 10 ppb Re, Rh, In and Bi as internal standards. Standardization was against artificial multi-element

standards, that is, using a five-point calibration curve with one point at the origin and four artificial multi-element standards with elemental concentrations of 10, 30, 50 and 100ppb.

The instrumental operating parameters were as follows: nebuliser gas flow = 0.84 litre.min^{-1}, main gas flow = 15 litre.min^{-1},auxiliary gas flow = 0.75 litre.min^{-1}; ICP RF forward power = 1100 V; autolens voltages: ^{9}Be = 7.8, ^{59}CO = 9.0, ^{115}In = 9.8. The number of sweeps and replicates was 20 and 3, respectively, the peak dwell time 35-50 ms, the total counting time per peak 2100-3000 ms, the total analytical time 101.58s, and the wash time between samples 180s. The instrument sensitivity was 30 529 cps.ppb^{-1}. ^{103}Rh and the background intensity at mass 220 was 3.1 cps. The nebulizer gas flow was optimized to minimized oxide and doubly-charged ion formation. Mathematical corrections were made for isobaric, oxide and doubly charged ion interferences. Procedural blank concentrations were <0.065 ppm for Pb; <0.030 ppm for Ba, Nb, Zr, Sr, Cu, Ni, and Sc; and <0.009 ppm for all other elements. Within-run precision was better than 3% (1σ relative standard deviation) for all elements, as was the precision between duplicate analyses, except for Co (3.36%). Lower limits of detection (based on 3 standard deviations of the procedural blank intensities) were <0.300 ppm for Sc; <0.085 ppm for Sr; <0.050 ppm for Pb, Ta, Ba, Nb, Zr, Rb, Cu, Ni, and Co; and <0.0095 ppm for all other elements.